NASA CONTRACTOR REPORT

NASA CR-2028

PULSED DIFFERENTIAL HOLOGRAPHIC MEASUREMENTS OF VIBRATION MODES OF HIGH-TEMPERATURE PANELS

by D. A. Evensen, R. Aprahamian, and K. R. Overoye

Prepared by
TRW SYSTEMS GROUP
Redondo Beach, Calif. 90278
for Langley Research Center

NATIONAL AERONAUTICS AND SPACE ADMINISTRATION • WASHINGTON, D. C. • JUNE 1972

1. Report No.	2. Government Accession No.	3. Recipient's Catalog No.
NASA CR-2028		

4. Title and Subtitle	5. Report Date
PULSED DIFFERENTIAL HOLOGRAPHIC MEASUREMENTS OF VIBRATION MODES OF HIGH-TEMPERATURE PANELS	June 1972
	6. Performing Organization Code
7. Author(s)	8. Performing Organization Report No.
D. A. Evensen, R. Aprahamian, and K. R. Overoye	AM 71-7
9. Performing Organization Name and Address	10. Work Unit No.
TRW Systems Group Redondo Beach, California	114-08-05-01
	11. Contract or Grant No.
	NAS1-10169
12. Sponsoring Agency Name and Address	13. Type of Report and Period Covered
National Aeronautics and Space Administration Washington, D. C. 20546	Contractor Report
	14. Sponsoring Agency Code

15. Supplementary Notes

16. Abstract

Holography is a lensless imaging technique which can be applied to measure static or dynamic displacements of structures. Conventional holography cannot be readily applied to measure vibration modes of high-temperature structures, due to difficulties caused by thermal convection currents. The present report discusses the use of "pulsed differential holography," which is a technique for recording structural motions in the presence of random fluctuations such as turbulence. An analysis of the differential method is presented, and demonstration experiments were conducted using heated stainless steel plates. Vibration modes were successfully recorded for the heated plates at temperatures of 1000, 1600, and 2000°F. The technique appears promising for such future measurements as vibrations of the Space Shuttle TPS panels or recording flutter of aeroelastic models in a wind-tunnel.

17. Key Words (Suggested by Author(s))	18. Distribution Statement
Pulsed holography Vibration measurements High-temperature panels	Unclassified - Unlimited

19. Security Classif. (of this report)	20. Security Classif. (of this page)	21. No. of Pages	22. Price*
Unclassified	Unclassified	139	$3.00

*For sale by the National Technical Information Service, Springfield, Virginia 22151

FOREWORD

This work was administered in the Loads Division, LaRC, and several NASA personnel contributed to the direction and emphasis followed in the course of this study.

Several major contributions were made by TRW staff members, such as Mr. J. E. Wright, who performed several tasks in support of the experiments. The work was performed in the Advanced Technology Staff Group, Space Vehicles Division of TRW Systems Group,

CONTENTS

PULSED DIFFERENTIAL HOLOGRAPHIC MEASUREMENTS OF VIBRATION MODES OF HIGH-TEMPERATURE PANELS

D. A. Evensen
R. Aprahamian
K. R. Overoye

TRW Systems Group

SUMMARY

Holography is a lensless imaging technique which can be applied to measure static or dynamic displacements of structures. Conventional holography cannot be readily applied to measure vibration modes of high-temperature structures, due to difficulties caused by thermal convection currents. The present report discusses the use of "pulsed differential holography," which is a technique for recording structural motions in the presence of random fluctuations such as turbulence. An analysis of the differential method is presented, and demonstration experiments were conducted using heated stainless steel plates. Vibration modes were successfully recorded for the heated plates at temperatures of 1000, 1600, and 2000°F. The technique appears promising for such future measurements as vibrations of the Space Shuttle TPS panels or recording flutter of aeroelastic models in a wind-tunnel.

1.0 INTRODUCTION

Holography is a lensless imaging process which allows the reconstruction of three-dimensional images of diffuse objects (Refs. 1 and 2). Discussions of the physical principles and some applications of holography are available in recent textbooks (e.g., Refs. 3, 4, and 5). A related technique, known as holographic interferometry (Ref. 6) allows the experimenter to measure static or dynamic displacements of interest in many structural mechanics problems (Refs. 7, 8, 9, 10).

In partieular, "double-exposure" holographic interferometry provides a measure of the relative structural displacement (say $\vec{u}_2 - \vec{u}_1$) between two exposures of the hologram. For high-speed dynamic events, such as elastic wave propagation, double-exposure holography requires the use of pulsed lasers (see Refs. 11, 12, and 13). A related technique, called "differential" holographic interferometry has been applied to static problems (Ref. 14) and large-amplitude vibrations (Ref. 15).

For small amplitude vibrations (on the order of a few wavelengths of light) "time-average holography" (Ref. 16) has proven very successful for recording vibration modes. Vibration modes of beams, plates, shells, turbine blades, and many other practical structures have been recorded using time-average holography (see Refs. 10 and 17, for example). Conventional time-average holography uses continuous-wave lasers and involves relatively long exposure times. During the exposure of the photographic plate (hologram), the optical system must be relatively free of random motions (i.e., optical path length changes) or the hologram will not be properly recorded (see Ref. 18). This problem of maintaining adequate stability during the exposure is a major drawback of conventional time-average holography.

Since holography had proven very useful in recording structural vibrations of plates at room temperature (see Ref. 17), the question arose as to whether or not similar techniques would work for tests on high-temperature Space Shuttle panels at 1500° - 2500°F. The major problem (for holography) which temperature effects introduce, involves thermal convection currents. These convection currents cause changes in the index of refraction of the air around the vibrating panel and thereby cause random fluctuations in the optical path length. Thus, the problem becomes one of recording the structural motion in the presence of "noise" (i.e., random fluctuations in the optical path).

This problem has been solved using a vacuum chamber (which eliminates the convection currents) and continuous-wave, time-average holography (see Ref. 10). However, the vacuum chamber introduces several mechanical complications and does not appear practical for the Space Shuttle TPS panels of interest to NASA. A more promising approach, which was demonstrated during the present study, involves "pulsed differential

holography" (see Refs. 11 and 15). With this technique, a pulsed laser is used to expose the hologram at two closely-spaced times, t_1 and t_2 separated by a small time-delay, Δt. Between these two exposure times, the vibrating plate undergoes a displacement, but the (slowly-varying) thermal convection noise does not change appreciably. The resulting "differential hologram" records primarily the relative structural displacement $(\vec{u}_2 - \vec{u}_1)$ between exposures, and provides good definition of the vibration modes of the plate. This holographic method has been used herein to record very clean vibration modes of plates at temperatures of 1000, 1600, and 2000°F, in the presence of thermal convection currents.

The pulsed differential technique appears applicable to many other problems where the rate of change of the structural deformation (say $\dot{u}$) is sufficiently larger than the rate of change of the "noise" terms. For example, a differential approach might prove workable for recording structural motions (e.g., flutter) in a wind tunnel, despite the presence of turbulence in the aerodynamic boundary layers.

The work reported herein is divided into five main parts, as follows:

- o Holography and Holographic Interferometry
- o Pulsed Differential Holography Applied to Vibrating Objects
- o Tests at 1000°F
- o Tests at 2000°F
- o Concluding Remarks

The section on holography is intended to provide background and explain the fundamentals of the technique to engineers not already familiar with holography. Pulsed differential holography is then discussed and applied to harmonically vibrating objects, such as a high-temperature plate. Analytical results are presented for the important case of "small" time-delay, and the question of optimum timing the laser pulses (with respect to the plate vibration) is discussed. Results are presented which outline the sensitivity, capabilities, and limitations of the differential technique. A probability analysis is presented for the case of "random timing of the first pulse"; random timing was actually used in some of the high-temperature experiments.

Details of the vibration tests and problems involved are presented in the next two sections. The tests at 1000°F were conducted using an 8" x 10" stainless steel plate and optimum sychronization of the laser with the plate vibration. Interferograms showing mode shapes are presented for several modes and frequencies, at temperatures of

approximately 250, 515, 700, and 1040°F. Similar results are presented in the next section for tests at 1600°F and 2025°F.

The final section on Concluding Remarks summarizes the main results obtained from this study.

Regarding future experiments involving differential holography, it appears that this technique may be applicable to holographic measurements of flutter in a wind tunnel. The major problems of making such measurements in a wind tunnel environment involve high vibration levels and the problem of turbulence in the aerodynamic boundary layer(s). By using pulsed differential holography, the structural deformation (between exposures) would be recorded, and (hopefully) the wind tunnel turbulence would not change appreciably and distort the interferogram. Preliminary calculations involving various boundary layer thicknesses and wind tunnel Mach numbers appear encouraging. The measurement of panel flutter by pulsed differential techniques has been suggested, and the approach might work equally well for larger structures, such as wings and small-scale aeroelastic models of aircraft.

A related problem (which may be amenable to a similar solution) involves the response of skin panels to the turbulent pressure fluctuations in the boundary layer on large flight vehicles. Tests are frequently conducted in large wind tunnels to simulate the response of the vehicle panels. The response can be viewed as the superposition of many structural modes responding simultaneously. Conventional instrumentation for such tests involves fixed transducers which give the (local) panel displacement as a function of time. By employing pulsed differential holography in such tests, one can record the structural velocity, $\dot{w}$, at time t_1. The differential hologram gives a measure of the instantaneous surface velocity $\frac{\partial w}{\partial t}$ (over the surface of the panel, x,y) at a particular time, t_1. Such spatial measurements may be correlated with the point transducers used conventionally and provide complementary information not currently available.

2.0 HOLOGRAPHY AND HOLOGRAPHIC INTERFEROMETRY

Introduction and Background

The term "holography" is used to describe a means of recording the amplitudes and phases of waves, such as light waves or sound waves. Holography originated with Gabor (Ref. 1) who pointed out the possibility of recording (on a piece of photographic film) the amplitudes and phases of coherent, monochromatic light waves transmitted through a transparent object. By then projecting light through the photographic film (which is called a "hologram") it is possible to reproduce a three-dimensional image of the original object.

The reproduction of images as Gabor suggested became practical with the advent of the laser as a source of monochromatic, coherent light. In 1964, Leith and Upatnieks (Ref. 2) demonstrated that a three-dimensional image of an opaque object could be reconstructed in a manner similar to that proposed by Gabor. Figure 1 shows a typical set-up of the apparatus used in the Leith and Upatnieks holographic method.

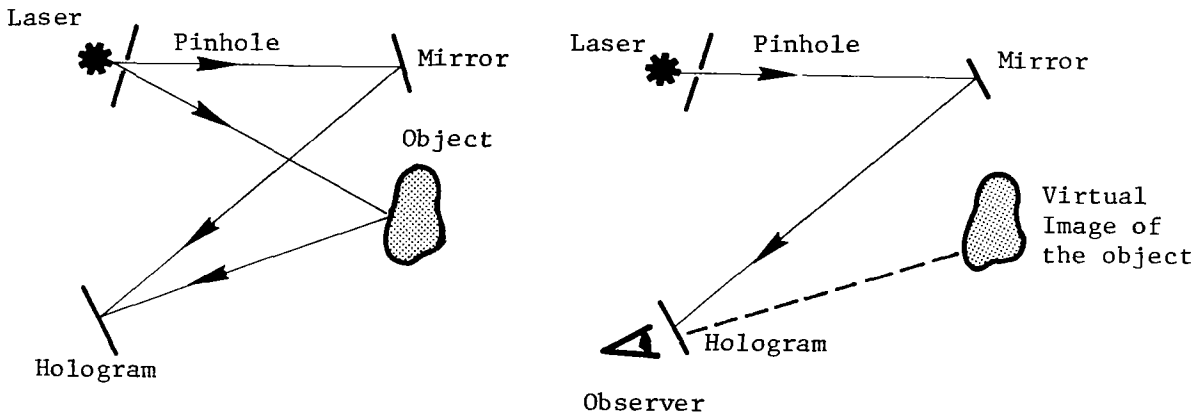

Figure 1 - Left: Image Recording Process

Right: Image Retrieval

In making the hologram, the light waves from the object (object beam) interact with the light from the mirror (reference beam). When the light from the mirror is in phase with the light from the object, the waves add; conversely, the waves cancel one another when they are out of phase. This type of interaction results in variations in the intensity of the light striking the photographic film (these are spatial variations in intensity, in the plane of the hologram). Since photographic film reacts to the intensity of light impinging on it, the exposed film gives a permanent record of the interaction of the two light beams.

To reconstruct the image of the object from the hologram, the developed photographic film is illuminated with any monochromatic light source, e.g., the original laser. Now the light interacts with the hologram, and the result is a three-dimensional image of the original object. The reconstruction of images in this fashion can be described mathematically, and derivations are available in many textbooks (Ref. 3, 4, 5).

Double-Exposure Holographic Interferometry

Although image reconstruction was one of the first applications of holography, a technique that has shown more potential from a research standpoint is "double-exposure holography," which is one form of holographic interferometry (Ref. 6). The essential ideas are as follows: first make a hologram of the object you wish to examine; then subject the object to loads which cause it to deform, and expose the same hologram for a second time. Now when this "double-exposed hologram" is developed and then illuminated, two images are produced: one is from the undeformed body, the other from the deformed body. These light waves (which form the two images) interact with one another, thereby creating interference fringe patterns. (See Figure 2, for example.) By analyzing the fringe patterns, one can determine the surface deformations of the body, which were caused by the applied load.

Several papers have been written showing how the interference fringe patterns can be related to the deformation of the object: see, for example, Ref. 7, 8. 9, and 10.

As just presented, "double-exposure holographic interferometry" can be used to record the relative deformation of a structure as it passes from one state ("undeformed", say) to another (the "deformed" state). It should be evident that the two states of deformation correspond to the first exposure and the second exposure of the hologram, respectively.

Initial work with double-exposure holograms involved measurement of deflections from an unstressed state (the initial displacement, $\vec{u}_1$ was zero) to a nearby stressed state of static equilibrium ($\vec{u}_2 \neq 0$).

Thus, the relative deformation measured between exposures was

$$\vec{u}_2 - \vec{u}_1 = \vec{u}_2 - 0 = \vec{u} \qquad (2\text{-}1)$$

where the displacement vector $\vec{u}$ was a function of position $(\vec{x})$ on the object, but did not vary with time, t. (See for example, Ref. 9 and 10.)

This work was soon extended to dynamic problems, however, in which the first exposure recorded the unstressed state $(\vec{u}_1 = 0)$ and the second exposure recorded the deformed state, $\vec{u}_2(x, t_i)$ where t_i denotes the particular instant in time when the second exposure was made. Typical examples of this type involve elastic wave propagation in structures; see References 11, 12, 13, and Figure 2. The significant difference between the static and dynamic events (from a holographic standpoint) is that static displacements can be recorded with continuous-wave lasers, but high-speed dynamic events require the use of pulsed lasers. (The main advantages and disadvantages of cw and pulsed laser holography are presented in a subsequent section.)

Another extension of double-exposure holography involves two states of deformation, with corresponding displacements $\vec{u}_1$ and $\vec{u}_2$. For example, the displacement $\vec{u}$ in static problems depends upon the applied load, P. When the load has a value P_1, displacement $\vec{u}_1$ results, and the first exposure of the hologram is made. The load is then changed to a value P_2, (the corresponding displacement state is denoted by $\vec{u}_2$) and a second exposure is made. The interference fringes which form (when the hologram is reconstructed) are related to the relative displacement $(\vec{u}_2 - \vec{u}_1)$ between exposures.

This type of (static) double-exposure holography was demonstrated in Ref. 14 for static loading and buckling of cylindrical shells. Similar results have been obtained for time-dependent displacements: see Ref. 11 and 15, for example. Imagine that we wish to study deformations $\vec{u}(\vec{x}, t)$ that depend upon position $(\vec{x})$ and time, t. With a pulsed ruby laser, we can expose the hologram twice, at times t_1 and t_2. Then the interference fringes give a measure of relative displacement,

$$\vec{\delta} = \vec{u}(\vec{x}, t_2) - \vec{u}(\vec{x}, t_1) \qquad (2\text{-}2)$$

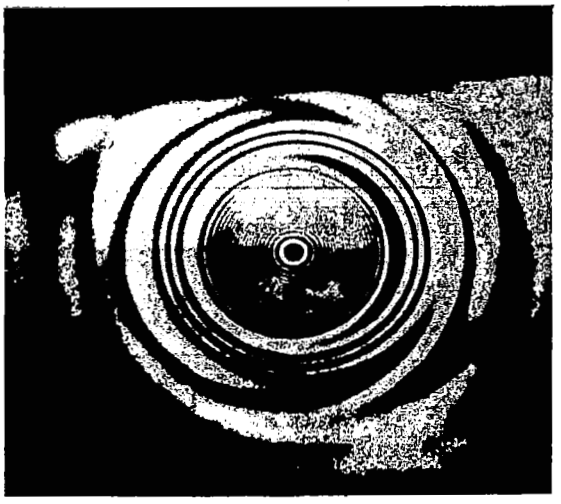

(a) Δ = 80 μsec

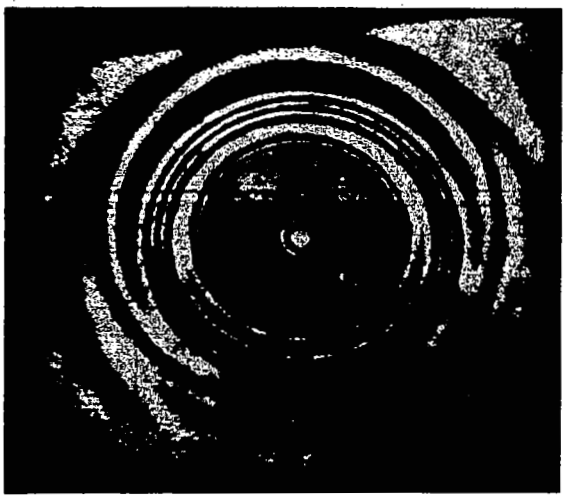

(b) Δ = 100 μsec

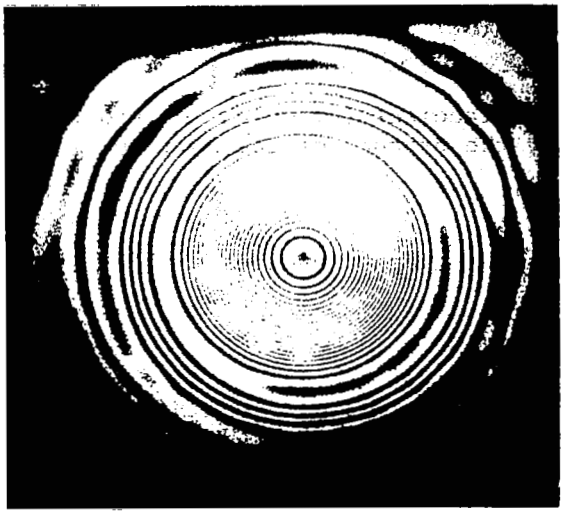

(c) Δ = 130 μsec

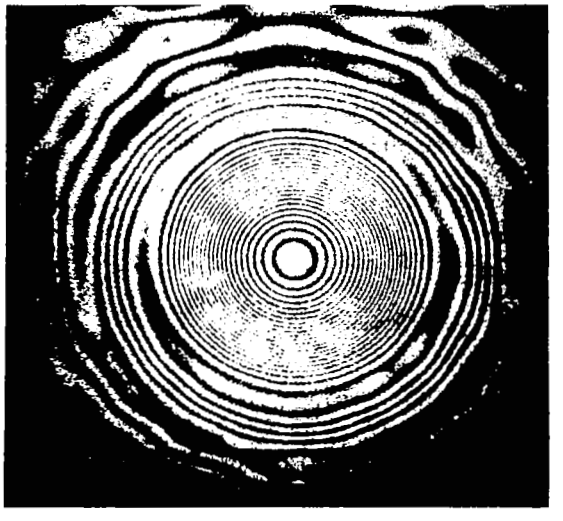

(d) Δ = 150 μsec

Figure 2 - Double-Exposure Holograms Showing Transverse Wave Propagation in a Plate (From Ref. 12)

Now suppose that time t_2 is very near t_1; that is,

$$t_2 = t_1 + \Delta t \tag{2-3}$$

where Δt (for problems of interest herein) is on the order of 50 microseconds. Assuming the displacement field $\vec{u}(\vec{x}, t)$ is a continuous function of time, we can expand $\vec{u}(\vec{x}, t_2)$ in a Taylor series about $t = t_1$. Equation (2-2) then becomes

$$\vec{\delta} = \vec{u}(\vec{x}, t_1) + \frac{\partial \vec{u}}{\partial t}\bigg|_{t_1} \Delta t + \frac{1}{2}\frac{\partial^2 \vec{u}}{\partial t^2}\bigg|_{t_1} (\Delta t)^2 + \ldots$$

$$- \vec{u}(\vec{x}, t_1) \tag{2-4}$$

which simplifies to

$$\vec{\delta} = \frac{\partial \vec{u}}{\partial t}(\vec{x}, t_1)\, \Delta t + O(\Delta t)^2 \tag{2-5}$$

Equation (2-5) simply states that the displacement $(\vec{\delta})$ which is recorded holographically, is well-approximated by the product of the surface velocity $\frac{\partial \vec{u}}{\partial t}$ and the time interval, Δt.

Since this type of double-exposure holography involves small differences,

$$\Delta \vec{u} = \vec{u}_2 - \vec{u}_1$$

and

$$\Delta t = t_2 - t_1$$

it has been termed "differential holographic interferometry". A separate section of this report is devoted to vibration analysis using this differential technique; but first some understanding of continuous-wave and pulsed laser holography is required, as outlined in the following paragraphs.

Continuous-Wave vs. Pulsed-Laser Holography

Continuous-wave lasers operate continuously, as their name implies. Typically the power output of cw lasers (used for holography) is on the order of 15 to 50 milliwatts. These power levels are such that relatively "long" exposure times are required to make holograms with cw lasers. For example, typical exposure times for cw holography range from 5 seconds to several minutes. (The exposure time required is a function of the sensitivity of the photographic emulsion and the intensity of the light reaching the hologram.)

For ordinary, single-exposure holography, it is common practice to require that the resultant of all changes in optical path length (due to noise, seismic disturbances, etc.) be less than 1/10th of a wavelength during the exposure time. For long exposure times, (such as those used in continuous-wave holography) this criterion of $\lambda/10$ places stringent mechanical stability requirements on the entire optical arrangement as well as on the object being recorded. These stability requirements are commonly satisfied by (i) using large, massive seismic tables that are vibration-isolated, (ii) turning off the air-conditioning (to reduce spurious air currents in the room), and (iii) using various other techniques to reduce noise, unwanted vibration, etc. These severe, long-term stability requirements, which apply to continuous-wave holography, have restricted its use and by-and-large limited it to the laboratory environment. On the other hand, pulsed laser holography usually involves exposure times which are very short: 50 nanoseconds is typical for a pulsed ruby laser. Such pulsed lasers emit very high-intensity light, which is sufficient to form a hologram on the photographic plate, despite the short exposure time. The basic stability requirement - i.e., that all path length changes must be less than $\lambda/10$, during the exposure - still is valid. However, since the exposure time is so short (50×10^{-9} sec), and most random mechanical disturbances are sufficiently "low-frequency", it becomes possible to make pulsed laser holograms on ordinary wooden tables, in noisy machine-shop environments, etc. (A discussion of the limits on the noise, what amplitude and frequency can be tolerated, etc. is given in Section 3.0.)

Now consider our problem of measuring the vibration modes of a high-temperature plate, using holographic interferometry (see Figure 3). The main problem to be overcome in such an experiment involves the thermal convection currents. Thermal convection causes changes in the index of refraction and results in random fluctuations in the optical path length. If the plate were at room temperature, it would be possible to record the vibration modes using "time-average" holography with a continuous-wave laser (see Ref. 16 and 17, for example). (An example of a time-average hologram of a vibrating plate is shown in Figure 4.)

In "time-average" holography, the intensity of the reconstructed image (from the developed hologram) is related to the square of time integral

$$I_r \sim E^2$$

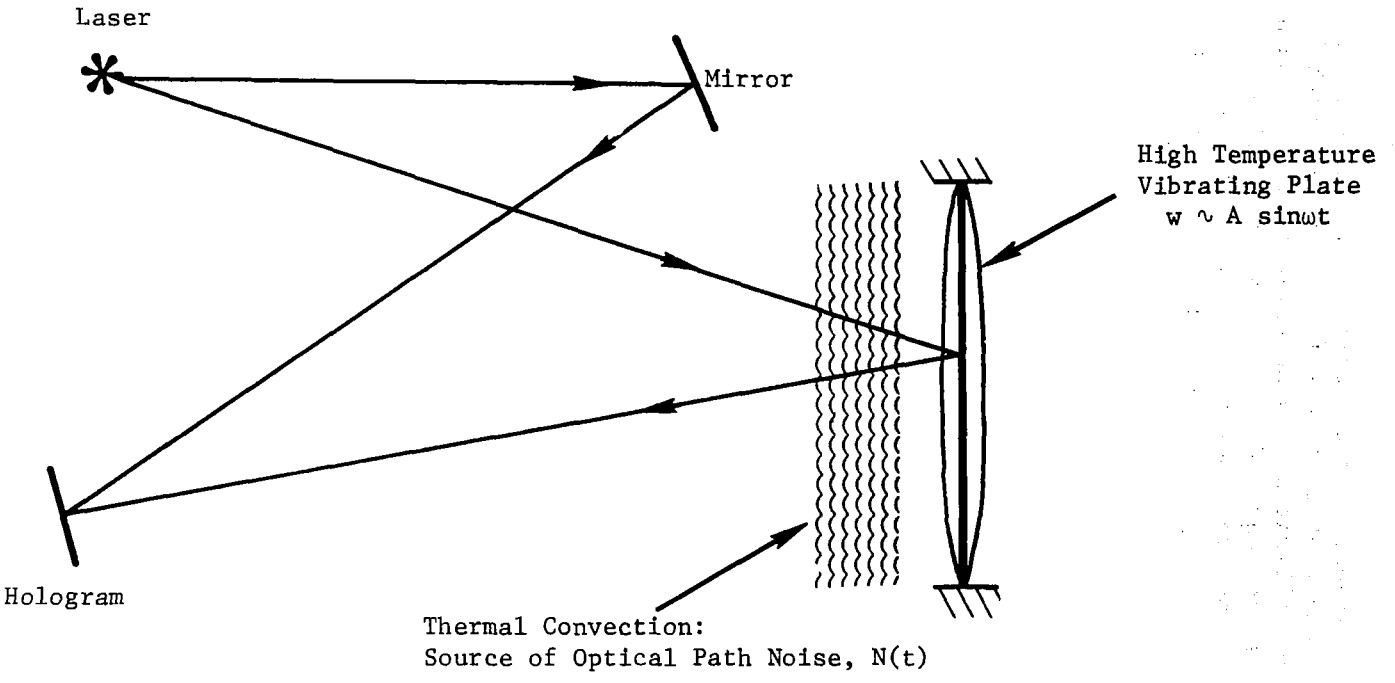

Figure 3: Holographic Arrangement for Recording Vibration Modes of High-Temperature Plates.

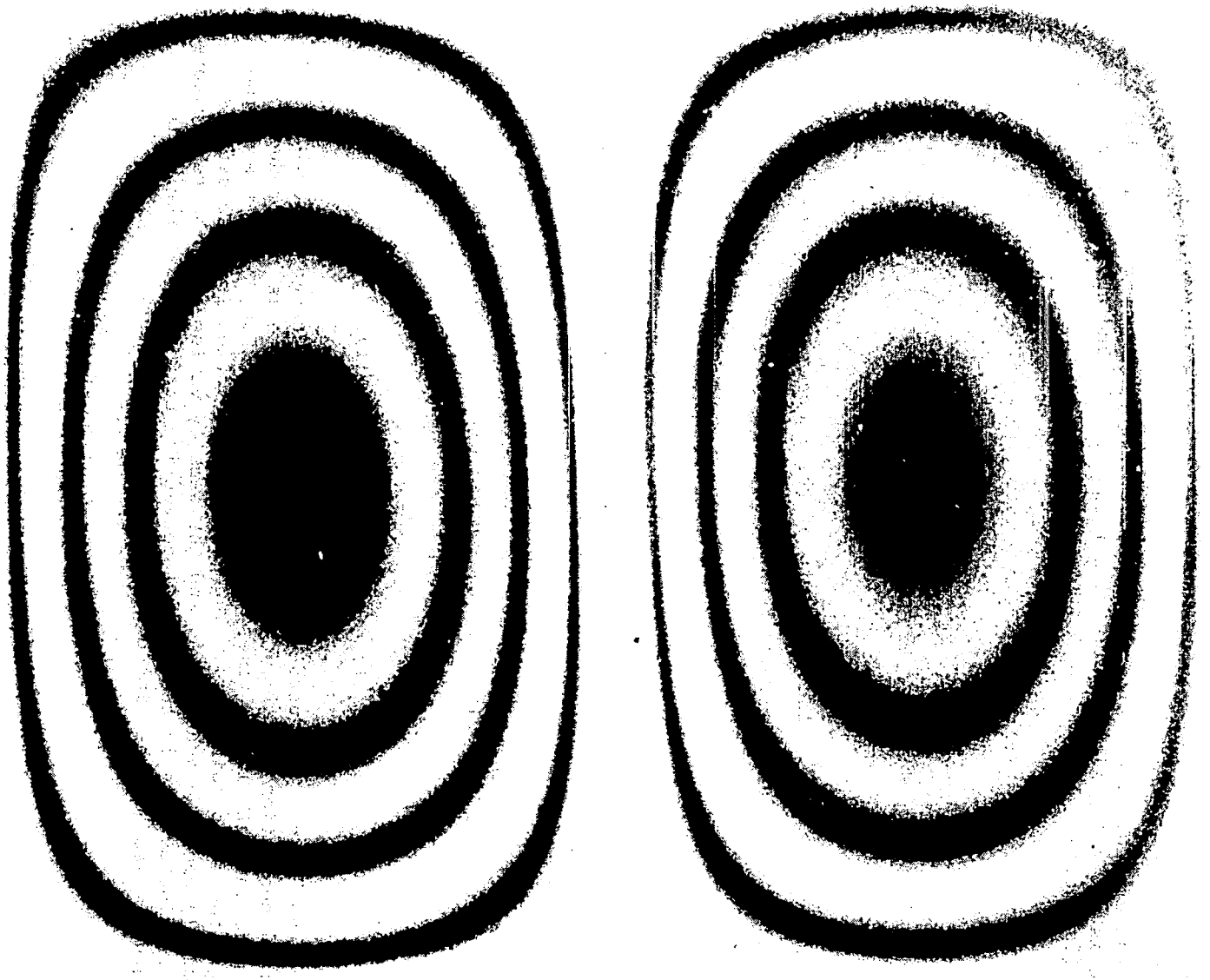

Figure 4 - Time-Average Hologram of the 1 x 2 Mode of a Vibration Rectangular Plate (f = 357 cps, Ref. 17)

where

$$E \sim \int_0^T e^{i\phi(t)}\, dt$$

T is the exposure time, and $\phi(t)$ is the time-varying phase. If the plate is vibrating sinusoidally with frequency Ω and amplitude m, then (for normal illumination and viewing)

$$\phi(t) = \frac{2\pi}{\lambda} (m \sin \Omega t)$$

$$E \sim \int_0^T e^{i \frac{2\pi}{\lambda} m \sin \Omega t}\, dt \sim J_o \left(\frac{2\pi}{\lambda} m\right)$$

(providing $T > \frac{2\pi}{\Omega}$). The intensity of the reconstructed image, I_r, is proportional to the zero-order Bessel function, squared:

$$I_r \sim J_o^2 \left(\frac{2\pi}{\lambda} m\right)$$

Thus, the zeroes of the Bessel function correspond to locations where the intensity I_r is zero, which are the black interference fringes (see Figure 4).

Now imagine that we try to use time-average holography when the plate is heated. In this case, the phase $\phi(t)$, contains a "noise" term, N(t):

$$\phi(t) = \frac{2\pi}{\lambda} \left[m \sin \Omega t + N(t)\right]$$

where the "noise" is caused by optical path length changes through the thermal convection currents. The optical path length is the product of the physical path length times the index of refraction, η, of the medium (e.g., the surrounding air). The index of refraction in gases depends primarily upon the density, ρ, and the density varies with the temperature. Thus, fluctuations in the thermal convection currents near the plate eventually lead to the time-dependent noise term, N(t).

In this case, the time-integration gives

$$E \sim \int_0^T e^{i \frac{2\pi}{\lambda} m \sin \Omega t} \; e^{i \frac{2\pi}{\lambda} N(t)} \, dt$$

Clearly, if we limit the noise amplitude, such that

$$\frac{2\pi |N|}{\lambda} << 1$$

or

$$|N| << \frac{\lambda}{2\pi}$$

then the term $e^{i \frac{2\pi}{\lambda} N(t)}$ is approximately unity and we regain (approximately) the standard, room-temperature result,

$$E \sim J_o \left(\frac{2\pi}{\lambda} m \right)$$

$$I_r \sim J_o^2 \left(\frac{2\pi}{\lambda} m \right)$$

which was presented previously.

Similarly, it appears that when $N(t)$ is sufficiently large (and also sufficiently random) the factor $e^{i \frac{2\pi}{\lambda} N(t)}$ can take any value (on the unit circle in the complex plane) in a random fashion and cause the time integral for E to vanish. (For a further discussion of this point, see Refs. 18 and 19 .) The important noise factor N(t) from the convection currents is a function of the temperature (call it Θ), and the time, t. From texts on fluid mechanics (e.g., Ref. 20) it is expected that the free convection boundary layer (on a heated, vertical plate) will be laminar (i.e., steady) at low temperatures and eventually become turbulent (random) as the temperature increases. When the flow is steady (i.e., not time-dependent) then the noise N(t) is zero and continuous-wave holography remains feasible. As the temperature increases, the turbulent eddies in the flow increase the random path length changes and eventually prevent the formation of continuous-wave holograms.

This qualitative description is in agreement with experiments involving cw holography of heated objects. For example, Reference 21 showed that good-quality continuous-wave holograms of vibrating turbine blades can be made in air at temperatures up to 300°C (572°F). Higher temperatures can be achieved by using a helium atmosphere (e.g., Ref. 22) which has a smaller change in index of refraction with temperature. Experiments have shown that good quality cw holograms can be made at temperatures from 800 - 1000°F in a helium atmosphere. Above these temperatures, the desired interference fringes (due to either static or vibratory displacements) eventually become weak (low-contrast) and gradually disappear.

Another approach, which was also demonstrated at TRW (Ref. 10), is to remove the thermal convection currents by using a vacuum enclosure. Double-exposure, cw holograms of a heated turbine blade (1400°F) are reported in Ref. 10. A similar approach was originally intended for use in the present study of heated, vibrating plates. However, this method involves significant heat loads on the vacuum chamber, which can cause problems with the windows, thermal creep, etc. The criteria of mechanical stability (random displacements less than $\lambda/10$) during exposure still applies, but it is complicated by the vacuum chamber and the heat input. In addition, since the intent of this study was to develop practical, workable means of measuring plate vibration modes at high temperatures, it became apparent that we should concentrate our efforts on "pulsed differential holography" (and thus avoid many mechanical complications, such as the vacuum chamber).

The use of "differential holography" as a means of eliminating the noise from convection currents is discussed in the following paragraphs.

Pulsed Differential Holographic Interferometry

The basic ideas involved in "differential holographic interferometry" have already been introduced in the discussion of double-exposure holography (see Equation 2-2). The present section will discuss the application of pulsed differential holography to eliminate the effects of the thermal convection currents.

When the plate is vibrating sinusoidally and significant thermal convection is present, the (time-varying) change in optical path length (e.g., from the laser, to the vibrating plate, and then to the hologram) is given by

$$\phi(t) = \frac{2\pi}{\lambda} \left[m \sin \Omega t + N(t) \right] \qquad (2\text{-}6)$$

where the amplitude, m, is a function of the co-ordinates (x, y) in the plane of the vibrating plate and the thermal convection noise, N(t), varies with space (x, y) as well as the time, t.

Now we use the pulsed laser to expose the hologram* at times t_1 and t_2. The resulting interferogram records the difference in phase, $\phi(t_2) - \phi(t_1)$. And, as before, if $t_2 = t_1 + \Delta t$, we have (by a Taylor's Series expansion)

$$\phi(t_2) - \phi(t_1) = \phi(t_1) + \left.\frac{d\phi}{dt}\right|_{t_1} \Delta t + \ldots - \phi(t_1)$$

$$= \dot{\phi}\ \Delta t + 0(\Delta t)^2 \qquad (2\text{-}7)$$

where $\dot{\phi}$ is the time rate of change of the phase, evaluated at $t = t_1$. Substituting Equation (2-6) into (2-7) we have

$$\phi(t_2) - \phi(t_1) \cong \frac{2\pi}{\lambda}\left[\, m\ \Omega\ \cos(\Omega t_1) \ + \ \dot{N}(t_1) \,\right]\ (\Delta t) \qquad (2\text{-}8)$$

In order to record the mode shape of the vibrating panel, we require that

$$m\ \Omega\ \ \cos\ \Omega\ t_1 \gg \dot{N}(t_1) \qquad (2\text{-}9)$$

which says that our <u>signal</u> (in this case, the velocity of the plate, at time t_1) be much greater than the "noise" (which in this case is $\dot{N}$, evaluated at time t_1). An alternate criterion to limit $\dot{N}(t)$ might be

$$\dot{N}\ \Delta t \ll \frac{\lambda}{2} \qquad (2\text{-}10)$$

which means that between the exposures at t_1 and t_2 the change in optical path length (due to the noise alone) will not be sufficient to cause a fringe on the interferogram. (The first interference fringe forms when the phase change $\phi(t_2) - \phi(t_1) = \frac{2\pi}{\lambda}\left(\frac{\lambda}{2}\right) \cong \pi$.)

In the case of noise due to thermal convection, the fluid mechanics and turbulence is such that relatively low-frequencies and amplitudes contribute to the noise. Thus, by an appropriate choice of Δt, we can largely eliminate the effects of thermal convection. In simplified form, the vibrating plate displaces an amount $(m\ \Omega \cos\ \Omega\ t_1)\Delta t$ between exposures

*The pulsed laser exposes the hologram in approximately 50×10^{-9} sec., and as such acts much like a Dirac delta function applied at times t_1 and t_2.

of the hologram, but the thermal convection currents simply do not change between exposures (since the convection is really "slowly-varying" in time).

The reader should recognize that the turbulence (which leads to the noise N) depends upon temperature. Thus, as the temperature increases, so does the noise and it might become necessary to adjust the time-delay Δt in order to satisfy the inequality (2-10). Our experiments were conducted using $\Delta t = 50$ μsec between pulses, and mode shapes were recorded successfully (with little or no noise) up to 2000°F. However, it appears that for each time delay Δt there is a maximum temperature Θ_{max} above which the noise effects become significant, i.e., when $\dot{N}\Delta t$ is not small in comparison to $\lambda/2$. At these extreme temperatures, the hologram becomes "corrupted" or distorted by the presence of the noise and does not faithfully record the deflection shape.

Interpretation of the Fringe Patterns: Displacements and Mode Shapes

The reconstructed image from a holographic interferogram possesses dark bands or lines, called interference fringes. (Examples of such fringes are given in Figures 2 and 4.) A major feature of holographic interferometry is that it allows us to measure the displacements of a vibrating structure, by relating the displacements to the dark interference fringes.

Several papers have been published which deal with the relations between a displacement field and the corresponding holographic interferogram. (For a general discussion of the problem, see References 7, 8, and 9.) A step-by-step, detailed derivation of the governing equations is given in Appendix A of Reference 17, which deals with time-average, real-time, and double-exposure holography.

We are concerned herein with the results for double-exposure holography, and the equations can be expressed conveniently in vector form, as shown in Ref. 9. In particular, Ref. 9 shows that the reconstructed image of a hologram exposed twice to an object which has deformed between exposures will exhibit dark fringes on parts of the object wherever the condition

$$\vec{\delta} \cdot (\vec{n}_i + \vec{n}_v) = \frac{(2n \pm 1)\lambda}{2} \qquad (2\text{-}11)$$

is satisfied; where

$\vec{\delta}$ = the displacement vector

λ = wavelength of the light from the laser used to make and reconstruct the holographic images

$\vec{n}_i$ = unit vector in the direction from the object to the illuminating source

$\vec{n}_v$ = unit vector in the direction of view, from the object through the hologram to the observer

n = integer, the fringe order, ± 1, ± 2, ± 3, etc.

The term $\vec{\delta} \cdot (\vec{n}_i + \vec{n}_v)$ is illustrated by the vector diagram shown in Figure 5. The term $(\vec{n}_i + \vec{n}_v)$ is a vector sum, and it is represented by a vector which lies in the plane containing $\vec{n}_i$ and $\vec{n}_v$ and bisects the angle between them. The magnitude of this vector sum is $2 \cos \frac{1}{2}(\vec{n}_i, \vec{n}_v)$ where $(\vec{n}_i, \vec{n}_v)$ is the angle which is bisected. Finally, the dot product $\vec{\delta} \cdot (\vec{n}_i + \vec{n}_v)$ is the projection of the displacement vector $\vec{\delta}$ in the direction of $(\vec{n}_i + \vec{n}_v)$, as shown in Figure 5.

A particular case of Equation (2-11) which occurs frequently in practice is illustrated in Figure 6. Referring to Figure 6, the structure of interest (the heated plate, for example) lies in the x-y plane. Ignoring variations in the y-direction, we have for the illumination and viewing vectors

$$\left.\begin{aligned} \vec{n}_i &= (\sin \theta_i)\,\vec{i} + (\cos \theta_i)\vec{k} \\ \text{and} \qquad \vec{n}_v &= -(\sin \theta_v)\,\vec{i} + (\cos \theta_v)\vec{k} \end{aligned}\right\} \tag{2-12}$$

where $\vec{i}$ and $\vec{k}$ are unit vectors in the x and z directions, and the angles θ_i and θ_v are shown in Figure 6. Now denote the displacement vector, $\vec{\delta}$, by its x, y, and z components:

$$\vec{\delta} = u\,\vec{i} + v\,\vec{j} + w\,\vec{k} \tag{2-13}$$

Forming the dot-product in Equation (2-11) we have

$$u(\sin \theta_i - \sin \theta_v) + w(\cos \theta_i + \cos \theta_v) = \frac{(2n \pm 1)\lambda}{2} \tag{2-14}$$

For transverse vibrations (of plates, beams, shells, etc.) it is usual that the deflection, w, is much greater than the in-plane displacement, u. In addition, many experiments are purposely designed such that the angles θ_i and θ_v are very small (i.e., less than 5°). Under these

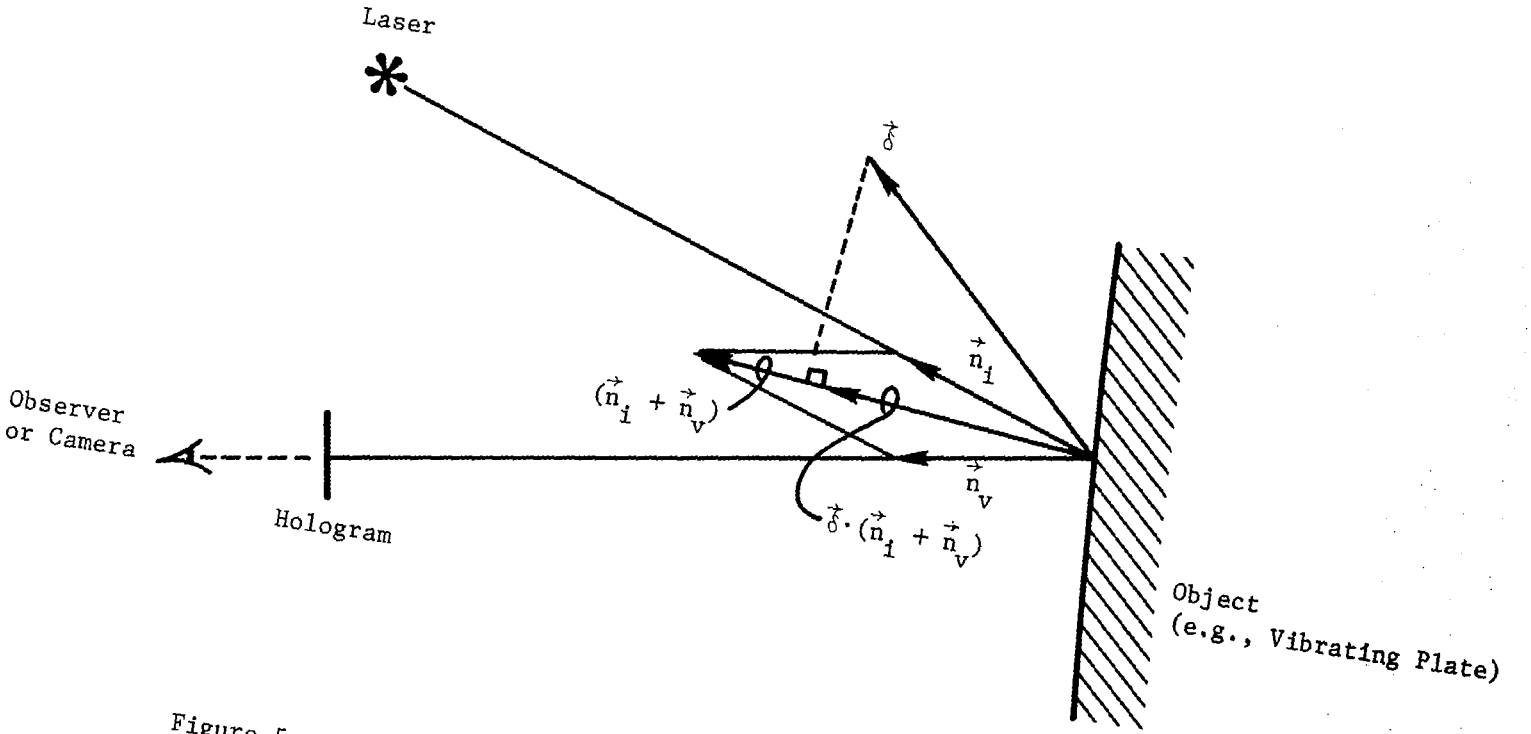

Figure 5: Vector Diagram Showing the Illuminating and Viewing Directions, with the Displacement $\vec{\delta}$ between Exposures.

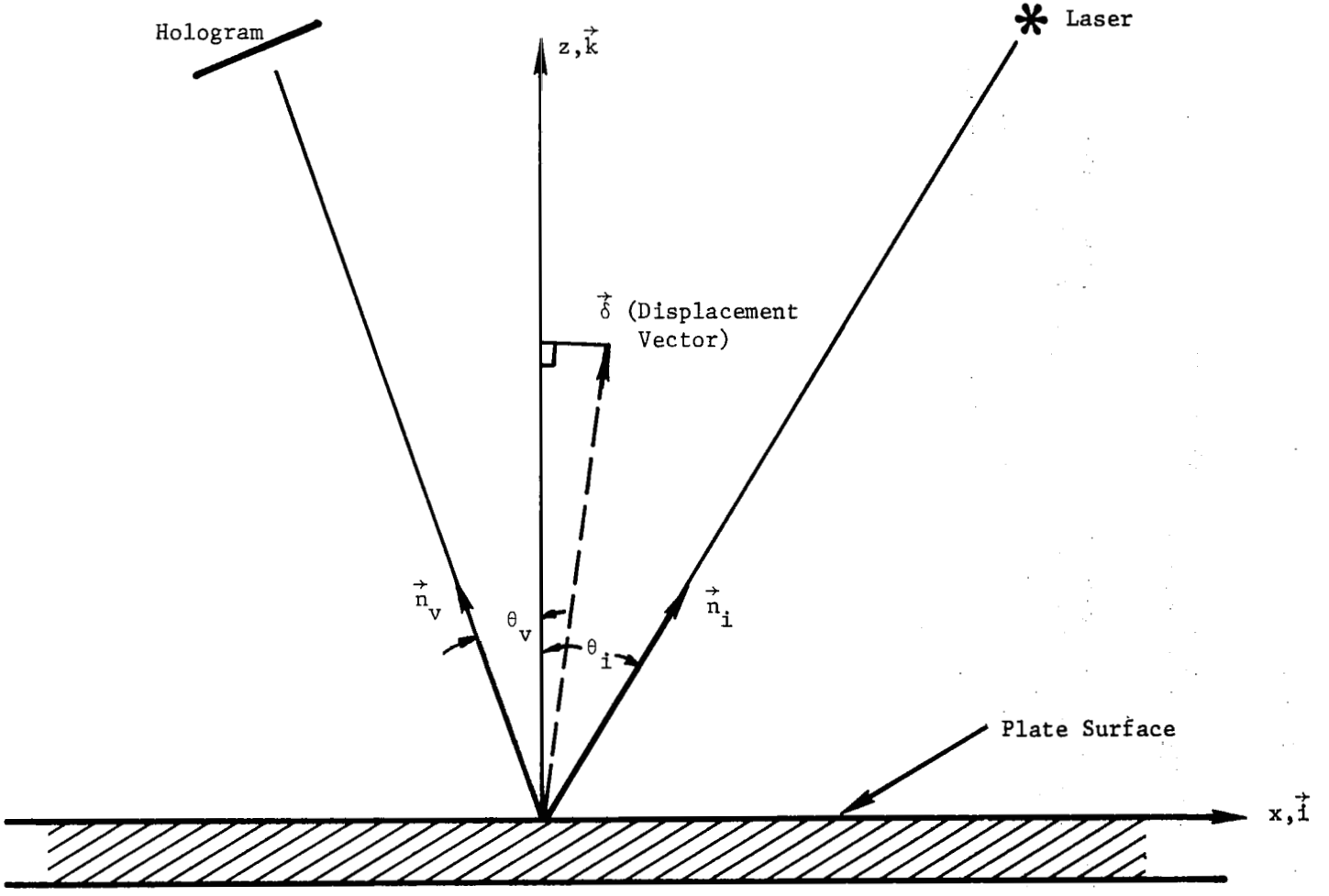

Figure 6: Diagram Illustrating the Illumination and Viewing Angles θ_i and θ_v.

conditions, Equation (2-14) is well-approximated by

$$w = \frac{(2n \pm 1)\lambda}{2(\cos \theta_i + \cos \theta_v)} \approx \frac{(2n \pm 1)\lambda}{4} \qquad (2\text{-}15)$$

Equation (2-15) relates the transverse deflection w (between two exposures of the hologram) to the interference fringe pattern of the reconstructed image. Thus, a black interference fringe for which the fringe order $n = +1$ corresponds to a deflection (at the fringe location) of $w = \frac{\lambda}{4}$ between exposures. Similarly, the $n = 2$ dark fringe corresponds to a deflection $w = \frac{3\lambda}{4}$. Thus, the interference fringes can be regarded as "contour lines" (as in the case of terrain maps of topology) of equal amplitudes of displacement. These contour lines (on which the fringe order is constant) vary over the surface of the plate, (x, y), and give a readily-interpreted overall view of the plate deflection. For example, the idea of axi-symmetric waves propagating radially outward is clearly apparent from Figure 2, and the vibration of a rectangular plate in the 1 by 2 mode is clear from Figure 4.

To obtain quanitatitive data for the deflection, w, as a function of space (x, y), it is necessary to employ the holographic equation (e.g., 2-15) and to locate the fringe on the surface of the plate. For example, by placing a ruler parallel to the edge of the plate on the photograph (such as Figure 4) we can locate the x-coordinate of the fringes for any given y value. Then, using Equation (2-15) we can determine the deflection, w, at these x-locations. The results give discrete data points, which show the deflection w at particular locations (x_i, y_i). As an example, for resonant vibrations of a simply-supported rectangular plate, the vibration mode shape is given by (Ref. 23)

$$w = \Phi_{mn}(x, y) = \sin \frac{m\pi x}{a} \sin \frac{n\pi y}{b} \qquad (2\text{-}16)$$

where a, b are the lengths of the sides of the plate, which coincide with the x and y axes. Normally, one determines the deflection w along lines where $\frac{m\pi y}{b} = \pi/2$ is a constant, and thus obtains the x-dependence (or vice-versa). A plot of a typical vibration mode obtained in this fashion is shown in Figure 7.* Similar results, obtained at

* The reader should note that Figure 7 was obtained from a time-average hologram, for which the fringe interpretation is different than Equation (2-15). See Ref. 16 for a discussion of time-average holography.

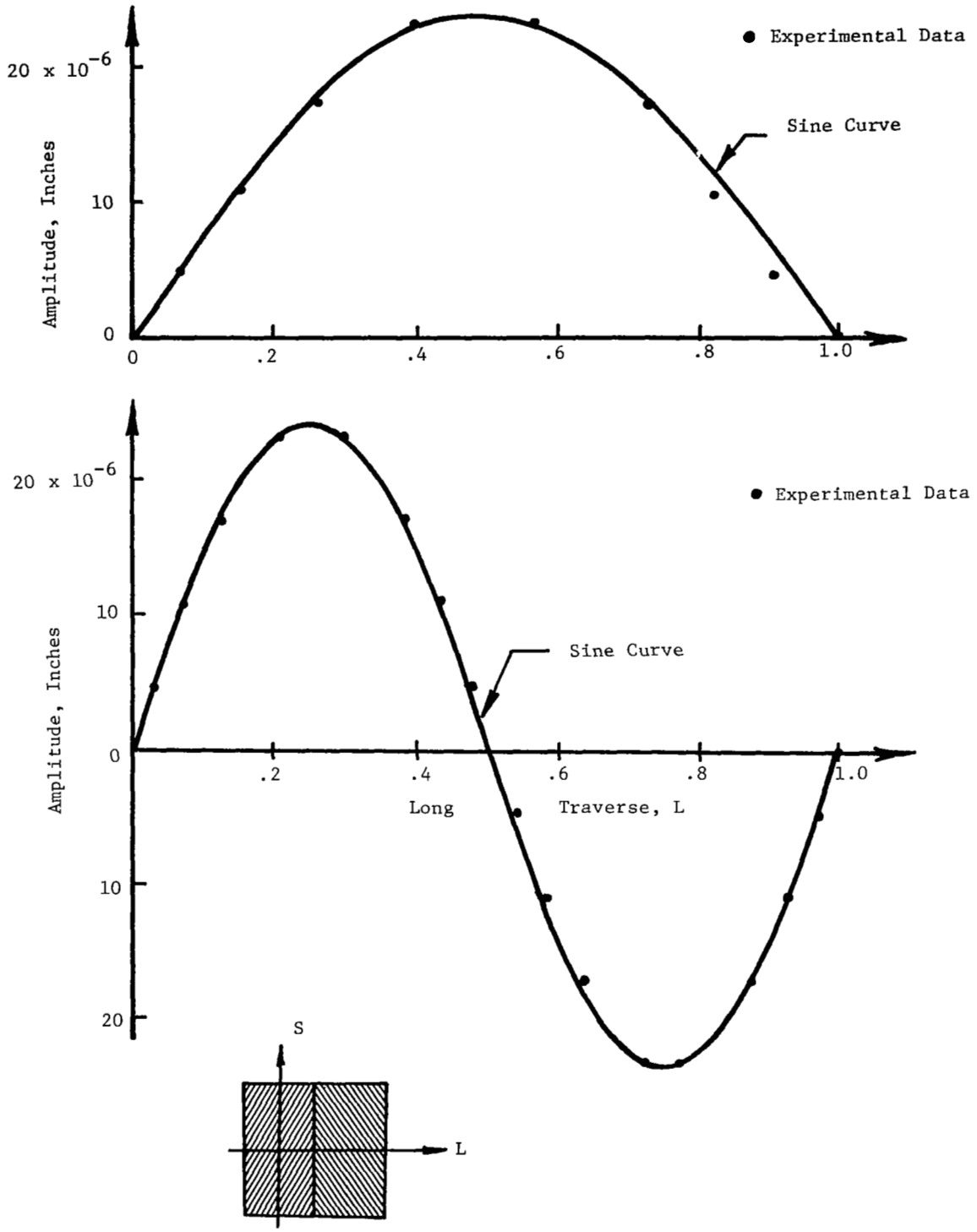

Figure 7 - Mode Shape of the 1x2 Mode Shown in Figure 2. (Ref. 17)

high temperatures through the use of pulsed differential holography, are presented herein (see Sections 4.0 and 5.0). With this information as background, let us now consider the special case of pulsed differential holography applied to sinusoidally vibrating objects.

3.0 PULSED DIFFERENTIAL HOLOGRAPHY APPLIED TO VIBRATING OBJECTS

Introduction

The basic ideas of pulsed differential holography have been described in Section 2.0. The present section discusses some of the practical aspects of the problem when the structure is vibrating sinusoidally in a normal mode. Approximate results for small time delay are given herein, as well as the general case of arbitrary Δt. The "sensitivity" of the pulsed differential technique is discussed, i.e., its ability to detect a particular vibration amplitude at a given frequency, assuming the time delay, Δt, is fixed. The influence of "noise" (due to random mechanical or optical disturbances) is also considered.

Harmonic Vibrations in a Single Mode

Consider the resonant, transverse vibrations of a flat plate; the lateral deflection, w, is given by

$$w(x, y, t) = A_o \Phi_{mn}(x,y) \sin \omega_{mn} t \qquad (3\text{-}1)$$

where A_o is the (maximum) vibration amplitude

$\Phi_{mn}(x, y)$ describes the shape of the m-nth vibration mode, and

$\omega_{mn} = 2\pi f_{mn}$ is the vibration frequency

For example, if the plate is rectangular, isotropic, and simply-supported, we have the familar results (Ref. 23)

mode: $$\Phi_{mn}(x, y) = \sin \frac{m\pi x}{a} \sin \frac{m\pi y}{b}$$

frequency: $$\omega_{mn} = \left(\frac{D}{\rho h}\right)^{1/2} \left[\left(\frac{m\pi}{a}\right)^2 + \left(\frac{n\pi}{b}\right)^2\right]$$

For discussion purposes, it is simpler to focus our attention on a particular point on the plate (point P, with co-ordinates x_p, y_p). Then Equation (3-1) can be written as

$$w(x_p, y_p, t) = A \sin \omega t \qquad (3\text{-}2)$$

where

$A = A_o \Phi_{mn}(x_p, y_p)$ is the local amplitude of vibration,

and $\omega = 2\pi f$ is the vibration frequency.

Now recall that our pulsed differential hologram records the relative displacement between two exposures, made at times t_1 and $t_2 = (t_1 + \Delta t)$, respectively. Equation (2-15) can thus be combined with Equation (3-2) above to yield the relative displacement

$$w_2 - w_1 = A \sin \omega(t_1 + \Delta t) - A \sin \omega t_1$$

$$= \frac{(2n + 1)\lambda}{4} \qquad (3\text{-}3)$$

Equation (3-3), describing sinusoidal motion that is instantaneously recorded at times t_1 and t_2 (by the light pulses from the laser) is illustrated schematically in Figure 8.

We refer to the product (ωt_1) as the "initial phase," and the term $(\omega \Delta t)$ as the "change in phase," respectively. Equation (3-3) is valid for all values of the initial phase and the time delay Δt. For small values of Δt, the results can be simplified somewhat, as shown in the following paragraphs.

Approximate Results for Small Time-Delays

Equation (3-3) can be expanded using trigonometric identities and the small-angle approximations

$$\sin(\omega \Delta t) \approx (\omega \Delta t)$$

$$\cos(\omega \Delta t) \approx 1 - 0(\Delta t)^2$$

which are valid when

$$\omega(\Delta t) << 1 \qquad (3\text{-}4)$$

The result is

$$w_2 - w_1 = \omega\, A(\Delta t) \cos \omega\, t_1 = \frac{(2n + 1)\lambda}{4} \qquad (3\text{-}5)$$

which is just a special case of the Taylors expansion discussed previously

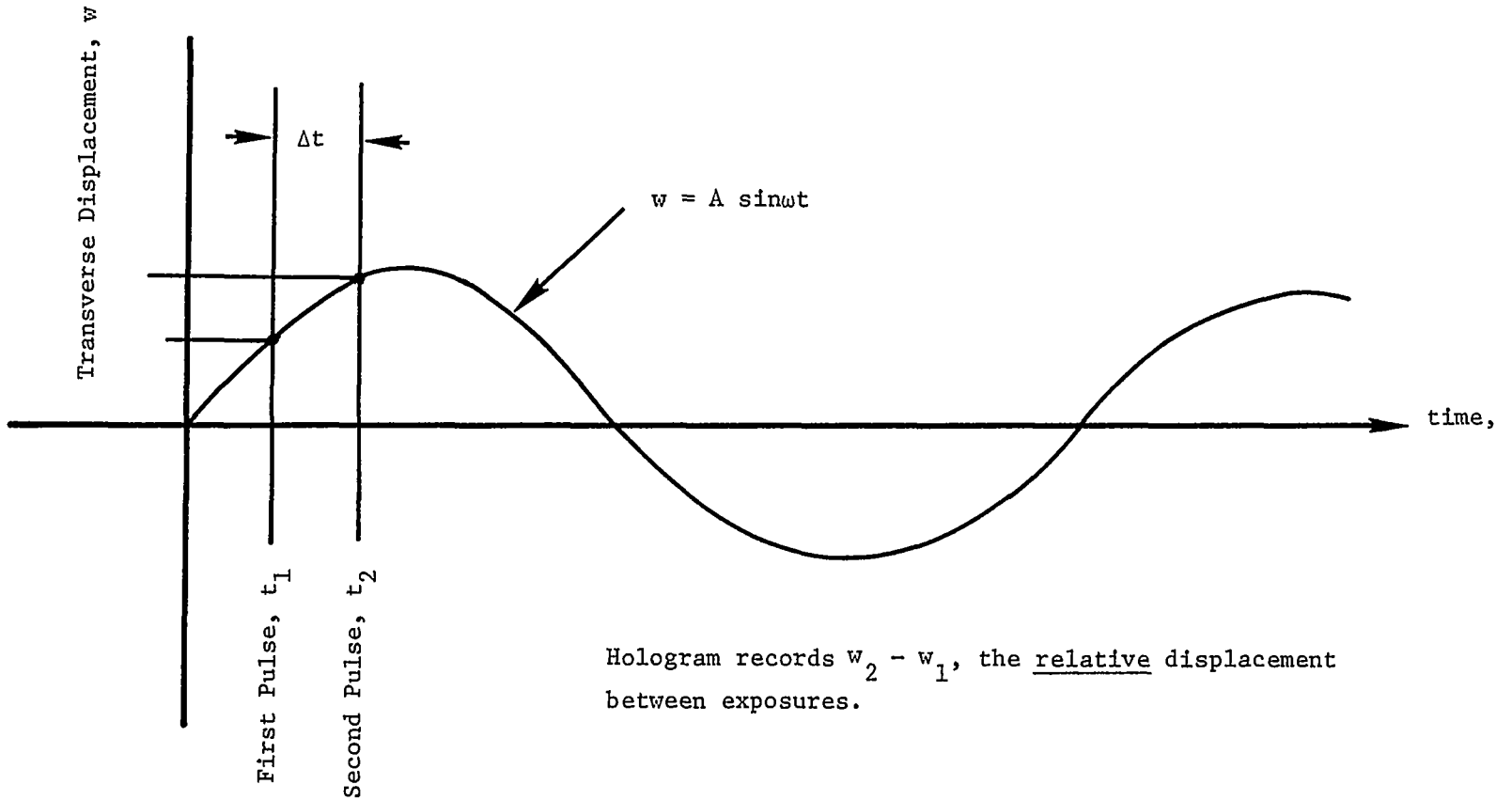

Figure 8: Sinusoidal Displacement of a Vibrating Plate. (The relative displacement $w_2 - w_1$ is recorded holographically by laser pulses at times t_2 and t_1.)

(see Equation 2-4). The product ω A cos ω t_1 in Equation (3-5) is just the velocity, $\dot{w}$, evaluated at time t_1.

The reader should note that the spatial (x, y) dependence of the deflection is hidden in Equation (3-5), but it is present, nevertheless. The interference fringes (lines along which the fringe order n is constant) are curves which vary in x and y (i.e., in the plane of the plate). Similarly, our "local amplitude", A, is really a function of x and y: $A = A_o \Phi_{mn}(x, y)$. Thus, a pulsed differential hologram can be used to determine mode shapes $\Phi_{mn}(x, y)$ by means of Equation (3-5). Two examples of holograms made in this fashion are shown in Figures 9 and 10, which involve vibrations of a plate at room temperature. It is clear from these results that differential holograms can be used to record vibration modes. The sensitivity of this technique - its capabilities and limitations - are discussed in the section which follows.

Sensitivity Curves: Capabilities and Limitations

Using the relation $\omega = 2\pi f$, Equation (3-5) can be written as

$$2\pi f\ (\Delta t)\ A \cos \omega\ t_1 = \frac{(2n \pm 1)\lambda}{4} \tag{3-6}$$

or, solving for the local amplitude, A, we have

$$A = \frac{(2n \pm 1)\lambda}{4(2\pi f)(\Delta t)\ \cos \omega\ t_1} \tag{3-7}$$

or

$$A = F(n, \lambda, f, \Delta t, t_1)$$

in functional form. Recall that Equation (3-7) is valid only when the inequality

$$\omega(\Delta t) \ll 1$$

is satisfied. This relation can be put in the form

$$\frac{\Delta t}{T} \ll \frac{1}{2\pi} \tag{3-8}$$

where $T = \frac{2\pi}{\omega} = \frac{1}{f}$ is the period of vibration. We see, then, that the time delay between exposures of the hologram must be small in comparison with the vibration period, for our approximate Equation (3-7) to remain valid.

Figure 9 - Differential hologram of the fundamental mode. (Δt = 50 μs between pulses). First pulse synchronized to occur when plate has maximum velocity. (f = 138 cps)

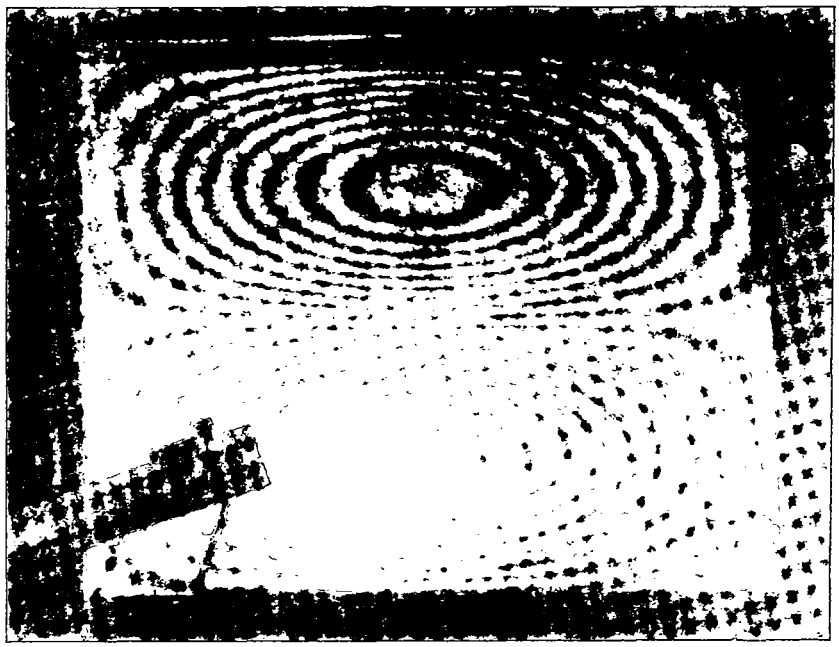

Figure 10 - Differential hologram of 1 x 2 mode. (Δt = 25 μs between pulses). Laser sychronized to displacement transducer. (f = 342 cps)

To determine the sensitivity of the pulsed holographic system, we want to find the minimum value, A, for which Equation (3-7) holds. The minimization is subject to practical constraints on the variables (n, λ, f, Δt, and t_1). For example, with the pulsed ruby laser used in our experiments, λ is fixed at 6943Å (i.e., 6.943×10^{-5} cm). Similarly, the time delay between successive laser pulses is limited (by the electronics) to the range

$$1\ \mu s \leq t \leq 500\ \mu s \tag{3-9}$$

Finally, for recording the mode shape, $\Phi_{mn}(x, y)$, we want at least some minimum number of fringes (n_{min}) enclosing each antinode.

To minimize A in Equation (3-7) it is clear that the term $\cos(\omega t_1)$ in the denominator should be made a maximum. This is accomplished expermentially by synchronizing the laser pulse with the plate vibration such that effectively $t_1 = 0$. (The plate velocity, $\dot{w}$, is a maximum at $t_1 = 0$.) With these restrictions on λ, Δt, n and t_1, Equation (3-7) yields

$$A = \frac{(2n_{min} - 1)(6.943 \times 10^{-5}\ \text{cm})}{4(2\pi f)(\Delta t)} \tag{3-10}$$

where Δt is subject to the inequalities (3-8) and (3-9).

At this point, it is simplest to consider Δt as a parameter, and also to fix n_{min} at some nominal value (say n = 5). Equation (3-10) gives the minimum amplitude, A_{min}, as a function of frequency. For example, with $n_{min} = 5$ and the time delay $\Delta t = 100\ \mu s$ we have

$$A_{min} = \left(\frac{9}{4}\right) \frac{(6.943 \times 10^{-5})}{(6.28)(100 \times 10^{-6})} \left(\frac{1}{f}\right)$$

$$A_{min} = \frac{.248}{f}\ , \tag{3-11}$$

where A_{min} is the vibration amplitude in centimeters.

Equation (3-11) has been plotted in Figure 11, for various values of Δt, and a fixed number of fringes, n = 5. Thus, with a time delay $\Delta t = 100\ \mu s$ (between laser pulses), and a plate vibration frequency of

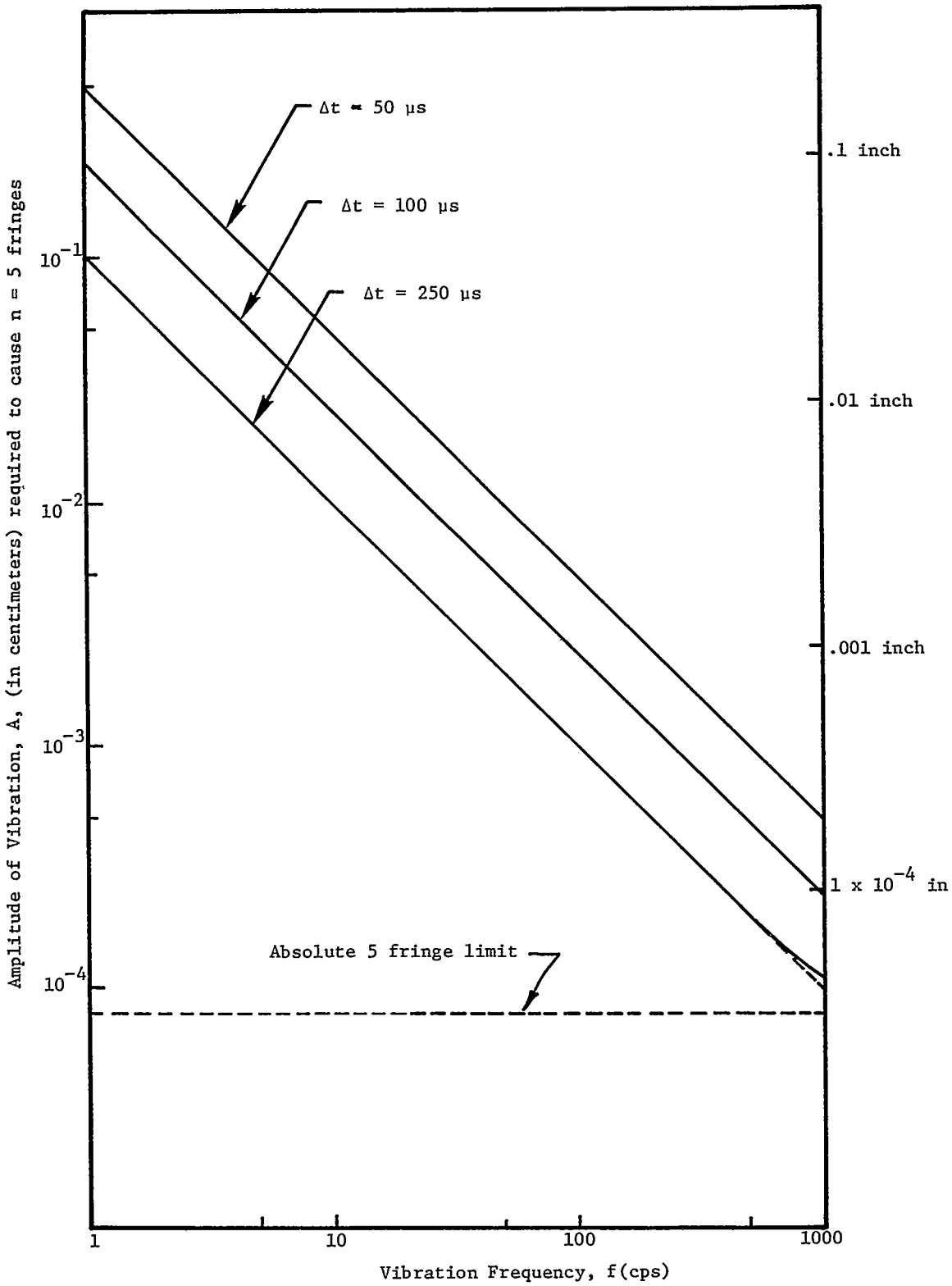

Figure 11: Vibration Amplitude A, Required to Produce Five Interference Fringes on a Pulsed Differential Hologram

1 cps, vibration amplitude $A = .248$ cm (approximately .1 inch) is required to produce <u>five</u> interference fringe contours around each antinode of the vibration mode. Similarly, if the vibration frequency $f = 100$ cps, the required amplitude (using the 100 μs time-delay) is 2.48×10^{-3} cm (or approximately one-thousandth of an inch) to produce <u>five</u> fringe contours.

The question of increasing the sensitivity of this pulsed differential technique naturally arises. If the experimenter is satisfied with fewer fringe contours (and correspondingly less definition of the vibration mode) he could operate with lower values for n_{min}, the fringe order. For example, using $n_{min} = 2$ (two fringe contour lines) Equation (3-10) gives

$$A_{min} = \frac{.0826}{f} \quad \text{(in cm)} \tag{3-12}$$

using $\Delta t = 100$ μs. Equation (3-12) represents an increase in sensitivity by a factor of <u>three</u>, when compared with Equation (3-11). (But, this increase in sensitivity has been accompanied by the formation of fewer fringe contours.)

Another means of increasing the sensitivity is to increase the time delay (Δt) between pulses. Thus, when Δt is increased from 100 μs to 250 μs, the sensitivity increases by a factor of 250:100 = 2.5. Thus, if the plate vibrates with frequency $f = 1$ cps, and a time-delay $\Delta t = 250$ μs is used, a vibration amplitude $A = .1$ cm is required (to produce five contour fringes). Conversely, if Δt is halved (from 100 μs to 50 μs) the sensitivity <u>decreases</u> by a factor of two. This inverse dependence on Δt is apparent from Equation (3-10) and accounts for the "parallel-line" nature of the curves shown in Figure 11.

It is not possible to continue increasing the sensitivity by using larger and larger values of Δt, however, since other effects (not described by Equation 3-10) enter the problem. First of all, Equation (3-10) is limited by the inequality (3-8) to "small" time-delays. Secondly, as Δt becomes larger we approach the time scale of the turbulence and fluid mechanics of thermal convection past the heated plate, and the hologram can become corrupted by this "noise". Nevertheless, it is instructive to examine Equation (3-3) for the case of large time-delays, when the limitation $\Delta t/T \ll \frac{1}{2\pi}$ does not apply.

For example, if we choose the times t_1 and Δt properly, and adjust them to correspond with the period of vibration, it is possible to find a minimum amplitude limit (i.e., a sensitivity curve) that is <u>independent</u> of frequency. In particular, we choose t_1 and Δt such that

$$\omega t_1 = \frac{3}{2} \quad \text{(initial phase)}$$

$$\omega \Delta t = \pi$$

which is equivalent to

$$t_1 = \frac{3\pi}{2\omega} = \frac{3}{4}\,T$$
$$\Delta t = \frac{\pi}{\omega} = \frac{T}{2} \qquad (3\text{-}13)$$

This timing is such that the first laser pulse (at time t_1) occurs when

$$w_1 = A \sin\left(\frac{3\pi}{2}\right) = -A$$

and the second pulse (one-half a period later) occurs when

$$w_2 = A \sin\left(\frac{3\pi}{2} + \pi\right) = A$$

The hologram gives interference fringe contours of the relative displacement

$$w_2 - w_1 = 2A = \frac{(2n \pm 1)\lambda}{4} \qquad (3\text{-}14)$$

(see Equation 2-15).

Equation (3-14) is independent of the vibration frequency, f, because the times t_1 and Δt were chosen to coincide with the maximum and minimum excursions of the sine wave, namely $\pm$ A. If we again choose a minimum number of fringes as $n_{min} = 5$, then Equation (3-14) gives the amplitude sensitivity

$$A_{min} = \frac{9}{8}\,\lambda = 7.8 \times 10^{-5} \text{ cm} \qquad (3\text{-}15)$$

as the vibration amplitude required to form 5 fringes around an antinode of the vibration mode. This "absolute, 5 fringe limit" (Equation 3-15) is plotted as a horizontal line in Figure 11. The reader should note that this "limit" was derived without regard for the constraint Equation $1\ \mu s \leq \Delta t \leq 500\ \mu s$ which is a physical limitation for our particular laser-electronics package.

Finally, if the number of fringe contours is reduced (to $n_{min} = 2$, say) so we have less definition but more sensitivity, then Equation (3-14)

gives

$$A_{min} = \frac{3\lambda}{8} = .26 \times 10^{-5} \text{ cm} \tag{3-16}$$

for our (idealized) case of "peak-to-peak" timing of the laser pulses.

Another special case of Equation (3-3) which is not limited to small time delays is given by the timing

$$t_1 = -\frac{\Delta t}{2}$$
$$t_2 = t_1 + \Delta t = \frac{\Delta t}{2} \tag{3-17}$$

which involves laser pulses that are symmetric in time about the point $t = 0$. In this case, Equation (3-3) gives

$$w_2 - w_1 = 2 A \sin \omega \frac{\Delta t}{2} = 2 A \sin(\pi f \Delta t)$$

or

$$2 A \sin(\pi f \Delta t) = \frac{(2n \pm 1)\lambda}{4} \tag{3-18}$$

Equation (3-18) is an exact result (assuming sinusoidal motion and the symmetrical timing just discussed) which reduces to Equation (3-10) when the linearization

$$\frac{\Delta t}{T} \ll \frac{1}{2\pi}$$

is applied. With $\Delta t \leq 250$ μs, Equations (3-18) and (3-10) give identical results for frequencies up to 1000 cps.

Effects of Geometry: Change in Sensitivity

The calculations of the preceding section are based upon the relation

$$w_2 - w_1 = \frac{(2n \pm 1)\lambda}{4} \tag{3-19}$$

which relates the relative displacement (between exposures) to the fringe order n and the laser wavelength, λ. This equation is discussed in Section 2.0, and is limited to "small" illuminating and viewing angles:

$$\theta_v \ll 1$$
$$\theta_i \ll 1 \tag{3-20}$$

(The angles θ_i and θ_v are illustrated in Figure 6, Section 2.0.) Initial tests were run using small angles θ_i and θ_v, and they are reported in Section 4.0. However, it later became necessary to examine the case of large values for θ_i and θ_v, as discussed in the following paragraphs.

For the 2000°F experiments on heated plates, it was desired to place quartz radiant heat lamps close to the vibrating plate and to record the holograms of the same (hot) surface. The close proximity of the heat lamps required that the vibrating plate be viewed (and illuminated) using very shallow, "grazing angles", as illustrated in Figure 12. These shallow angles (labeled ε_i and ε_v in Figure 12) are related to θ_i and θ_v by the equations

$$\theta_i = \pi/2 - \varepsilon_i$$
$$\theta_v = \pi/2 - \varepsilon_v \tag{3-20}$$

which are apparent from the geometry. Under these conditions, the angles θ_i and θ_v are large, which means the cos θ terms must be retained in Equation (2-15). The result is

$$w_2 - w_1 = \frac{(2n \pm 1)\lambda}{2(\cos\theta_i + \cos\theta_v)} \tag{3-21}$$

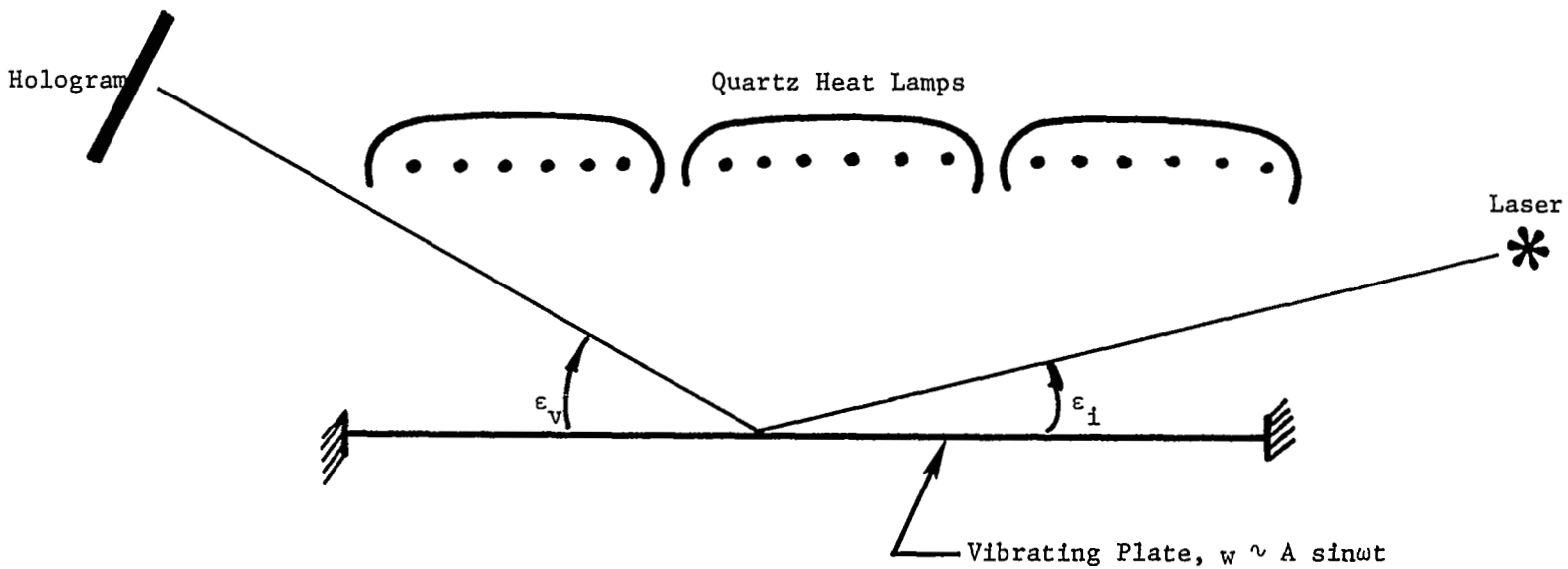

Figure 12: Illustration of the Grazing Angles ε_i and ε_v

which may be written in terms of the complementary angles (ε_i and ε_v) as

$$w_2 - w_1 = \frac{(2n + 1)\lambda}{2(\sin \varepsilon_i + \sin \varepsilon_v)} \tag{3-22}$$

For simplicity, consider the case of equal angles when $\varepsilon_i = \varepsilon_v = \varepsilon$. Then Equation (3-22) becomes

$$w_2 - w_1 = \frac{(2n \pm 1)\lambda}{4 \sin \varepsilon} \tag{3-22}$$

which is <u>identical</u> to the previous case (Equation 3-19), <u>except</u> for the factor $(\sin \varepsilon)^{-1}$.

The influence of the grazing angle ε is clear, then, and we can simply modify the calculations of the preceding section by the factor $(\sin \varepsilon)^{-1}$. For example, when $\varepsilon = \pi/2$, we regain the previous results, such as Figure 11. When the angle ε is reduced to 20°, we have a loss in sensitivity by the factor 1/sin 20°. In other words, the vibration amplitude required to cause five contour fringes is (cf. Equation 3-22)

$$A_{min} = \frac{.248}{f}\left(\frac{1}{\sin 20°}\right)$$

$$A_{min} = \frac{.725}{f} \qquad (\varepsilon = 20°) \tag{3-23}$$

where A_{min} is the vibration amplitude in cm,

f is the vibration frequency in cps,

$n_{min} = 5$ (five fringe contours form)

and $\Delta t = 100$ μs time-delay between laser pulses.

Equation (3-23) represents a loss in sensitivity by approximately a factor of three, when compared to the case of "normal" viewing given by Equation (3-11). Similarly, when the angle $\varepsilon = 10°$, the result is

$$A_{min} = \frac{.248}{f}\left(\frac{1}{\sin 10°}\right) = \frac{1.43}{f} \text{ (cm)} \tag{3-24}$$

which represents a loss in sensitivity by a factor $(\sin 10°)^{-1} \approx 6$, with respect to normal viewing.

These results are illustrated graphically in Figure 13, in which the line ($\varepsilon = 90°$) is identical to the line $\Delta t = 100$ μs of Figure 11. Figure 13 shows the effect of changes in the grazing angle, where Figure 11 illustrates changes in Δt. It is of practical interest to note at this point that the experiments described in Section 5.0 employed a grazing angle in the range

$$5° \leq \varepsilon \leq 10° \tag{3-25}$$

and achieved successful results. The extreme case ($\varepsilon = 0$) is a "singular point" in the theory which implies that an "infinite" displacement $(w_2 - w_1)$ is required to cause a fringe on the interferogram. To analyze the case of very small angles ($\varepsilon \to 0$) requires that the finite size of the experiment be considered. That is, the finite path of the light rays from the laser, to the object, and to the hologram becomes involved, and the approximation that the laser source (or hologram) is "off at infinity" can no longer be employed.

Effects of Initial Phase and Large Time-Delays

For small values of Δt, the relation between the vibrating object (with frequency ω and amplitude A) and the fringe order n (of the interferogram) is

$$w_2 - w_1 = A\omega(\Delta t)\ \cos\omega t_1 = \frac{(2n+1)\lambda}{4} \tag{3-5}$$

where the product ωt_1 is referred to as the "initial phase" and relates to the timing of the first pulse of the laser.

By the use of a displacement transducer (e.g., an inductance pick-up or a capacitance probe, etc.) mounted near the vibrating plate, the sinusoidal displacement of the plate can be electrically monitored. And, by means of an oscilloscope (with a variable time-delay and gate output) it is fairly straightforward to synchronize the laser pulse(s) with the transducer signal from the vibrating plate. Thus, it is possible to readily adjust the "initial phase" (ωt_1) in Equation (3-5), and we made use of this fact previously in going from Equation (3-7) to Equation (3-10), where the latter is based upon $\omega t_1 = 0$, $\cos\omega t_1 = 1$.

A simple experimental demonstration of the more general expression (Equation 3-5) was made as follows. If the vibration frequency and the amplitude A are held constant, as well as the time-delay Δt, then Equation (3-5) can be expressed as

$$\frac{(2n \pm 1)\lambda}{4} = K\ \cos\omega t_1 \tag{3-26}$$

where $K = A\omega(\Delta t)$ is a constant.

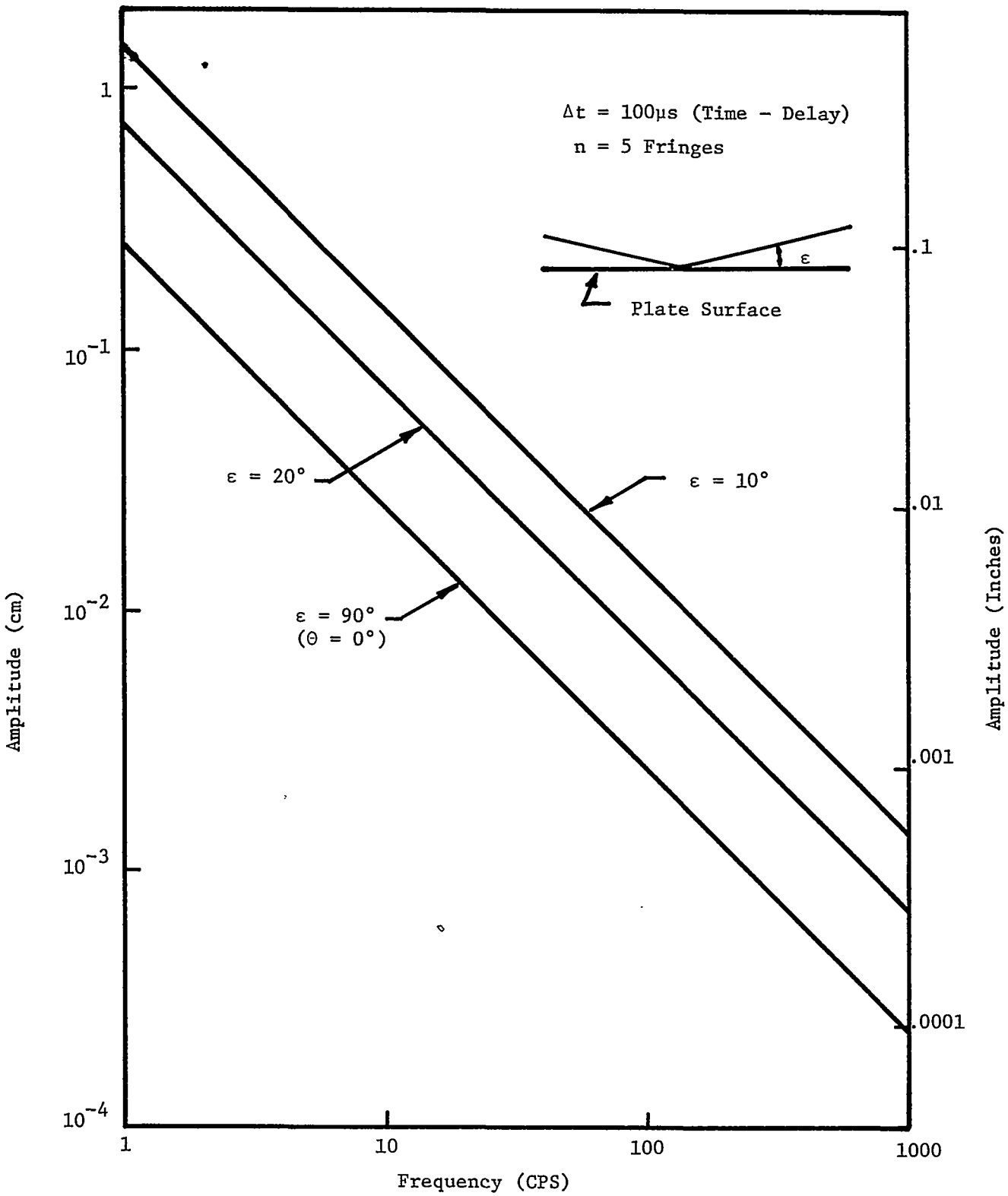

Figure 13 - Vibration Amplitude, A, Required to Produce Five Contour Fringes, for Various Grazing Angles, ε.

The test was run by vibrating a plate at constant amplitude and frequency, but varying the time t_1 of the initial laser pulse. The time delay between pulses (Δt) was held constant at 50 μs. Several differential holograms were obtained in this fashion, and the factor $(2n \pm 1)\lambda/4$ was determined at an antinode of the vibration mode. The results are plotted in Figure 14, which shows the factor (2n - 1) plotted vs. the initial phase (ωt_1).

Equation (3-26) predicts that the factor $(2n \pm 1)$ should vary at a cosine function, and this conclusion is borne out by the data shown in Figure 14. Each data point in Figure 14 required a separate interferogram, corresponding to each value of the phase ωt_1. A total of fifteen differential holograms were made in this fashion, and the corresponding phase values (ωt_1) were varied to span a full period of the cosine, as illustrated in Figure 14.

Additional tests were conducted to verify Equation (3-3)

$$w_2 = w_1 = A \sin (t_1 + \Delta t) - A \sin \omega t_1$$

$$= \frac{(2n \pm 1)\lambda}{4} \tag{3-3}$$

This equation can be written as

$$\frac{(2n \pm 1)\lambda}{4} = A[\sin(\psi_o + \Delta\psi) - \sin\psi_o] \tag{3-27}$$

where $\psi_o = \omega t_1$ is the initial phase and $\Delta\psi = (\omega\Delta t)$ is the change in phase between exposures of the hologram.

Tests were run to verify Equation (3-27), in which the amplitude and frequency of vibration were held constant, the initial phase ψ_o was kept fixed, and the phase change ($\omega\Delta t$) was varied. The results are shown in Figure 15, which gives $(2n \pm 1)$ plotted vs. ($\omega\Delta t$). The number of quarter wavelengths recorded on each interferogram were determined at the antinode of the vibration mode. Equation (3-27) predicts that the quantity $(2n \pm 1)\lambda/4$ should vary sinusoidally with $\Delta\psi$, and the results depend upon the initial phase, ψ_o. For our tests, the initial phase was very nearly given by

$$\psi_o \approx - \pi/2$$

in which case Equation (3-27) gives

$$\frac{(2n \pm 1)\lambda}{4} \cong A[1 - \cos\Delta\psi] \tag{3-28}$$

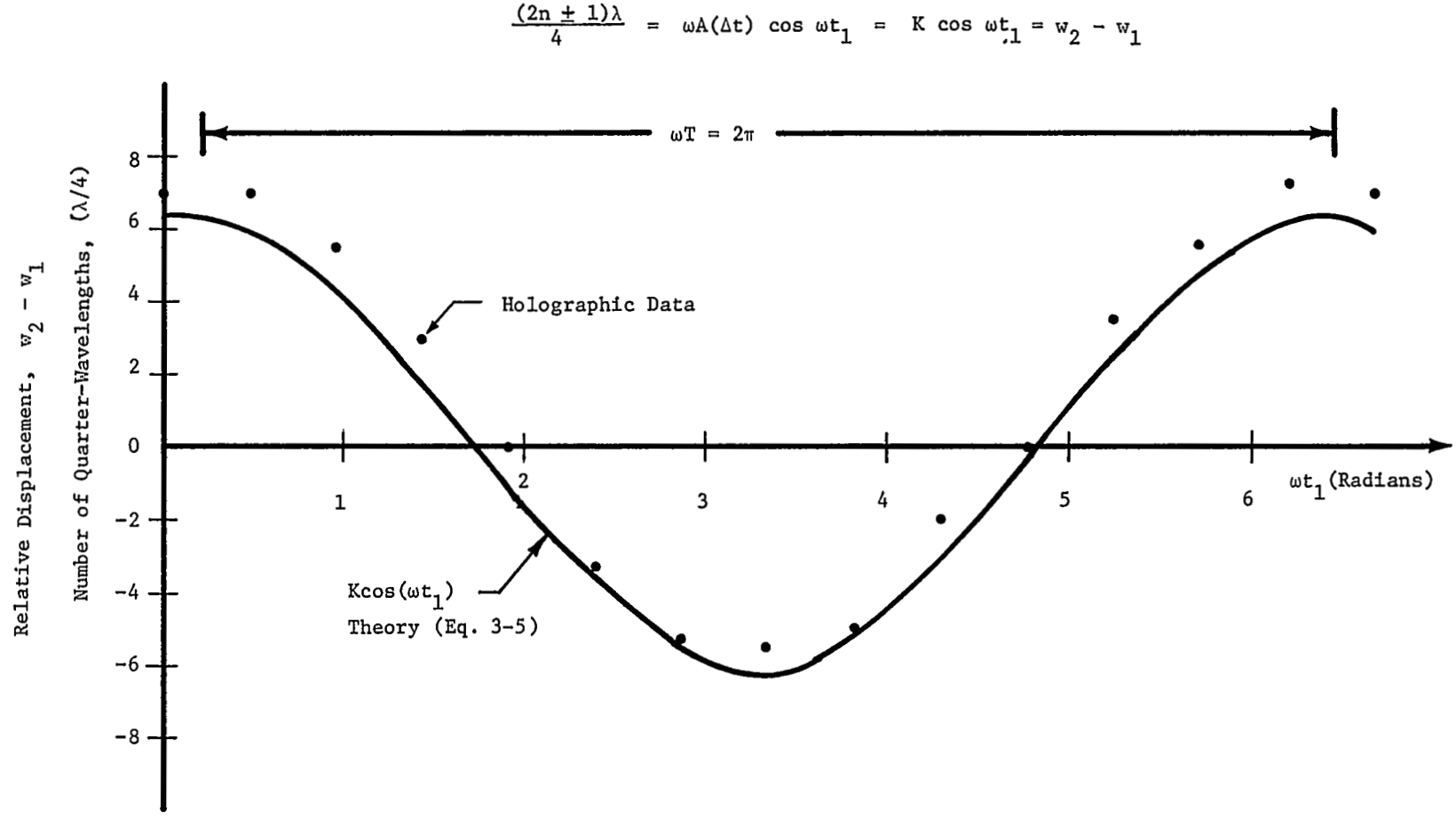

Figure 14 - Holographic Data Showing Variation of Displacement (in Quarter-Wavelengths) with Initial Phase, ωt_1

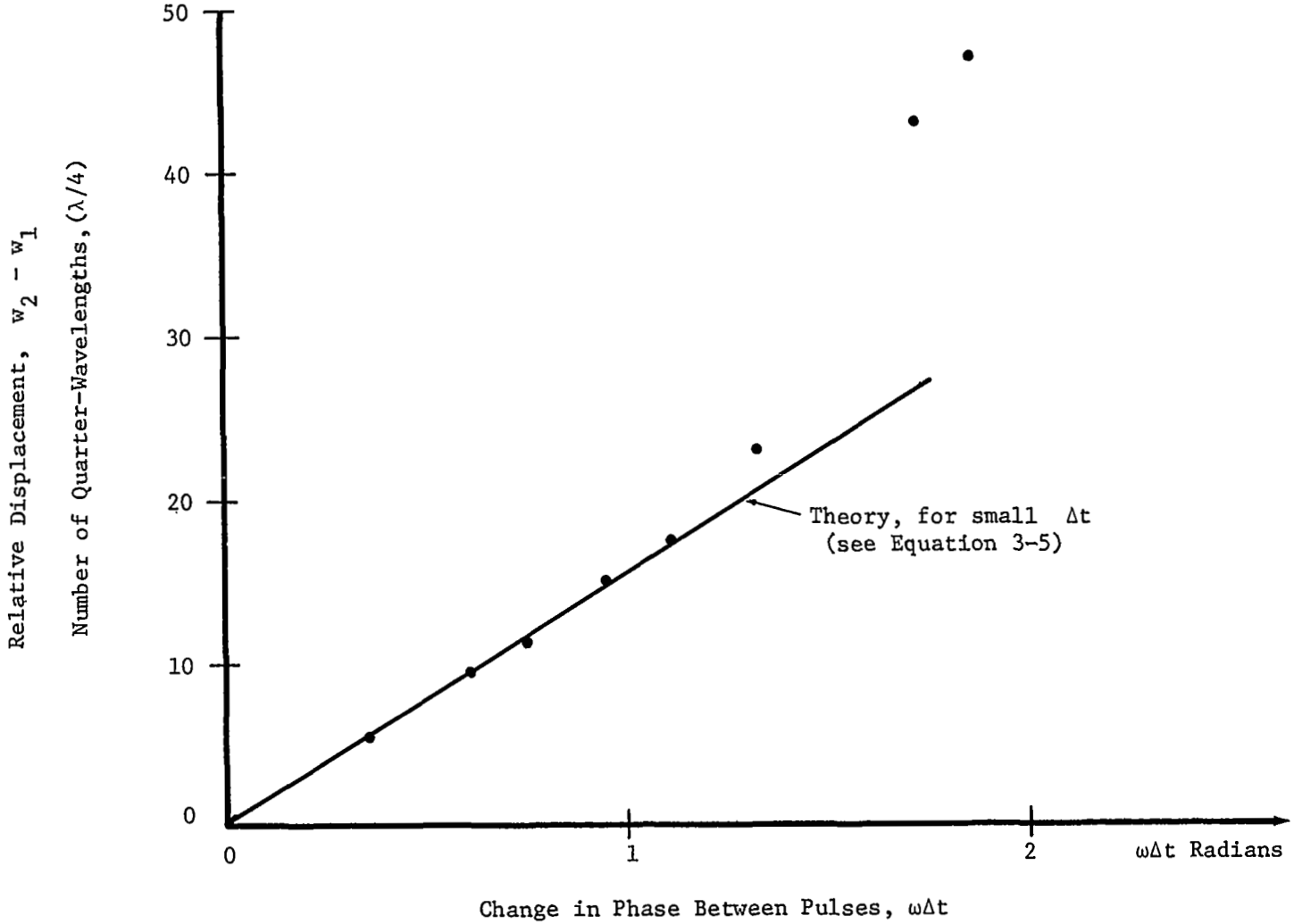

Figure 15 - Displacement between Exposures (in Quarter-Wavelengths) vs. Change in Phase ($\omega\Delta t$)

The data of Figure 15 have the general form of Equation (3-28), and the slight differences between theory and experiment are attributed to the fact that the initial phase was not exactly $-\pi/2$.

These tests were conducted using a vibration frequency of 645 cps, and the time delay Δt was varied from 90 μs to a maximum of 460 μs between exposures. Additional tests were run using very short time delays, and the results are shown in Figure 16. Equation (3-5) predicts that for small time-delays, $(2n - 1)\lambda/4$ should vary linearly with Δt, and this result is borne out by the data of Figure 16.

These experimental results serve to verify the functional forms predicted by analysis. For any given vibration amplitude and frequency, the number of fringes that will form can be accurately calculated, given the initial time t_1 and the delay Δt. Conversely, if the time delay is fixed (Δt = 50 μsec, for example) and the time t_1 is known, the sensitivity can be calculated in terms of vibration amplitude (A) and frequency ($\omega = 2\pi f$). Such results have been presented in previous paragraphs.

Mechanical Noise: Stability Requirements

The effects of noise (i.e., undesirable vibrations of one type or another) and the mechanical stability required of the experimental set-up can be estimated as follows. Consider a total deflection $w(x,y,t)$ that is a combination of a signal (which we wish to detect) plus noise.

$$w = S(x,y,t) + N(x,y,t) \tag{3-29}$$

In particular, let the signal S and the noise N both be oscillatory:

$$\begin{aligned} &\text{Signal:} \quad S(x,y,t) = A_o\Phi(x,y)\ \sin\omega t \\ &\text{Noise:} \quad N(x,y,t) = N_o g(x,y)\ \sin(\nu t + \gamma) \end{aligned} \tag{3-30}$$

The signal has a maximum amplitude A_o, a distribution $\Phi(x,y)$, which is the mode shape, and a frequency ω. Similarly, the "noise" has amplitude N_o, a spatial distribution $g(x,y)$, a frequency ν and a phase γ (which is relative to the signal, $\cos\omega t$).

A differential hologram records the relative displacement, $w_2 - w_1$, given by

$$w_2 - w_1 = \Delta t[A_o\omega\Phi\cos\omega t_1 + \nu N_o g\cos(\nu t_1 + \psi)] \tag{3-31}$$

where the "small time-delay" assumption

$$\begin{aligned} \omega\Delta t &<< 1 \\ \nu\Delta t &<< 1 \end{aligned} \tag{3-32}$$

has been used (cf. Equations 3-4 and 3-5).

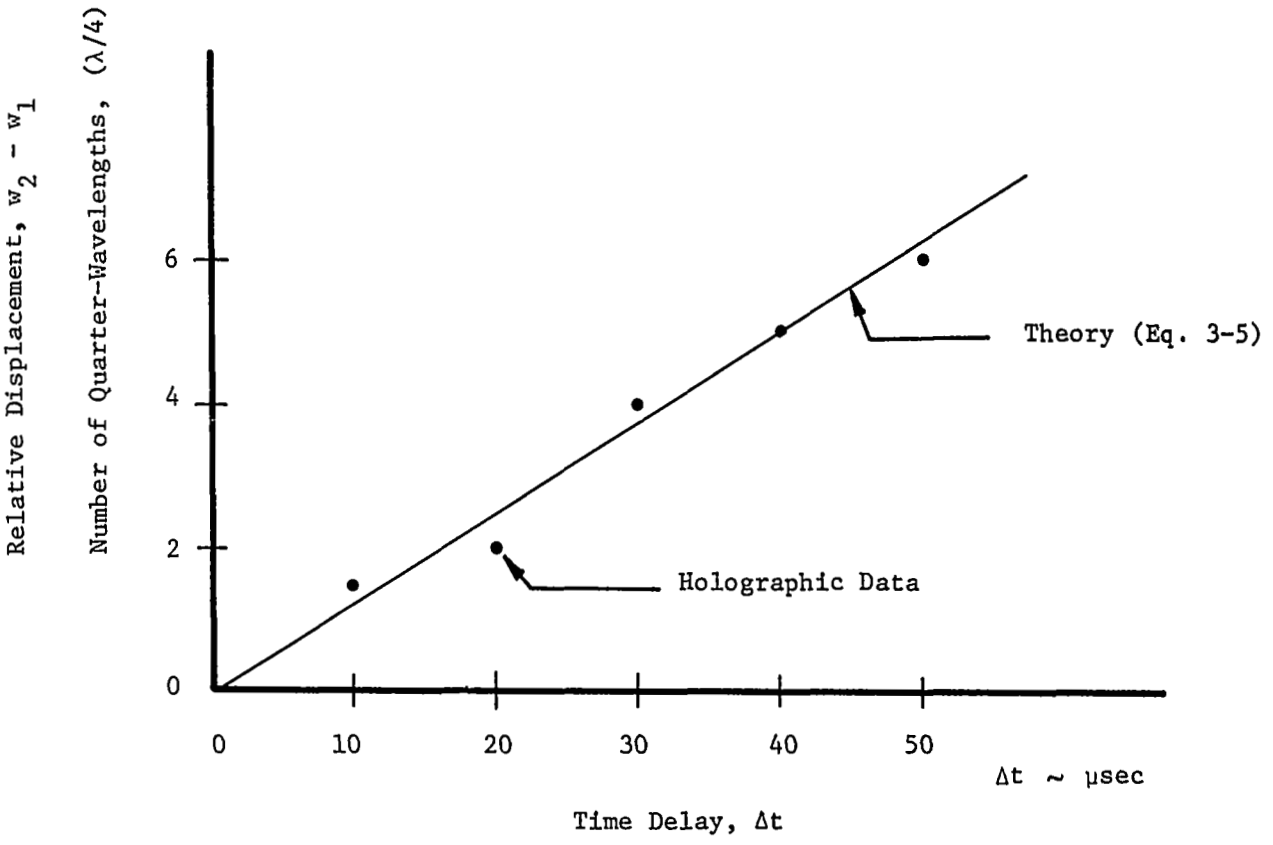

Figure 16 - Displacement between Exposures (in Quarter-Wavelengths) vs. Time Delay (Δt)

Referring to Equation (3-31), we want to record the term $A_o\Phi(x,y)$ (the vibration mode shape) and reject the noise $N_o g(x,y)$. The shape distributions $\Phi(x,y)$ and $g(x,y)$ are assumed to be normalized, and thus satisfy the conditions

$$|\Phi(x,y)| \leq 1 \quad , \qquad |g(x,y)| \leq 1 \tag{3-33}$$

and similarly, we have

$$|\cos\omega t_1| \leq 1 \quad , \qquad |\cos(\nu t_1 + \psi)| \leq 1 \tag{3-34}$$

Thus, to have a large signal-to-noise ratio, Equation (3-31) suggests the requirement

$$\omega A_o >> \nu N_o \tag{3-35}$$

which says that the maximum velocity (ωA_o) of the plate vibration we wish to record should be significantly greater than the velocity (νN_o) of the oscillatory noise.

Equation (3-35) does not tell the complete story, however. For example, with very poor timing, we might have $|\cos\omega t_1| << 1$, which would greatly reduce the signal term in Equation (3-31). In practice, the signal from the displacement transducer will usually allow accurate synchronization, such that $\omega t_1 = 0$ and $\cos\omega t_1 = 1$. With this "exact" timing, Equation (3-35) can be revised to

$$\omega A_o\Phi(x,y) >> \nu N_o g(x,y) \tag{3-36}$$

For all but the fundamental mode, the mode shape $\Phi(x,y)$ has <u>nodal lines</u>, where

$$\Phi(x,y) = 0 \tag{3-37}$$

and, <u>if</u> the distribution $g(x,y)$ does not coincide with the mode shape (Φ) then <u>the inequality (3-36) cannot be satisfied near the nodal lines</u>.

As a practical example, the plate might be vibrating in a mode

$$\Phi(x,y) = \sin\frac{m\pi x}{a}\sin\frac{n\pi y}{b} \tag{3-38}$$

and the plate boundaries (i.e., its support frame) might be moving in a "rigid-body" fashion, corresponding to

$$g(x,y) = 1 \tag{3-39}$$

In this case, the "noise" $\nu N_o \cos(\omega t_1 + \gamma)$ might cause fringes on the interferogram near the nodal lines

$$\frac{mx}{a} = \frac{k}{2} \quad , \qquad \frac{ny}{b} = \frac{\ell}{2} \tag{3-40}$$

(where m,n,ℓ, and k are integers).

One way to largely eliminate the effect of the noise is to insure that its amplitude and frequency satisfy the "no fringe" condition

$$|\nu N_o(\Delta t)| << \frac{\lambda}{4} \tag{3-41}$$

along with the inequality (3-35). Equation (3-41) states that the noise will not cause a fringe to form, even in the vicinity of nodal lines. Equation (3-35) insures that the contour fringes which do form will be caused primarily by the vibration $A_o\Phi(x,y)\sin\omega t$ which we desire to measure.

A feeling for the amplitudes and frequencies involved in Equation (3-41) can be obtained from Equation (3-10) and the related discussion on sensitivity. Using Δt = 100 μs, and n = 5, the sensitivity of the pulsed differential technique was calculated to be

$$A_{min} = \frac{.248}{f} \qquad \text{(in cm)} \tag{3-11}$$

Equation (3-41) corresponds to $n_{min} = 1$ and gives

$$N_o << \frac{2\pi(.248)}{\nu}\left(\frac{1}{9}\right) = \frac{.0276}{f_N} \tag{3-42}$$

as the noise amplitude (in centimeters) in terms of noise frequency f_N, (using the same Δt = 100 μs between pulses of the laser). Equation (3-42) is directly analogous to Equation (3-11), and the sensitivity curves presented previously (Figure 11) can be used to estimate the maximum noise amplitude N_o at a given noise frequency f_N. (The factor of 2π arises because $\nu = 2\pi f_N$ is a circular frequency).

Thus, with Δt = 100 μs, Equation (3-42) results in a linear "noise boundary" parallel to the diagonal lines of Figure 11, and at a factor of nine lower in amplitude than the corresponding sensitivity curve. In the special case where the undesirable noise N_o and the signal A cosωt have the same frequency ($\nu = \omega$, $f_N = f$) then Equation (3-35) simply states that the noise must be appreciably less than the signal.

In actual practice, many industrial environments are such that the noise amplitude falls off as frequency increases. Building vibrations, seismic disturbances, and motions due to vehicular traffic tend to be low frequency. High-frequency vibrations, on the other hand, tend to be damped out more readily, do not generally propagate far from their source, and can (if necessary) be prevented from influencing the hologram by vibration-isolation and simple mechanical filtering.

Although we have examined the special case of harmonic noise,

$$N(x,t,t) = N_o g(x,y) \cos(\nu t + \psi)$$

the more general case of random vibrations (with N characterized by its power spectral density) can also be treated. For example, the power spectral density P(f) gives a measure of the amplitude (squared) at a particular frequency f. As a first approximation, one might require

$$2\pi f[P(f)]^{1/2} \ (\Delta t) \ << \frac{\lambda}{4} \tag{3-42}$$

by analogy with Equation (3-41). Thus, for any value of Δt, we can compute an upper bound on the power spectral density P(f) of the mechanical noise. The limitations on P(f) computed from Equation (3-42) are expected to be very conservative; that is, one anticipates that in many cases fringes (due to noise) will <u>not</u> form even though P(f) fails to satisfy Equation (3-42).

A thorough treatment of the problems of noise and stability would involve a careful analysis using probability theory and random variables. For a given noise input (characterized by its P.S.D., say) one can then calculate the probability of the event

$$\dot{N}(\Delta t) \geq \frac{\lambda}{4} \tag{3-43}$$

i.e., the probability that the noise will cause a fringe to form. Such an analysis was beyond the scope of the present study. The problem of extracting signals in the presence of noise is fundamental to communications theory (e.g. Ref. 24) and is related to holographic measurements in the presence of random vibrations. (See Refs. 18 and 19, for example).

For the experiments reported herein, there were virtually no problems which arose due to noise, spurious vibrations, or lack of mechanical stability. Wooden tables and ordinary lab benches were used to support the optics, the plate specimen, the shaker, etc., and no attempt was made at vibration isolation of these components. The individual stands for the mirrors, lenses, etc., were generally held lightly in place with a small drop of glue, which is a carry-over from cw holography and helps keep the optics aligned. This represents the extent of the stability problems which were encountered experimentally. The development of precise limitations on noise (which are less stringent than those presented herein) will very likely depend upon pending applications of pulsed laser holography in noisy environments. For example, some applications of holographic nondestructive testing (HNDT) involve operations near noisy machinery, production lines,

etc. If the noise in these applications becomes a problem, then the question of recording structural deformations (while rejecting the noise) will receive the increased attention necessary for its solution.

Limitations on the Time-Delay and Plate Temperature

It is expected that most plate vibration problems of interest to NASA will fall somewhere in the ranges

$$\begin{aligned} &\text{Frequency:} && 1 \text{ cps} \leq f \leq 1000 \text{ cps} \\ &\text{Temperature:} && 78^\circ\text{F} \leq \Theta \leq 2500^\circ\text{F} \\ &\text{Amplitude:} && 1.75 \times 10^{-5} \text{ cm} \leq A \leq 100 \text{ cm} \\ &\text{Velocity:} && .25 \text{ cm/sec} \leq \omega A \leq 10^{5} \text{ cm/sec} \end{aligned} \tag{3-43}$$

where it is assumed that the plate is vibrating sinusoidally with a transverse deflection $w = A \sin(\omega t) = A \sin(2\pi f t)$.

These limits (specified as Equation 3-43) are only approximate, and they are given here primarily as a basis for discussion. Some of the limits given are flexible and readily changed to meet new situations; others are fixed by physical limitations, such as the wavelength of light, etc. For example, the frequency range could just as easily be

$$.1 \text{ cps} \leq f \leq 10{,}000 \text{ cps} \tag{3-44}$$

providing the velocity criterion

$$\omega A \geq .25 \text{ cm/sec} \tag{3-45}$$

is still satisfied. This velocity requirement (3-45) is based on the approximation of a small time-delay Δt between exposures on the order of 100 μsec. If it is possible to use $\Delta t = 250$ μsec, then the velocity requirement can be relaxed to

$$\omega A \geq .1 \text{ cm/sec} \tag{3-46}$$

The lower limit on vibration amplitude is fixed by the wavelength of light (λ) and the theory of double-exposure holography. Thus, we have the constraint on the vibration amplitude

$$A \geq \frac{\lambda}{4} \approx 1.75 \times 10^{-5} \text{ cm} \tag{3-47}$$

in order that at least one fringe forms on the interferogram.

For harmonic motion, the maximum vibration amplitude (set at $A \leq 100$ cm) and maximum velocity ($\omega A \leq 10^5$ cm/sec) have been chosen arbitrarily, and they are subject to considerable leeway. By appropriate synchronization of the laser pulses with the plate vibration, it is possible to record the relative displacement $w_2 - w_1$ when the plate velocity is nearly zero. When the plate reaches its maximum excursion, the velocity goes to zero, and small relative displacements $w_2 - w_1$ will occur in the time $\Delta t = t_2 - t_1$, regardless of the maximum vibration amplitude, A. This idea was demonstrated in Ref. 15, which showed holographic measurements on a plate vibrating to large amplitudes (.5 inch, peak-to-peak). Similarly, the maximum velocity ωA is not strongly limited, as long as the velocity $\dot{w}$ goes to zero periodically (harmonic motion again).

Now consider the limitations on the maximum temperature, Θ_{max}. The maximum temperature at which the differential pulse technique will successfully record vibration modes depends upon

- The time delay, Δt, between exposures
- The vibration amplitude A and frequency f
- The atmospheric medium, and its index of refraction as a function of temperature
- The orientation of the heated plate surface, e.g. vertical or horizontal
- The size of the plate

A thorough discussion of this problem involves fluid mechanics and heat transfer in free-convection boundary-layers (Ref. 20). However, we can imagine a hypothetical example in which the plate is standing vertically in air and vibrating with a given amplitude and frequency; the time-delay Δt between pulses is presumed to be set (at 250 μsec, say) and differential holograms made at room temperature Θ_o produce an adequate number of contour fringes. Now, imagine we begin heating the plate, and keep the parameters A, f, and Δt fixed. We continue recording differential holograms at various increasing temperatures, Θ_i. Eventually, the turbulence from the convection currents becomes significant, such that the noise (due to random changes in optical path length) can no longer satisfy Equation (2-10):

$$\dot{N}\,\Delta t \ll \lambda/2 \qquad (2\text{-}10)$$

At this point, the noise begins to distort or corrupt the mode shape we are trying to record on the differential hologram. Some noise will be tolerable, however, depending upon the quality of the mode shape data required.

As the temperature continues to increase, we reach the point where

$$\dot{N}(\Delta t) \gg \lambda/2 \tag{3-48}$$

and the noise can overwhelm the signal from the vibrating plate. Depending upon the mode shape, amplitude, frequency, etc., we can thus establish a maximum temperature, Θ_{max}, above which the holograms are too "noisy" and unacceptable for determining the mode shape.

Now suppose we determine this temperature to be Θ_{max} = 1400°F, and we wish to conduct tests at 2200°F. The most direct approach for increasing the allowable temperature is to shorten the time-delay. For example, if Θ_{max} = 1400°F using Δt = 250 μs between exposures, we can shorten Δt and reduce the noise term $\dot{N}(\Delta t)$. Thus, using Δt = 100 μs, we might be able to record mode shapes up to a new maximum temperature, Θ_{max} = 2000°F. Finally, we might try Δt = 50 μs and reach the goal of recording mode shapes at 2200°F.

The relationship between the maximum plate temperature, Θ_{max}, at which mode shapes can be adequately recorded and the time delay, Δt, between exposures, involves complicated fluid mechanics of thermal convection on vibrating surfaces and is not readily calculable. It seems clear, however, that long time-delays will result in lower operating temperatures, Θ_{max}. For the experiments described in Sections 4.0 and 5.0, a time-delay Δt = 50 μs was used throughout, and good quality noise-free mode shapes were recorded at 1000, 1600, and 2000°F.

Results for Random Firing of the First Pulse: Probability Calculations

Many of the preceding results (e.g., Figures 56, 57, 58) are based on the idea of synchronizing the laser pulse(s) with the vibration of the plate. In particular, by electronic synchronization we can (in most cases) control the "initial phase" (ωt_1) and achieve the maximum sensitivity of the pulsed differential technique. (See Equations 3-7 and 3-10, and the related discussion.)

The experimental details of timing the laser pulses, and the holographic results obtained using such synchronization are reported in Section 4.0. However, in some of the experiments (see Section 5.0) it was simpler to operate without synchronization. In this case, the interferograms were obtained using a small time-delay, ($\omega\Delta t$) << 1, and "random firing," i.e., the initial phase (ωt_1) varied randomly. Successful results were obtained with this approach, and the experiment is amenable to analysis using probability theory, as outlined in the following paragraphs.

Basic to probability analysis is the definition of an event (Ref. 25). For our purposes, the event is defined by such statements as "five or more contour fringes are recorded on the interferogram," or "the interferogram recorded at least one fringe contour," etc. In the case of normal

illumination and viewing ($\theta_i << 1$, $\theta_v << 1$, Equation 2-15) the event can be described mathematically by

$$|w_2 - w_1| \geq \frac{(2n - 1)\lambda}{4} \tag{3-49}$$

where we have chosen the fringe order, n, to be positive, and the absolute value of $w_2 - w_1$ is required since the interferogram is not sensitive to the sign (i.e., phase) of the relative displacement.

For small time-delays, Equation (3-49) is equivalent to

$$|\dot{w}\Delta t| \geq \frac{(2n - 1)\lambda}{4} \tag{3-50}$$

where $\dot{w}$ is the velocity, evaluated at time t_1. For the problem at hand we have the relations for the vibrating plate

$$\begin{aligned} &\text{(Displacement)} && w = A \sin \omega t \\ &\text{(Velocity)} && \dot{w} = (A\omega) \cos \omega t = V \cos \omega t \end{aligned} \tag{3-51}$$

Reference 25 shows that a motion

$$x = V \cos \omega t$$

(where t is a random variable) has associated with it the probability density function

$$\begin{aligned} p(x) &= \frac{1}{\pi\sqrt{V^2 - x^2}} && -V \leq x \leq V \\ p(x) &= 0 && |x| > V \end{aligned} \tag{3-52}$$

In our "random firing" experiments, the velocity $\dot{w}$ is evaluated at time t_1, where t_1 is a random variable corresponding to the time of the first laser pulse.

Thus, using our event (3-50) and the probability density (3-52) we can calculate the probability that the event actually occurs:

$$P\left[|\dot{w}\Delta t| \geq \frac{(2n - 1)\lambda}{4}\right] = \int_{x_1}^{x_2} p(x)dx \tag{3-53}$$

where appropriate limits for the integral x_1 and x_2 will be determined shortly. Since the time delay Δt is positive, we have the equivalence

$$P\left[\left|\dot{w}\Delta t\right| \geq \frac{(2n-1)\lambda}{4}\right] = P\left[\left|\dot{w}\right| \geq \frac{(2n-1)\lambda}{4(\Delta t)}\right] \tag{3-54}$$

The term involving n, λ, and Δt defines a velocity, v_o:

$$v_o = \frac{(2n-1)\lambda}{4(\Delta t)} \tag{3-55}$$

And, using Equations (3-52) through (3-55), we have the desired result

$$P\left[\left|\dot{w}\right| \geq v_o\right] = \int_{v_o}^{V} p(x)dx + \int_{-V}^{-v_o} p(x)dx$$

$$= 2\int_{v_o}^{V} p(x)dx \qquad \text{(by symmetry)}$$

$$= 2\int_{v_o}^{V} \frac{dx}{\pi\sqrt{V^2 - x^2}}$$

$$= \frac{2}{\pi}\left[\sin^{-1}\left(\frac{x}{V}\right)\right]_{v_o}^{V}$$

$$= \frac{2}{\pi}\left[\frac{\pi}{2} - \sin^{-1}\left(\frac{v_o}{V}\right)\right]$$

$$P\left[\left|\dot{w}\Delta t\right| \geq \frac{(2n-1)\lambda}{4}\right] = 1 - \frac{2}{\pi}\sin^{-1}\left(\frac{v_o}{V}\right) \tag{3-56}$$

where we have assumed that

$$v_o \leq V$$

$$\text{i.e.,} \qquad \frac{(2n-1)\lambda}{4\Delta t} \leq \omega A \tag{3-57}$$

Equation (3-56) gives "The probability that the velocity $|\dot{w}|$ is greater than or equal to v_o," which is equivalent to "The probability that the relative displacement between exposures $|w_2 - w_1|$ is greater than or equal to $\frac{(2n-1)\lambda}{4}$," which in simplest terms, means "The probability that n contour fringes form on the interferogram." Equation (3-56) can be interpreted in physical terms as the ratio of (1) the time during which

the velocity $|\dot{w}|$ exceeds v_o, divided by (2) the total period of vibration, T. This concept is illustrated graphically in Figure 17.

To get a feeling for these results, suppose we want five or more fringe contours to form (n = 5) and wish to use a time-delay $\Delta t = 100$ μsec. Then Equation (3-55) gives

$$v_o = \frac{(2n-1)\lambda}{4(\Delta t)} = \frac{9}{4} \times \frac{6.943 \times 10^{-5} \text{ cm}}{100 \times 10^{-6} \text{ sec}}$$

$$v_o = 1.56 \text{ cm/sec} \tag{3-58}$$

At this point, it is convenient to select a desired value for the probability $P\left[|\dot{w}\Delta t| > \frac{9\lambda}{4}\right]$, Equation (3-57). For example, a probability value $P = 2/3$ might be acceptable, meaning that "2 out of 3 interferograms would have five or more contour fringes." Thus, if we take

$$\sin^{-1}\left(\frac{v_o}{V}\right) = \frac{\pi}{6}$$

$$\text{i.e.,} \qquad \left(\frac{v_o}{V}\right) = .5 \tag{3-59}$$

Then Equation (3-57) yields

$$P\left[|\dot{w}\Delta t| \geq \frac{9\lambda}{4}\right] = 1 - \frac{2}{\pi}\left(\frac{\pi}{6}\right) = 2/3$$

which is the acceptable probability just postulated.

Equations (3-58) and (3-59) can then be combined to give the amplitude-frequency relation which must be met in order to achieve the probability $P = 2/3$. That is, from Equation (3-59) we have

$$\omega A = V = \frac{v_o}{.5} = \frac{1.56 \text{ cm/sec}}{.5} \tag{3-60}$$

and, using $\omega = 2\pi f$, this becomes

$$A = \frac{1.56 \text{ cm/sec}}{(2\pi f)(.5)} = \frac{.496}{f} \tag{3-61}$$

where A is the required vibration amplitude in centimeters, and f is the corresponding frequency in cps.

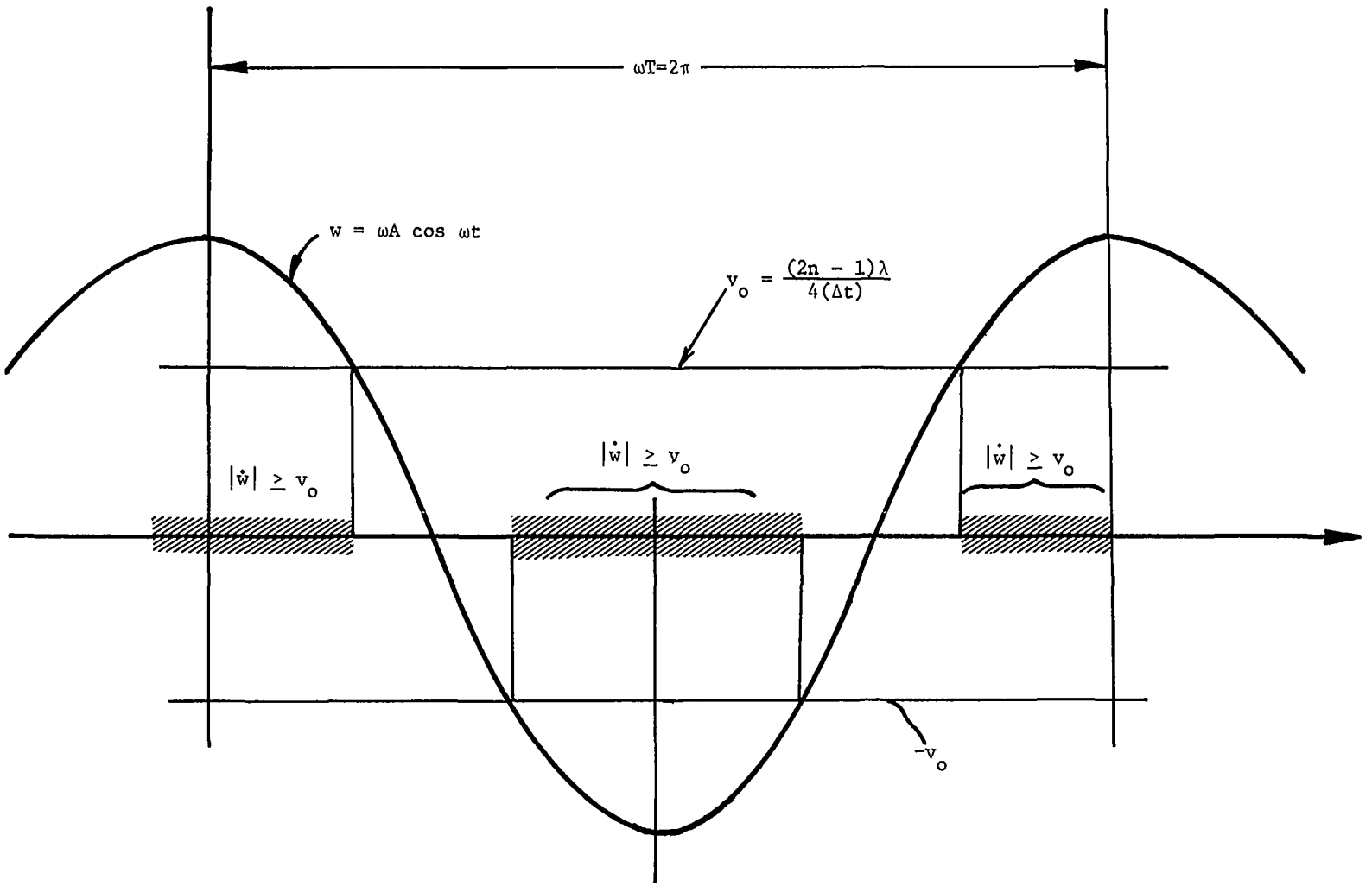

Figure 17 - Illustration of the Condition $|\dot{w}| \geq v_o$ and its Relation to the Probability Results

This result can be put into words, as follows. When the amplitude and frequency of vibration are such that Equation (3-61) is satisfied, and the timing of the first pulse t_1 is random, and a time-delay $\Delta t = 100$ μs is used between exposures, then a pulsed differential hologram will produce five fringe contours with a probability of 2/3.

The reader should note the similarity in form between Equation (3-11)

$$A = \frac{.248}{f} \tag{3-11}$$

(which assumes ideal synchronization between the laser and the vibration) and Equation (3-61) just derived, which assumes random firing of the first pulse. Both equations are based upon (n = 5) and $\Delta t = 100$ μs, but the former gives maximum sensitivity and probability <u>one</u>, whereas the latter requires a larger vibration amplitude (in the ratio .496/.248) and results in a probability of 2/3.

The probability of producing five fringes (n = 5) can be increased by using a larger time-delay (Δt) or increasing the plate velocity $V = \omega A$, i.e., making

$$Af > .496 \text{ cm/sec}$$

The reader should be aware of the approximations used in this analysis, such as the expansion

$$w_2 - w_1 \cong \dot{w}(\Delta t) \tag{3-62a}$$

and the inequalities

$$\frac{\Delta t}{T} << \frac{1}{2\pi} \tag{3-62b}$$

$$\frac{(2n - 1)\lambda}{4(\Delta t)} \leq \omega A \tag{3-62c}$$

which together imply the condition

$$\frac{(2n - 1)\lambda}{4} < A \tag{3-62d}$$

The probability analysis presented herein is limited by these approximations, and Equation (3-61) therefore applies only for those amplitudes and frequencies which meet the preceding requirements.

From an experimental standpoint, it is desirable to fix the time delay (say $\Delta t = 50$ μs, which was actually used) and calculate the probability of obtaining one fringe, two fringes, ($n = 1,2$, etc.) as a function of amplitude and frequency. This result can be determined using Equation (3-56) and various n values. Thus, with $\Delta t = 50$ μs and $n = 1$, we have

$$P\left[\left|\dot{w}\Delta t\right| \geq \frac{\lambda}{4}\right] = 1 - \frac{2}{\pi}\sin^{-1}\left(\frac{v_o}{\omega A}\right) \tag{3-63}$$

where $$v_o = \frac{\lambda}{4(\Delta t)} = \frac{6.943 \times 10^{-5}}{4(50 \times 10^{-6})} = .347 \text{ cm/sec}$$

Similarly, for $n = 3$, we have

$$P\left[\left|\dot{w}\Delta t\right| \geq \frac{5\lambda}{4}\right] = 1 - \frac{2}{\pi}\sin^{-1}\left(\frac{1.735}{\omega A}\right)$$

and for $n = 5$,

$$P\left[\left|\dot{w}\Delta t\right| \geq \frac{9\lambda}{4}\right] = 1 - \frac{2}{\pi}\sin^{-1}\left(\frac{3.123}{\omega A}\right)$$

These results are plotted in Figure 18 giving the probability P as a function of the velocity (ωA) in cm/sec.

The similar appearance of the curves in Figure 18 suggest a "similarity solution," which is readily developed as follows. For any value of n, we have from Equation (3-56) the probability

$$P\left[\left|\dot{w}\Delta t\right| > \frac{(2n-1)\lambda}{4}\right] = 1 - \frac{2}{\pi}\sin^{-1}(z) \tag{3-64a}$$

which can be inverted to read

$$\cos\left(\frac{\pi}{2}P\right) = z \tag{3-64b}$$

where $z = \frac{v_o}{\omega A}$ can be expressed as

$$z = \frac{\frac{(2n-1)\lambda}{4(\Delta t)}}{\omega A} = \frac{1}{2\pi(R\tau)} \tag{3-65}$$

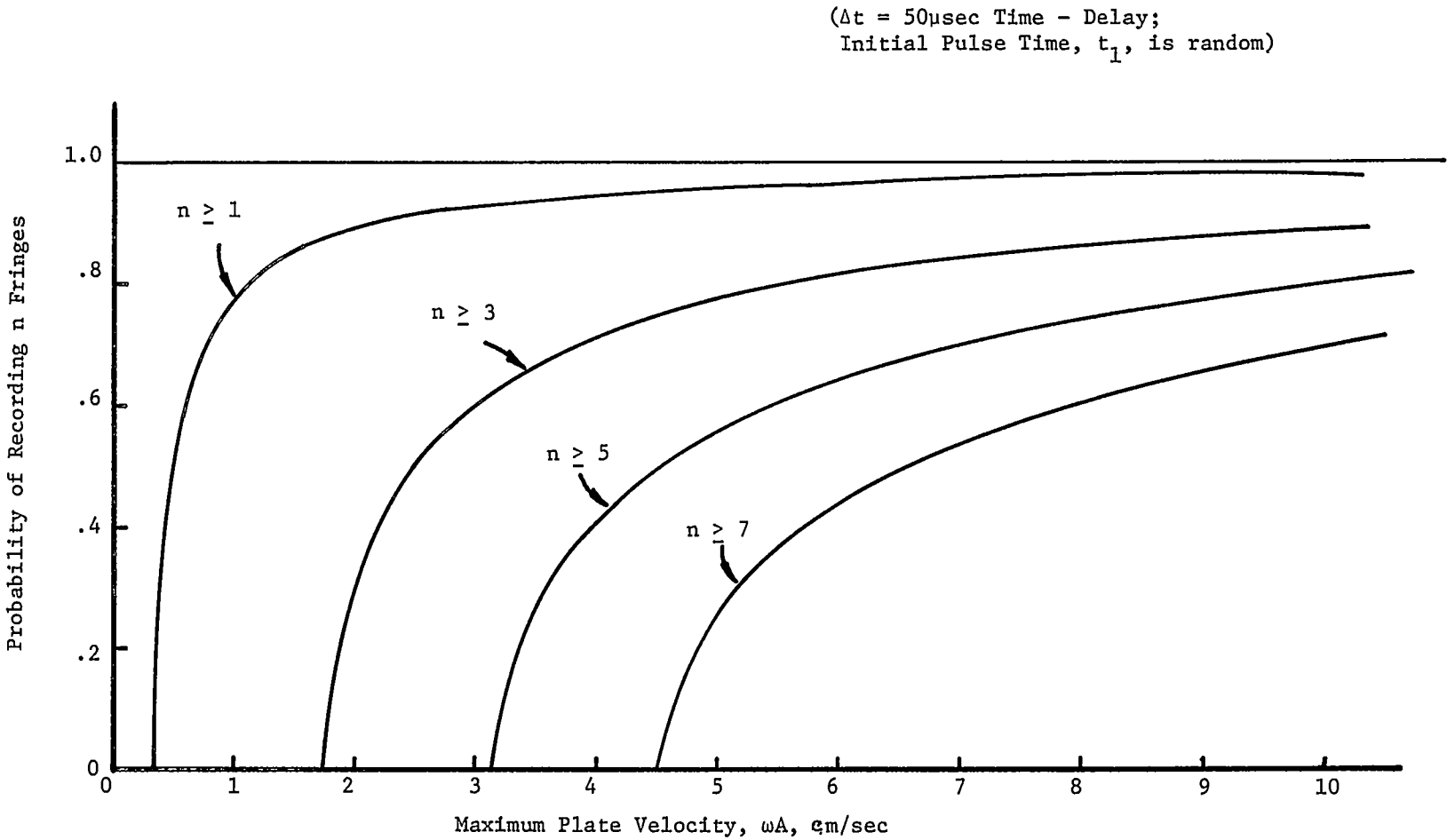

Figure 18 - Probability of Recording n Contour Fringes, as a Function of the Maximum Plate Velocity (Δt = 50 μs, Random Firing)

$\tau = \frac{\Delta t}{T}$ is a non-dimensional time, the ratio of time-delay to the vibration period, and

$$R = \frac{A}{\frac{(2n - 1)\lambda}{4}}$$

is a non-dimensional amplitude, the ratio of the vibration amplitude to the number of quarter-wavelengths recorded on the hologram.

Note from Equations (3-62) that $R > 1$ and $2\pi\tau << 1$, for the analysis to be valid. Equation (3-64) gives the probability of obtaining n fringe contours, as a function of the similarity variable $z = (2\pi\tau R)^{-1}$. The results are plotted in Figure 19, which is a universal curve that can be used for various fringe numbers (n), time-delays (Δt), amplitudes (A) and frequencies $\omega = \frac{2\pi}{T}$. For a fixed value of n (say n = 5, again) the probability of success (i.e., recording five fringes) increases as the amplitude, frequency, or time-delay is made larger. Note once again that these results cannot be applied indiscriminately, and are valid only when the approximations (3-62) are satisfied.

Random Firing Compared to Optimum Synchronization

For given values of the amplitude, frequency, and time-delay, the "optimum timing" (i.e., maximum velocity) approach presented in Equation (3-10) gives

$$\omega A(\Delta t) = \frac{(2n_{max} - 1)\lambda}{4} \tag{3-66}$$

where the fringe order n_{max} represents the "maximum number of fringes that can be obtained with optimum synchronization." (The term "optimum synchronization" or "optimum timing" simply means firing the laser when the plate velocity $\dot{w}$ is a maximum, thus maximizing the product $|\dot{w}\Delta t|$.)

With "random timing" (i.e., random firing of the first laser pulse) Equation (3-56) gives the probability of recording n or more fringes, in terms of the variable (v_o/V). Using the relation (3-55) for the velocity v_o and $V = A\omega$, we have

$$\frac{v_o}{V} = \frac{\frac{(2n - 1)\lambda}{4(\Delta t)}}{(A\omega)} = \frac{\frac{(2n - 1)\lambda}{4}}{(A\omega\ \Delta t)} \tag{3-67}$$

The denominator $(A\omega\ \Delta t)$ is related to the optimum, maximum fringe number, n_{max}, through Equation (3-66). Thus, Equations (3-66) and (3-67) can be combined to give

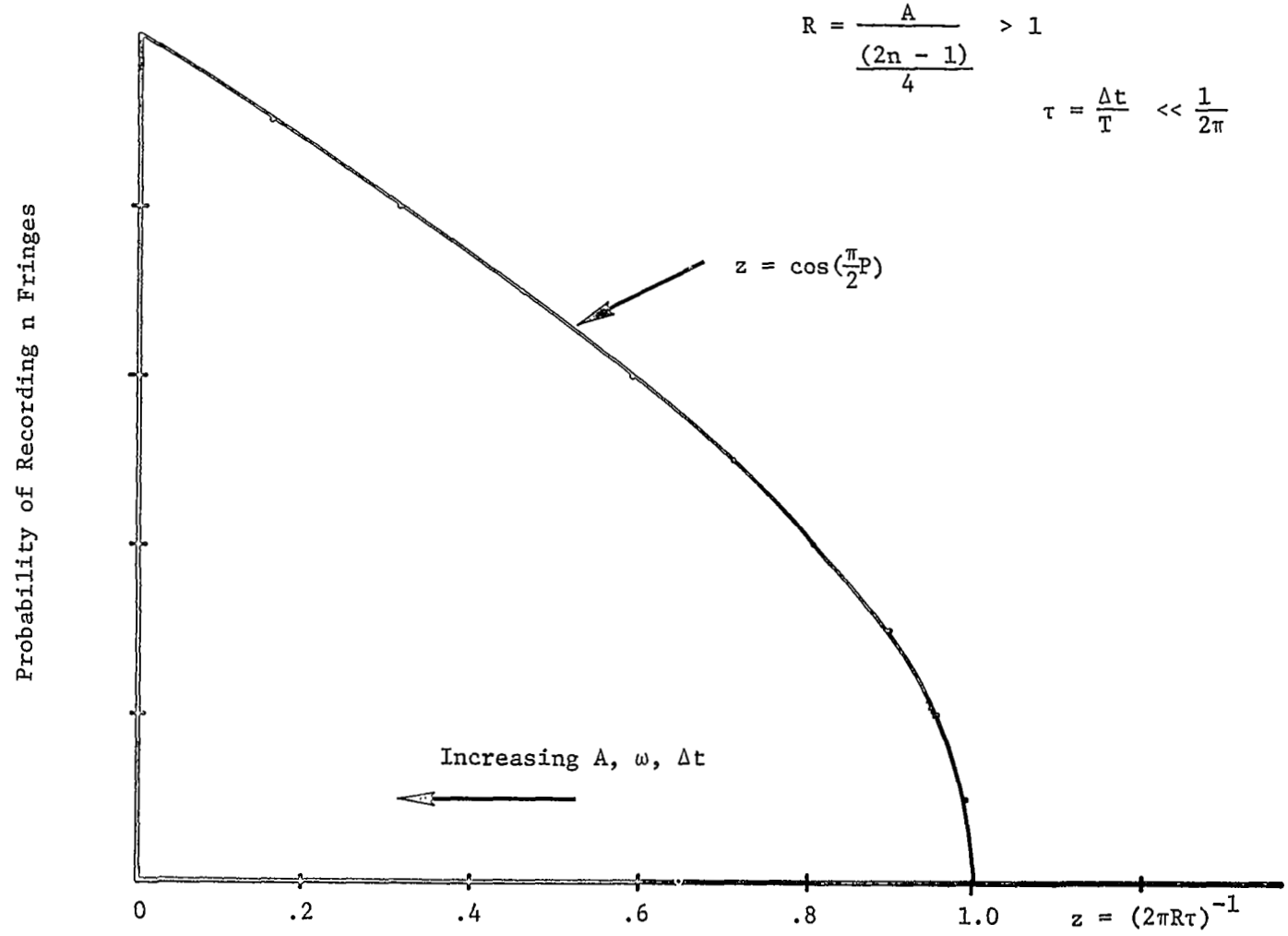

Figure 19 - Probability of Recording n Fringes, For a Given Amplitude, Frequency, and Time - Delay

$$\frac{v_o}{V} = \frac{(2n - 1)}{(2n_{max} - 1)} \tag{3-68}$$

and we can then substitute this expression for (v_o/V) in the probability Equation (3-56). The result is

$$P\left[|\dot{w}\Delta t| \geq \frac{(2n - 1)\lambda}{4}\right] = 1 - \frac{2}{\pi} \sin^{-1}\left[\frac{(2n - 1)}{(2n_{max} - 1)}\right] \tag{3-69}$$

Equation (3-69) gives "The probability of recording n contour fringes (using random firing of the first laser pulse) when optimum timing of the laser will produce n_{max} contour fringes. (The amplitude, frequency and time-delay are the <u>same</u> for both the optimum and random synchronization.) Since the fringe order, n, is an integer (n = 1,2,3, ...), the variable $(2n - 1)/(2n_{max} - 1)$ is <u>discrete</u>, and a plot of Equation (3-69) results in a "stair-step" appearance. Equation (3-69) is illustrated graphically in Figure 20 for the case $n_{max} = 5$ and in Figure 21 for $n_{max} = 10$.

These results are of particular interest from an experimental standpoint, since Equation (3-69) is <u>independent</u> of the amplitude, frequency, time-delay, and the illuminating and viewing angles (Θ_i, Θ_v), <u>providing</u> the approximations inherent in the derivation (e.g. Equations 3-62) are not violated. The similarity between the continuous curve of Figure 19 and the stair-steps of Figures 20 and 21 is readily apparent. The continuous variable $(2\pi\tau R)^{-1}$ in the smooth plot is analogous to the discrete variable $(2n - 1)/(2n_{max} - 1)$ in the stair-step graphs. As $n_{max} \to \infty$, the discrete variable approaches the continuous one and Figure 19 applies, with z replaced by (n/n_{max}).

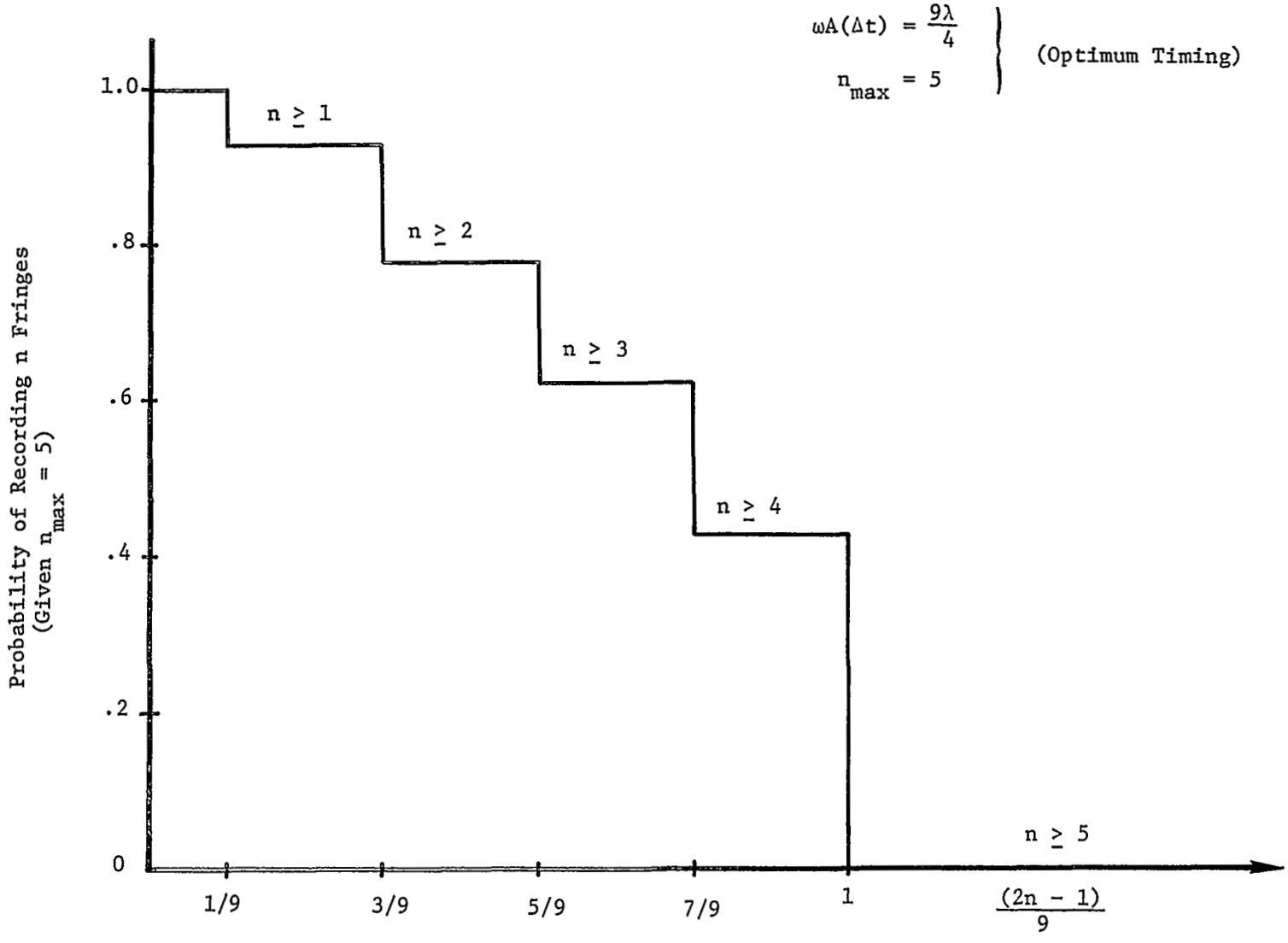

Figure 20 - Probability Distribution for Random Firing of the Laser, Given $n_{max} = 5$

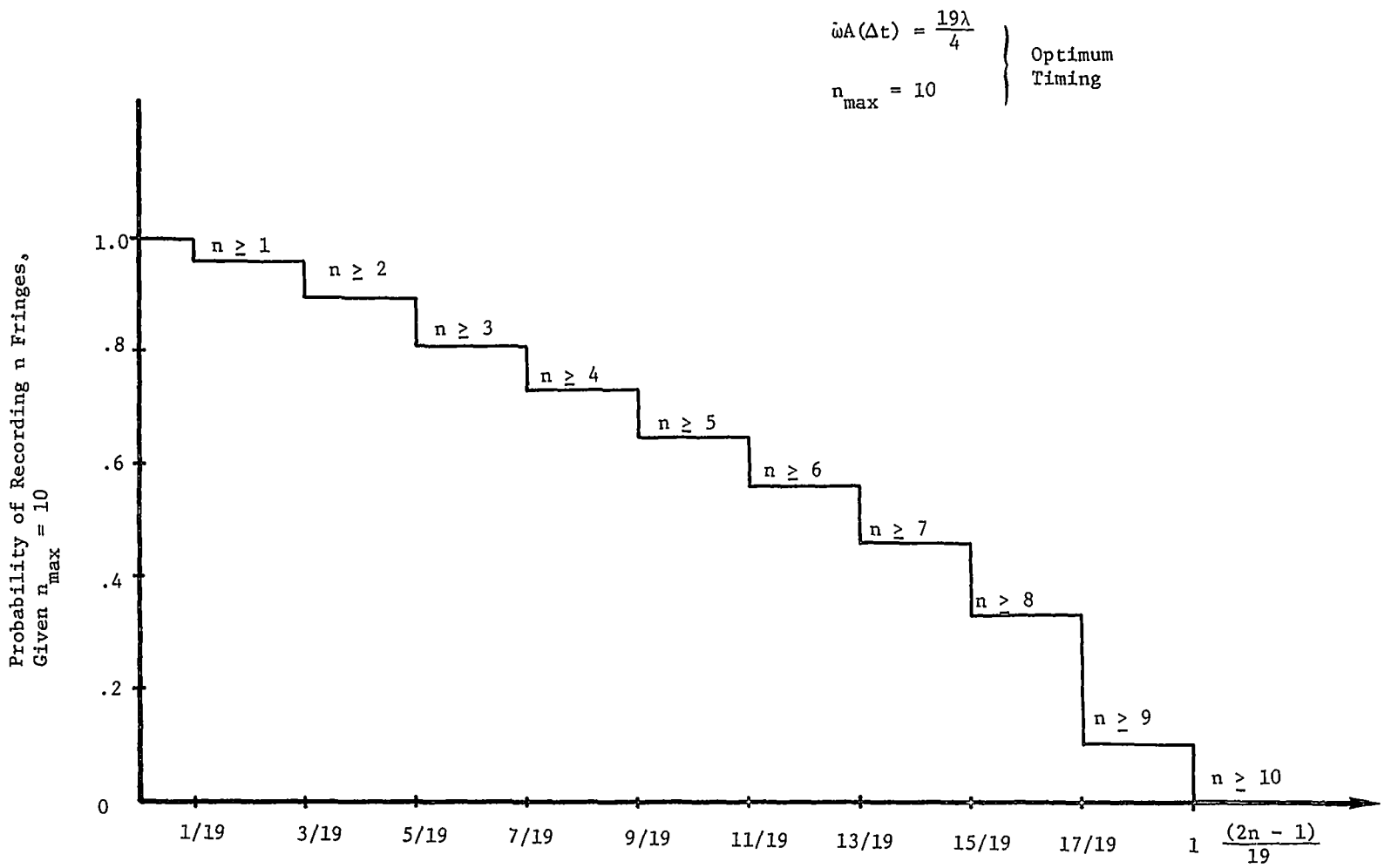

Figure 21 - Probability Distribution for Random Firing of the Laser, Given $n_{max} = 10$

Discussion of Results

The basic ideas of pulsed differential holography (presented in Section 2.0) have been applied herein to objects vibrating harmonically in a single mode. It appears that most practical measurements will involve small time-delay Δt, and approximate results have been given for this important case. The effects of geometry (i.e., low grazing angles), mechanical noise, and limitations on the time-delay and plate temperature have been briefly examined. A probability analysis was presented for the case of random firing of the initial laser pulse and small time-delays Δt between pulses.

It is clear that similar problems (of making holograms through random, turbulent media) arise in other areas, such as holographic measurement of flutter in a wind-tunnel, which involves passing the laser beam through the boundary layer(s). Whether such measurements will be successful or not depends upon (i) the signal-to-noise ratio (based upon velocities)

$$\dot{S}(\Delta t) >> \dot{N}(\Delta t)$$

and, (ii) limiting the path length changes due to noise

$$\dot{N}(\Delta t) << \frac{\lambda}{2}$$

The experimental fact that these requirements <u>can</u> be satisfied for heated, vibrating plates (to 2000°F) is discussed in Sections 4.0 and 5.0 which follow.

4.0 TESTS AT 1000°F

Introduction

Originally, it was planned to measure plate vibration modes at 1000 - 1500°F using time-average holography (in a vacuum enclosure) and pulsed differential holography (in the atmosphere). The pulsed holographic measurements appeared more promising, and they were completed first. Problems involving the plate support (to avoid thermal buckling), exciting and detecting resonance, timing the laser pulses, etc. were successfully solved and several mode shapes recorded at 1000°F. The techniques used, the problems encountered, and the results are presented in the paragraphs which follow.

Plate Specimen and Support Structure

A plate size of 8" by 10" was selected as the platform of the rectangular plate(s) to be vibrated. It was desired to use a relatively thin plate, to produce sufficiently low resonant frequencies. Stainless steel (302 or 304 stainless) was selected as the plate material, because of its high-temperature capability and availability from suppliers.

The main problem to be overcome in designing the supporting structure for the plate was to prevent thermal buckling.* It was desirable to prevent buckling, because it results in considerable distortion of the vibration modes (i.e., the modes of a buckled plate do not coincide with those of an unloaded, isotropic plate). (From a pragmatic viewpoint, when the vibration modes were recorded at 1000°F, we wanted to be sure they looked like plate modes and were credible results.)

Thermal buckling was avoided by using soft tension springs** to apply an in-plane preload to the plate. The design is shown schematically in Figure 22, and the actual structure is shown during assembly in Figures 23 and 24. When the plate was heated, thermal expansion occurred in the plane of the plate, and this expansion was "taken up" by the tension springs around the edges of the plate. During initial tests of this design, local buckling (i.e., crinkling) took place near the individual support clamps (which acted as heat sinks). This problem was overcome by making saw-cuts through the plate between the clamps, and inserting mica washers as thermal insulation to inhibit heat flow into the clamps. With this design, and a plate thickness h = .047", the stainless steel plate withstood temperatures as high as 1200°F without buckling.

Care was taken to achieve fairly uniform boundary conditions at the edges of the plate. This was accomplished by machining vee grooves part-way through the plate, to approximate the case of simply-supported

*It would have been possible to allow the plate to buckle, and then vibrate it to find the resonant modes of a buckled plate; however, this was not the objective of the contract.
**Stainless steel springs were used, to prevent relaxation at high-temperatures.

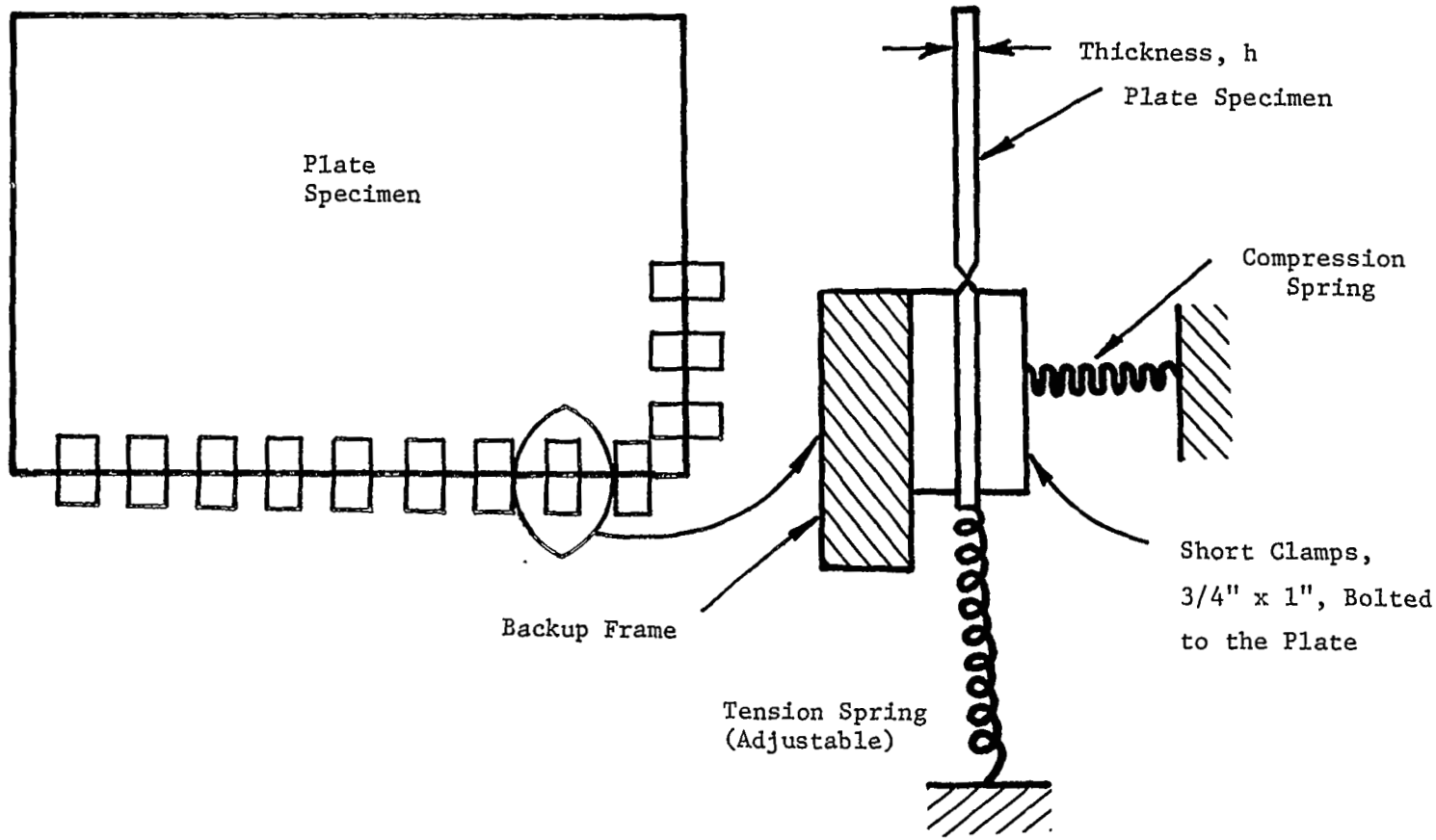

Figure 22 - Plate Edge Support and Tension Springs

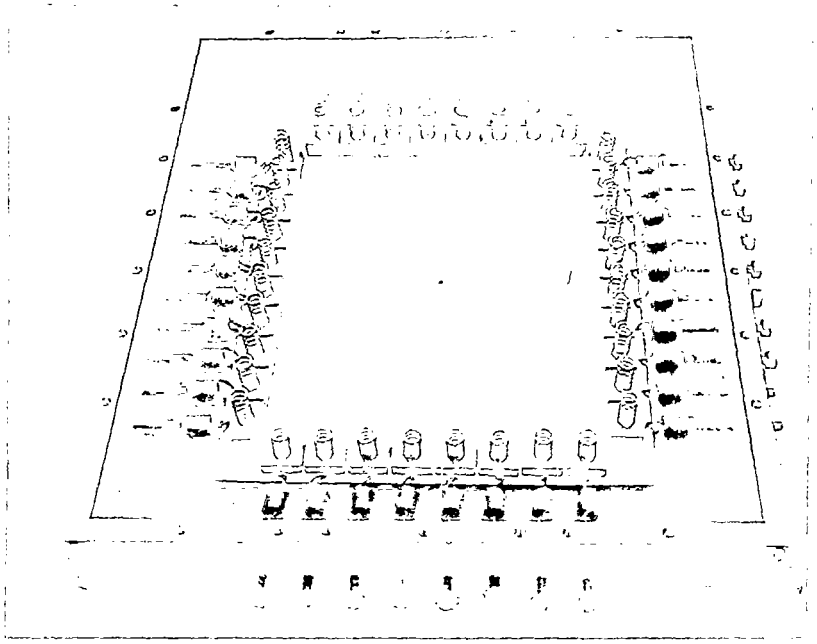

Figure 23 - Plate and Support Showing Tension Springs

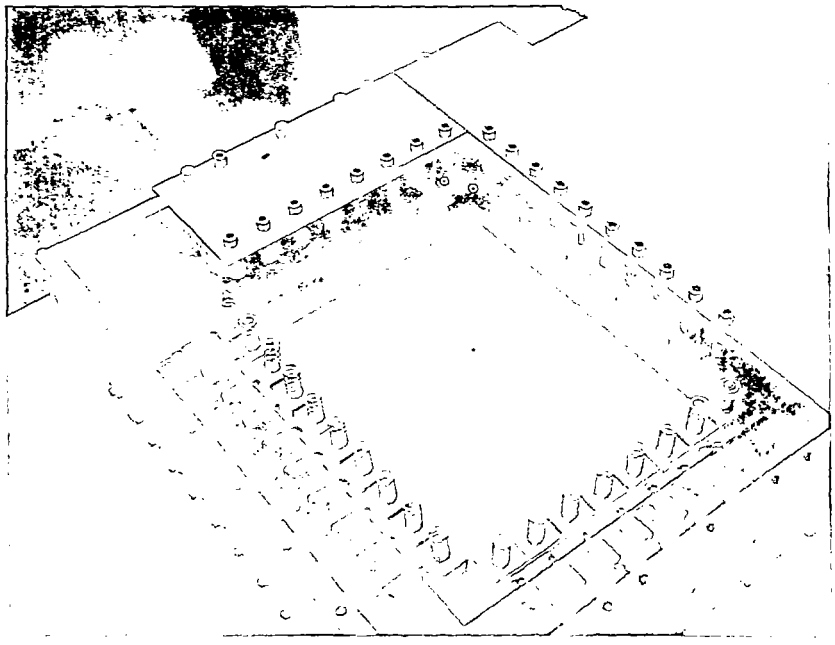

Figure 24- Plate and Support Partly Assembled

boundaries (see Figure 25). Mode shapes were recorded holographically at room temperature which demonstrated (by their symmetry) the uniformity of the boundary conditions. (For example, see Figures 9, 10 and 26).

Excitation and Detection of Resonance

The related problems of excitation and detection of resonance are fundamental to vibration studies. In the experiments reported herein, the problem was complicated by the high-temperature (1000°-2000°F). High-temperature piezoelectric transducers are available, and attempts were made to use them (i) to vibrate the plate, and (ii) to detect the plate vibrations. (Piezoelectric excitation has certain advantages, and this method had been used in related holographic studies, Ref. 10 and 17). The piezoelectric constants of available high-temperature crystals are very small, however, and the technique proved marginal, at best.

The excitation problem was solved directly by using a standard 25-lb. electrodynamic shaker, which drove the plate by means of a stinger and spring arrangement (See Figure 27). The spring (which contacted the plate) was made of stainless steel and was relatively soft to avoid distorting the plate vibration modes. It was not certain that the spring would continue to transmit forces when the plate was heated, since relaxation and creep frequently occur in springs at elevated temperatures. However, this arrangement operated successfully and was later used in the 2000°F tests. (From the standpoint of vibration testing and subsequent designs, this discussion serves to point out that excitation of the heated structure may present problems, and electro-mechanical driving through springs is a possible solution.)

The detection of resonance was also complicated by the high-temperatures. Special piezoelectric crystals (with high Curie temperatures) were tried without success. A condenser microphone was tried, but the tone from the shaker was detected by the mike and masked the plate response. (Furthermore, it was necessary to place the microphone near the heated plate, and it might not have survived the associated thermal input.) Capacitor pick-ups for detecting resonance can reportedly be operated at 2000°F, and they were considered. However, the detection problem was solved by using a Bently-Nevada inductance-type transducer*, which is rated by the manufacturer to operate at 1300°F.

This transducer responds to the plate displacement, provides a strong output signal, and has good frequency-response characteristics. With the associated electronics, the transducer produced a sinusoidal signal in-phase with the plate displacement, A $\sin\omega t$. The fact that the output from the transducer was in-phase with the motion of the plate was necessary for purposes of synchronizing the laser pulses with the plate vibration. With respect to future experiments of this type, the test designer should note that adequate frequency-response of the transducer-electronics (with constant phase-lags preferably zero) is necessary for proper synchronization of the laser. Details of the timing technique are given in subsequent paragraphs.

*Model 350TM24

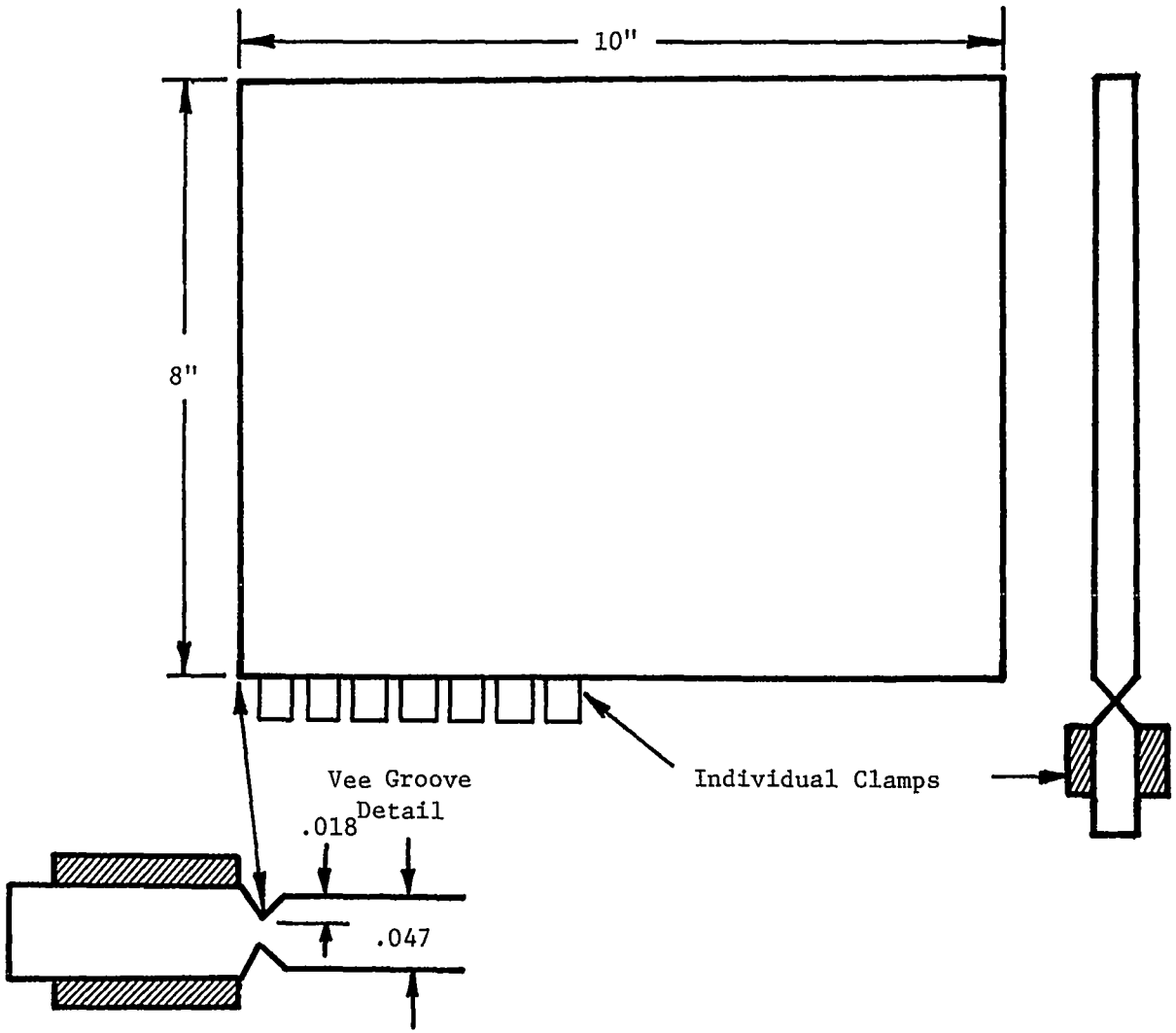

Figure 25 - Plate Planform and Groove Details

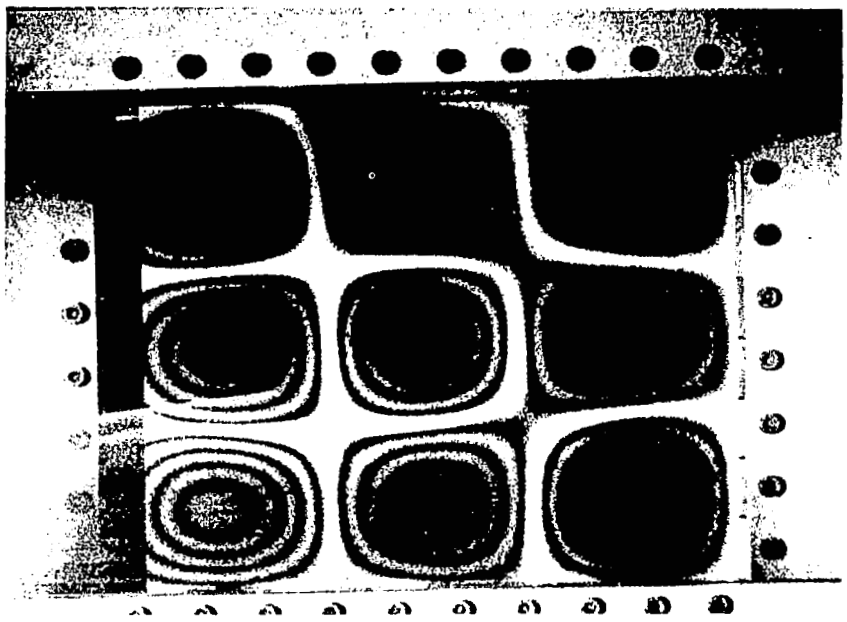

Figure 26: Time-average interferogram of the 3 x 3 mode (f = 994 cps)

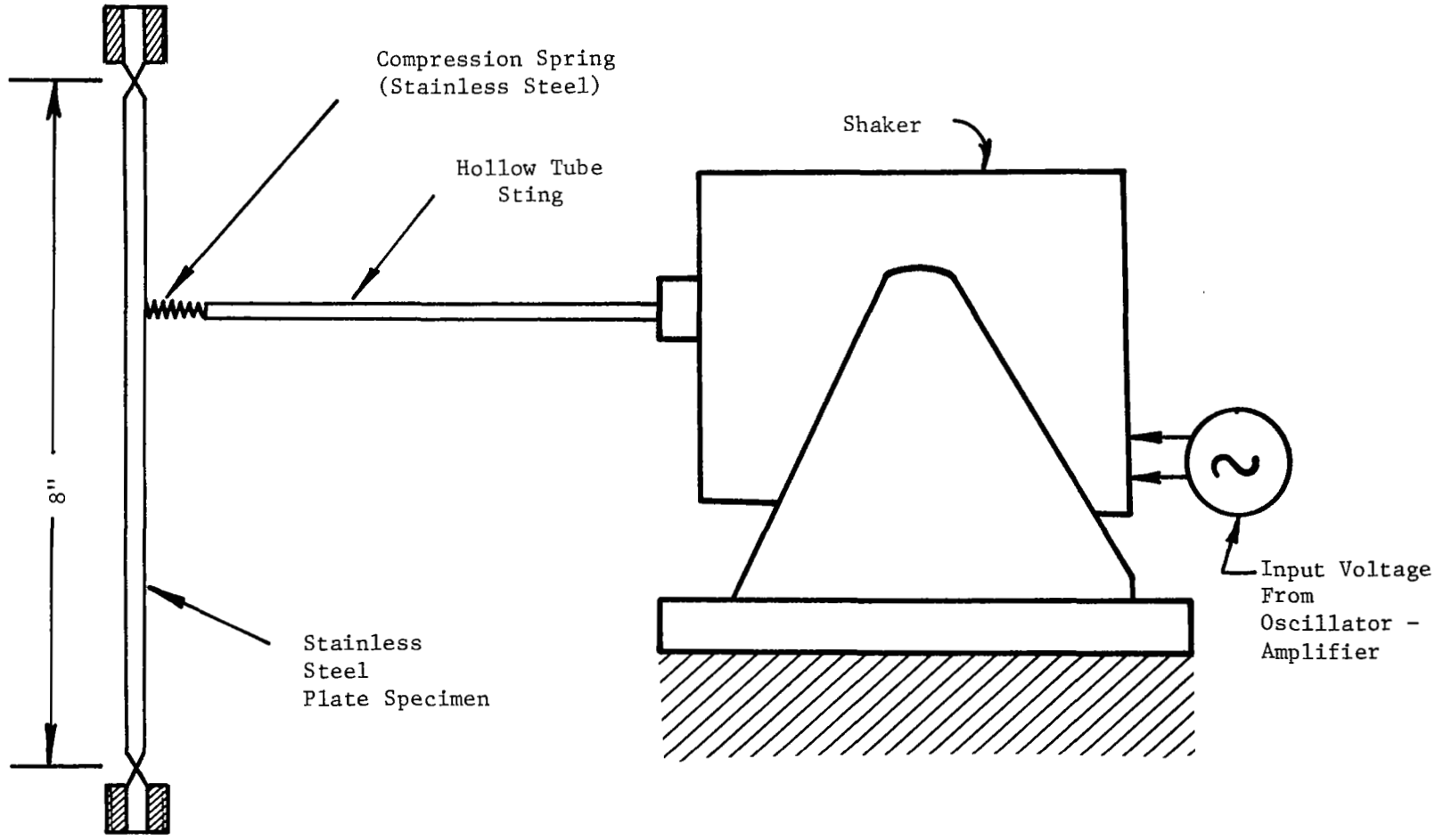

Figure 27 - Schematic Diagram of Excitation System

Experimental Set-Up

A schematic diagram of the experimental set-up is shown in Figure 28. An overall view showing the actual equipment is given in Figure 29. Referring to Figure 29, a standard oscillator-amplifier arrangement was used to drive the electrodynamic shaker at the desired amplitude and frequency. An electronic counter was used to measure the frequency of the input signal. The displacement transducer (which was used to monitor the plate response) was positioned in the lower left-hand quadrant of the plate (cf. Figures 9 and 10). The oscillator, counter, and transducer-related equipment are grouped in the area labelled "Electronics" in Figure 29.

The temperature of the plate was monitored by a chrome-alumel thermocouple welded to the plate surface in the lower right hand quadrant. The thermocouple output was read with a standard millivoltmeter designed for such applications. Light baffles (large aluminum sheets) were used to prevent the light from the radiant quartz heaters from reaching the hologram plate. (The hologram is represented by a white card in the center of Figure 29.)

Two quartz heat lamps were mounted directly behind the plate, about an inch or so away from its surface. A standard ther-mac control unit was used to provide manual adjustment of the voltage to the heat lamps. The heat lamps are shown in Figure 30, with the sting from the shaker passing between them. A photograph showing the sting (with the stainless-steel coil spring at its end) is given in Figure 31. Note that the input force (supplied through the spring) was located <u>off</u> the centerlines (i.e., the lines of symmetry) of the plate. This arrangement was used to allow adequate excitation of both the symmetric and anti-symmetric modes.

The optical arrangement used to make the holograms is shown schematically in Figure 32. The hologram and object beam were arranged such that the illumination and viewing angles θ_i and θ_v were small (e.g., less than 10 degrees; cf. Figure 6). This results in the case of "normal viewing and illumination" discussed with respect to Equation (2-15). The pulsed ruby laser used in these experiments is shown in Figure 33 along with its control units. This laser was built at TRW Systems and has the capability of producing multiple light pulses (at 6943Å) where the time between pulses (Δt) is individually adjustable within the range

$$1\ \mu s \leq \Delta t \leq 500\ \mu s \qquad (3\text{-}9)$$

mentioned previously in Section 3.0. The multiple pulses produced in this fashion are <u>mutually coherent</u>, which is a necessary requirement for holographic interferometry. (For a discussion of coherence and interferometry, see Ref. 26).

The synchronization of the laser pulses with the plate vibration ($A \sin\omega t$) was accomplished electronically as discussed in the following paragraphs.

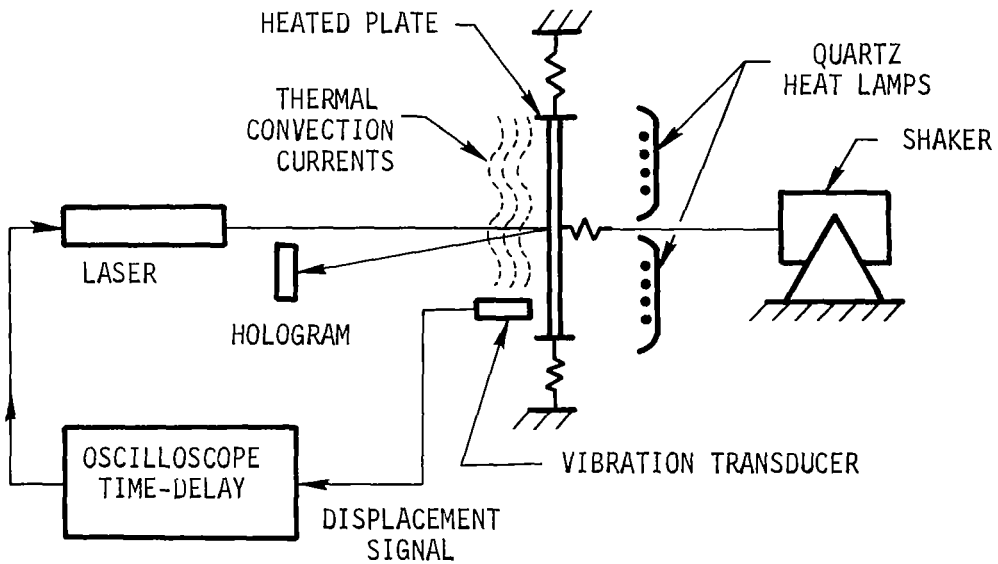

Figure 28: SCHEMATIC OF THE EXPERIMENTAL SET-UP
(HEATED PLATE, VIBRATION TEST 1000°F)

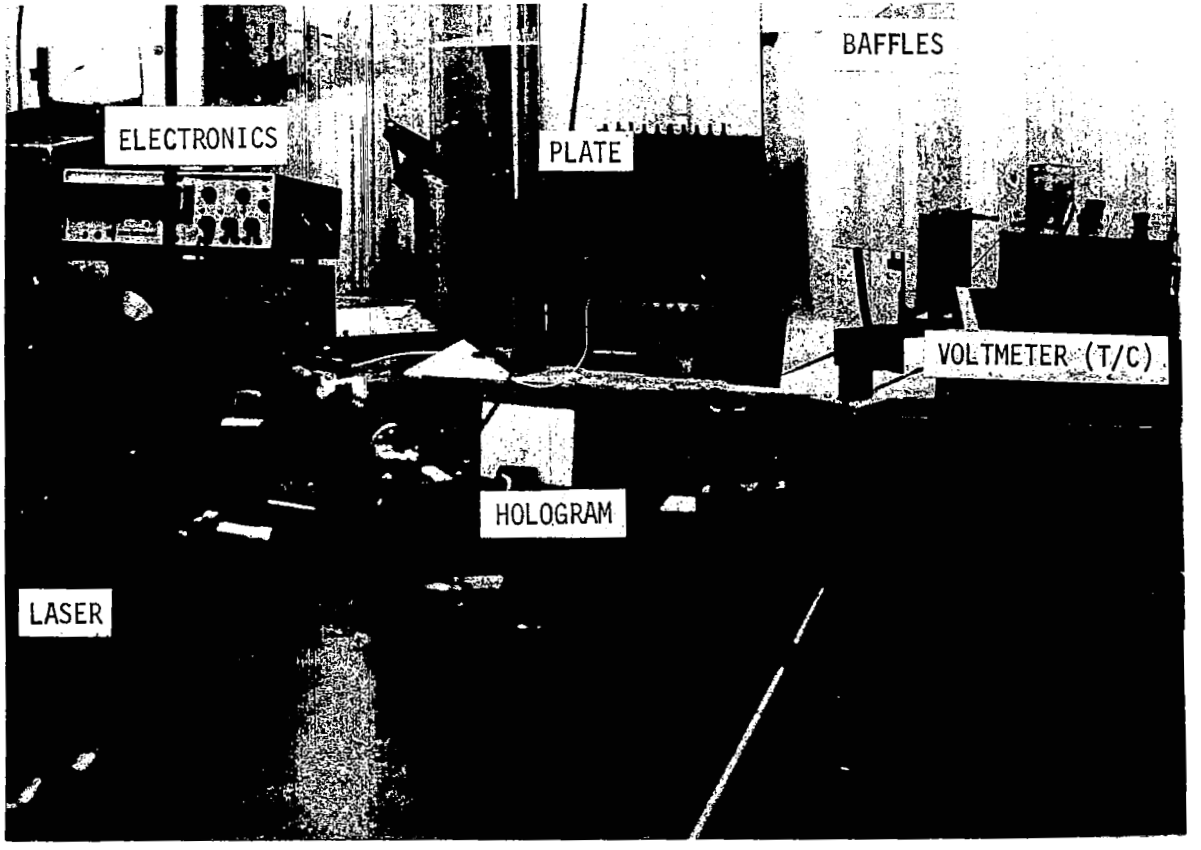

Figure 29 - Overall View of Experimental Set-Up, 1000°F Test

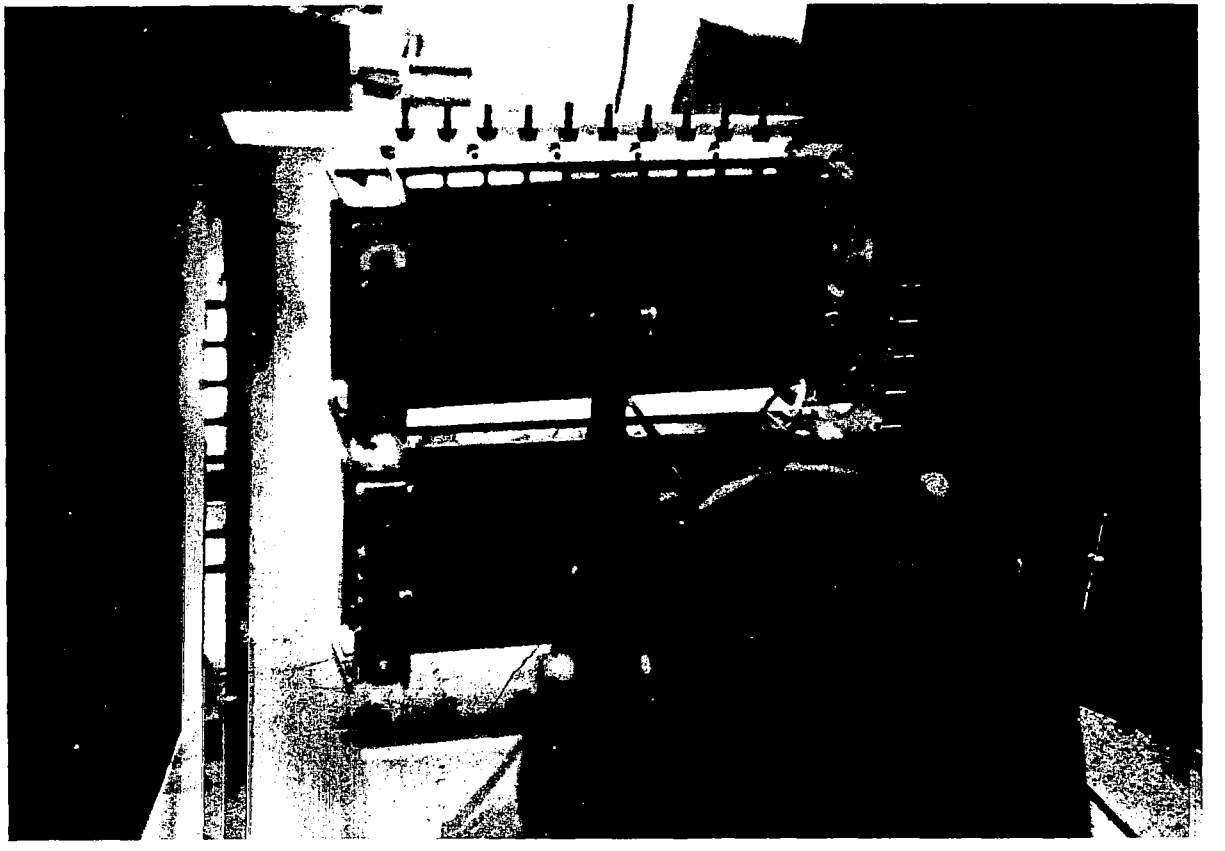

Figure 30 - Photograph Showing Heat Lamps
and Shaker Behind the Plate (1000°F Test)

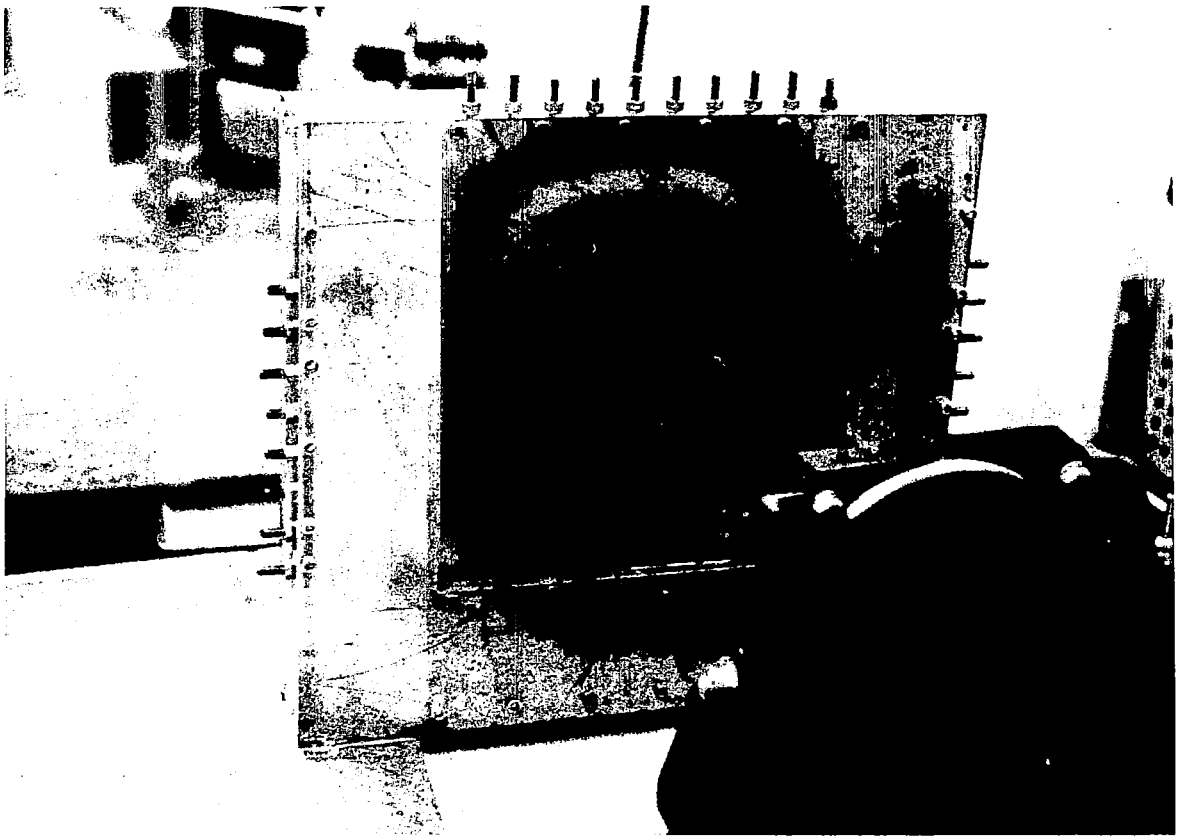

Figure 31 - Photograph Showing Shaker, Drive Rod,
and Compression Spring to Excite Vibrations

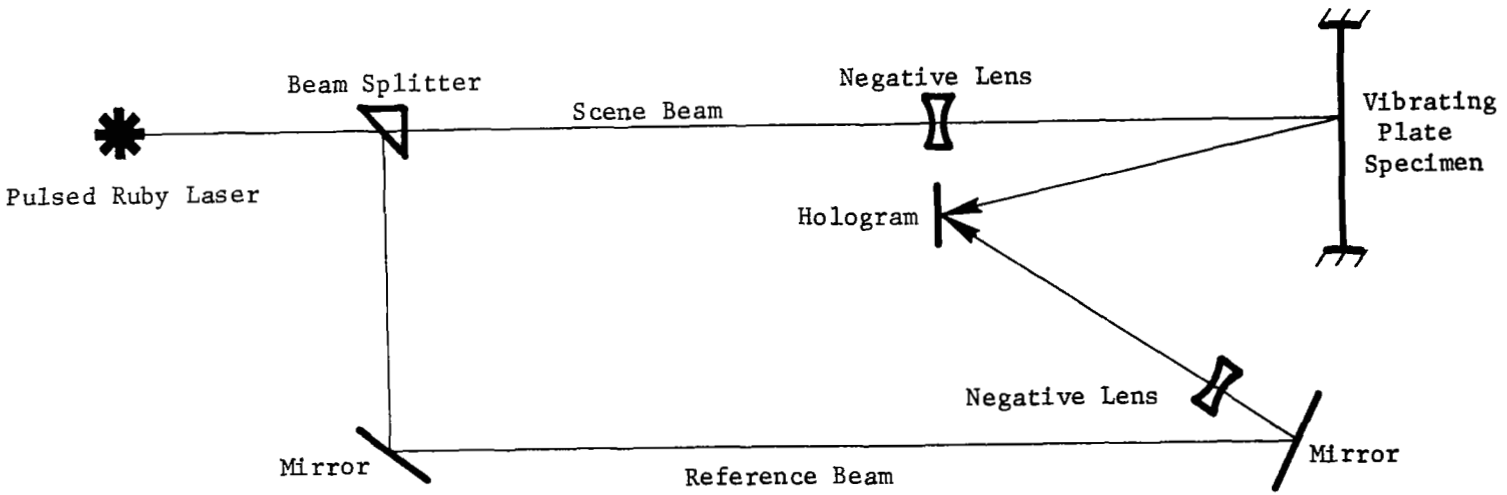

Figure 32 - Basic Optical Elements for Pulsed Laser Vibration Survey

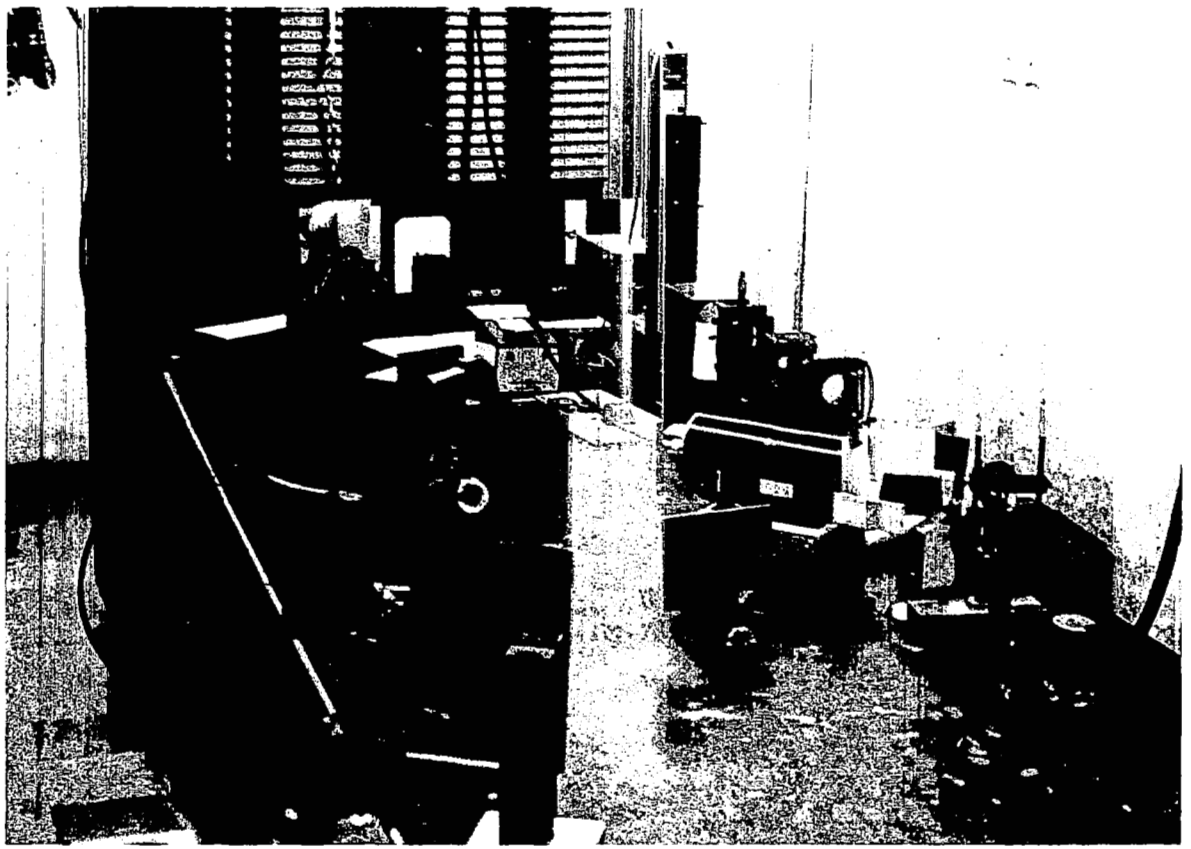

Figure 33 - Pulsed Ruby Laser, Optics, and Control Units

Timing of the Laser Pulses

The electrical connections of the equipment used to drive the plate to resonance and monitor its response are shown schematically in Figure 34. Both the driving and the motion sensor signals were displayed simultaneously on a Tektronix 535A oscilloscope, employing a 1A1 plug-in using the chopped mode. (In this mode, to achieve a stable display, a special connection was required between the Channel 1 Trigger Out connector on the plug-in and the External Trigger terminal for the time base used). To detect the peak of a resonance, the driving oscillator frequency was adjusted to give maximum amplitude from the motion pick up.

Display of the signals in the manner described also provided a convenient means for synchronizing the laser output to the plate motion. The laser required three trigger pulses. The first trigger pulse initiated the flash lamp discharge to optically pump the ruby rod.* The second and third pulses triggered the Pockels Cell Q-Switch twice in succession, to produce the two laser light pulses required for differential holographic interferometry. The time between the first and second pulses was long enough for sufficient population inversion to accumulate in the ruby. Both the second and third pulses were derived internally in the laser system from the first trigger pulse. They were set to occur 850 and 900 microseconds, respectively, after the first. This setting produced the desired 50 μsec time-delay between laser pulses.

The method for synchronizing the laser output to the plate motion involved operation of the 535A display scope in the "B Intensified by A" mode. The sweep rate of the display was determined by the B Time Base and a portion of the trace was brightened for a time determined by the A Time Base. The start of the intensified portion was set by the Delay Time Multiplier dial. Figure 35 is a photograph of the vibration wave-forms displayed in this mode. Using this mode of the scope, any desired portion of the motion waveform could be intensified. Coincident with the beginning of the intensified portion of the sweep, an output gate pulse appeared at the A-Gate terminals of the scope. The rise of this gate pulse was used to trigger the laser flash lamps (Figure 36 schematically shows the hook-up).

By manipulation of the A Time Base, the intensified portion of the waveform was set to be about 875 microseconds long, a time falling half-way between the two times set for the Q-Switch pulses. Hence, the start of the intensified portion was coincident with the firing of the laser flash lamps, and the end of the bright portion fell about mid-way between the two laser output pulses. It was an easy matter then to set the laser light pulses to occur at any point on the motion waveform. The delay time multiplier dial was simply adjusted so that the end of the intensified portion fell at the desired point on the vibration waveforms. (For example, see Figure 35).

*For a discussion of the laser, Pockels Cell, etc., see Ref. 17.

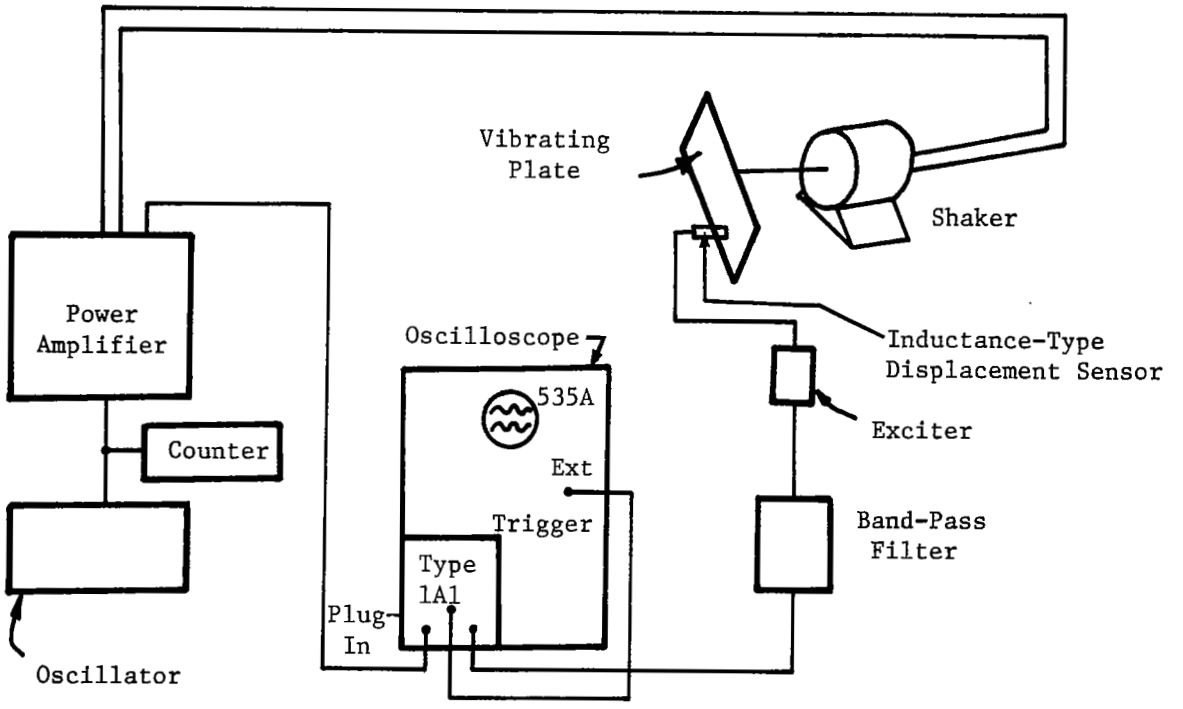

Figure 34: Schematic of the electrical arrangement to excite and monitor the plate vibration modes

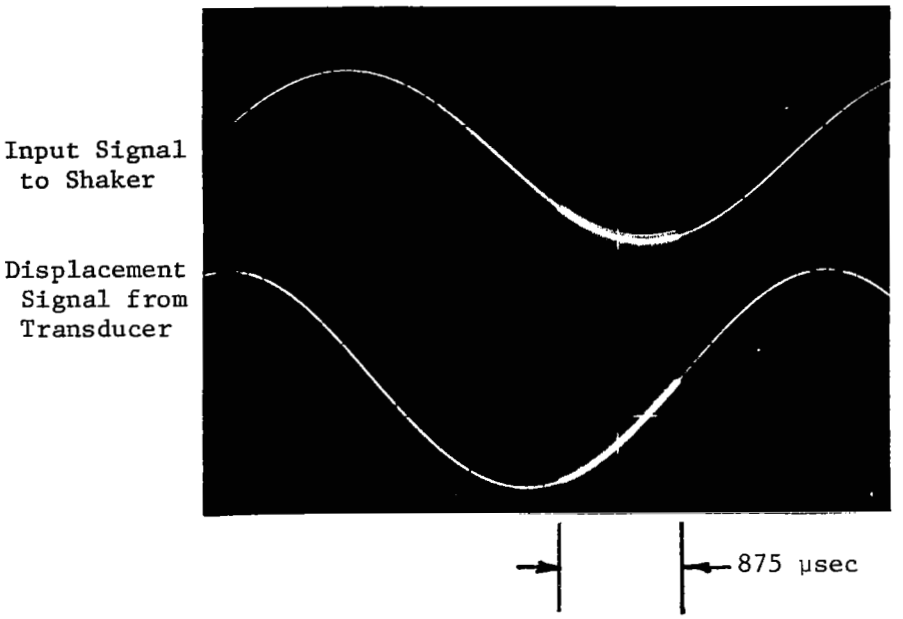

Figure 35(a): Oscilloscope trace showing "A" intensified by "B"

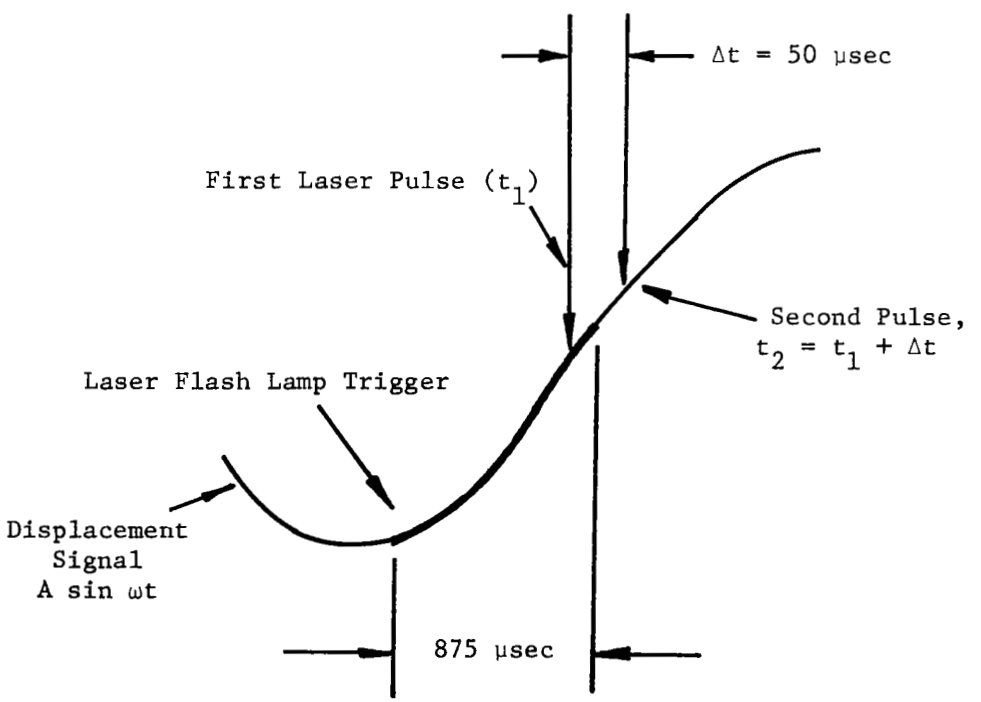

Figure 35(b): Timing of the laser pulses with the plate vibration

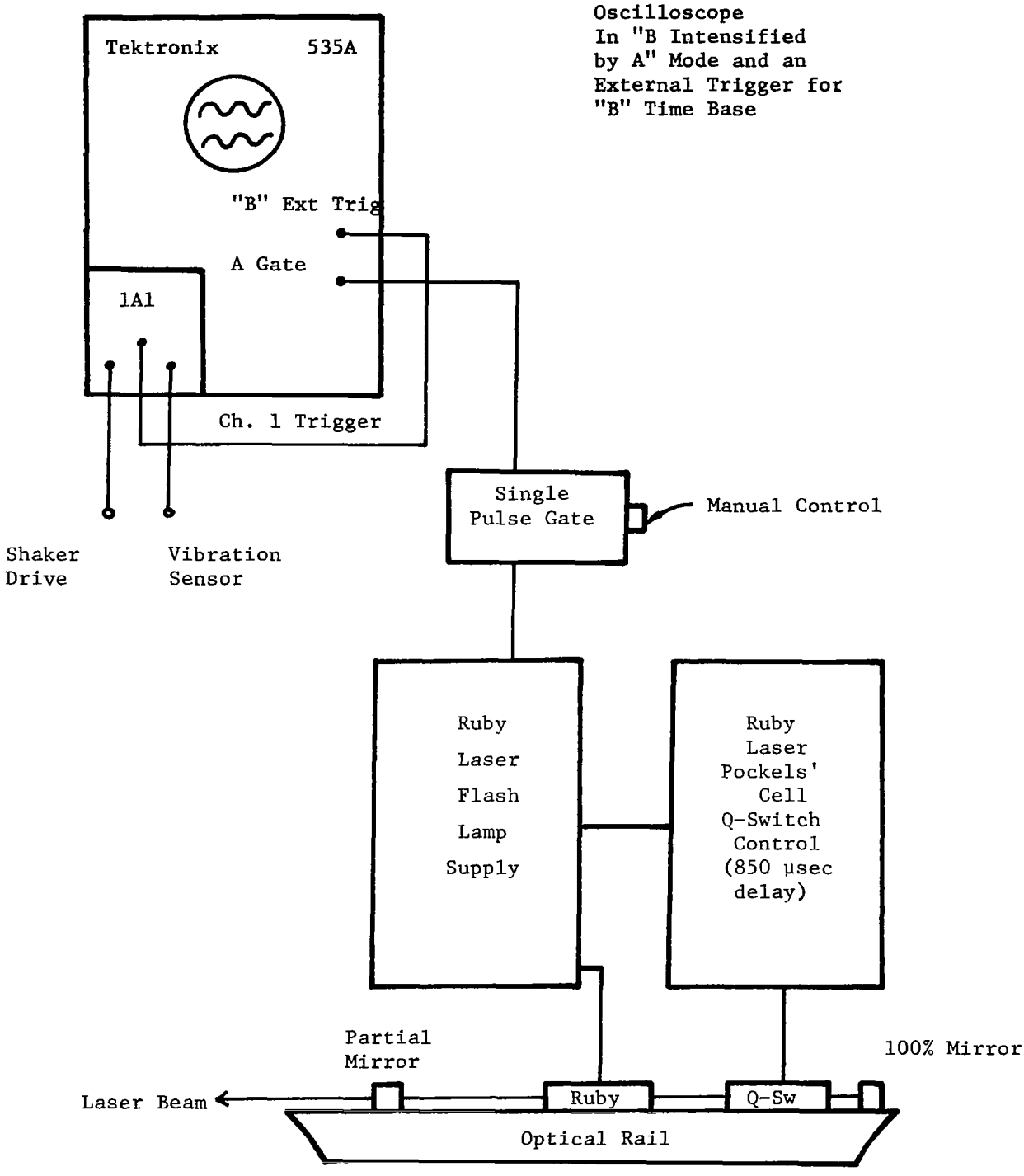

Figure 36 - Schematic of the Arrangement
Used to Obtain Laser Pulses
Synchronized to the Plate Motion

The 535A oscilloscope used in the set up had one short-coming in that it lacked a single-sweep feature. Consequently, a continuous train of pulses was present at the A Gate terminals while the plate was in motion. Such a continuous repetition of pulses would have resulted in damage to the laser circuits even while the laser storage capacitors were uncharged. Hence, a single pulse gate was included in the input leg to the laser (another oscilloscope having a single sweep feature, was used). Manual tripping of the gate allowed a single trigger pulse to reach the laser from the 535A oscilloscope on command, which activated the firing sequence and exposed the hologram.

Some Preliminary Results

Room temperature experiments were conducted first to verify the electronic timing arrangement just presented. Several pulsed differential holograms were made at room temperature and compared with time-average holograms of the same modes. Typical examples are shown in Figures 37 through 40, which gave us confidence in the differential method. As a demonstration that the differential technique would work at high-temperature, a hologram was made with the flame from a cigarette lighter in the path of the object beam. The result is given in Figure 41, which shows the fundamental mode of the plate, unaffected by the turbulence from the flame. (The lighter is barely visible in Figure 41). This successful demonstration was followed by the full-scale, high-temperature tests described in the following section.

Test Procedure

First, a brief resonance survey was conducted at room temperature, with the displacement pick-up used as a detector. Several modes were detected, ranging in frequency from 180 cps (the fundamental mode) to 745 cps. The quartz lamps were then turned on, and the thermocouple allowed to stablize at a temperature of 255°F, whereupon differential holograms were made of the fundamental mode (Figure 42) and the 1 x 2 mode (Figure 43).

The procedure used in conducting a test and making the holograms was

(1) Vary the excitation frequency of the shaker until a particular resonance was detected with the displacement transducer. Record the resonant frequency, as displayed by the counter.

(2) Using the sinusoidal displacement signal displayed on the oscilloscope, adjust the time-delay to fire the laser at the time of maximum velocity of the resonating plate.

(3) Load the (unexposed) photographic plate into its holder, then charge and fire the laser, giving the necessary differential hologram.

(4) Develop the hologram and reconstruct the images to see if the vibration mode in question had been adequately recorded.

(5) Adjust the excitation frequency to locate the next resonance and repeat steps 1 through 4 just presented.

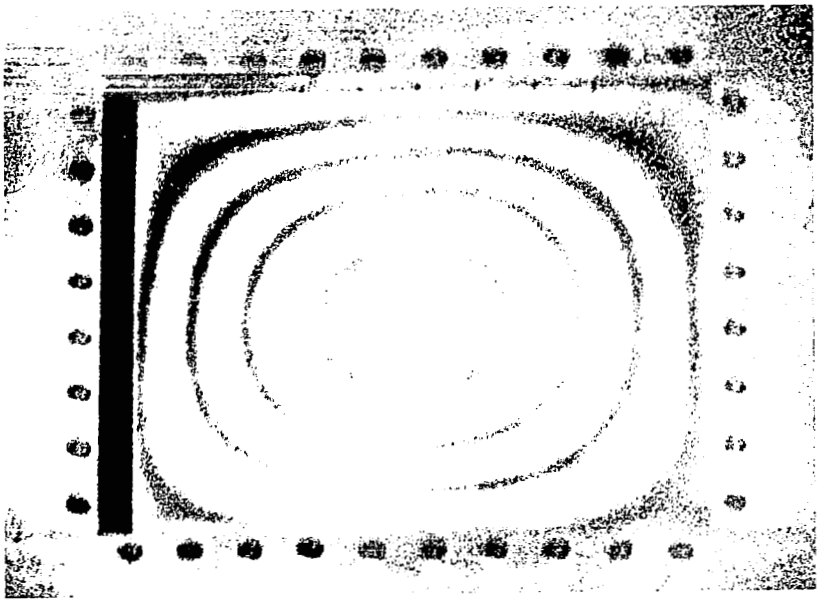

Figure 37(a): Pulsed differential hologram
of the First Mode (m = 1, n = 1) f = 122 cps

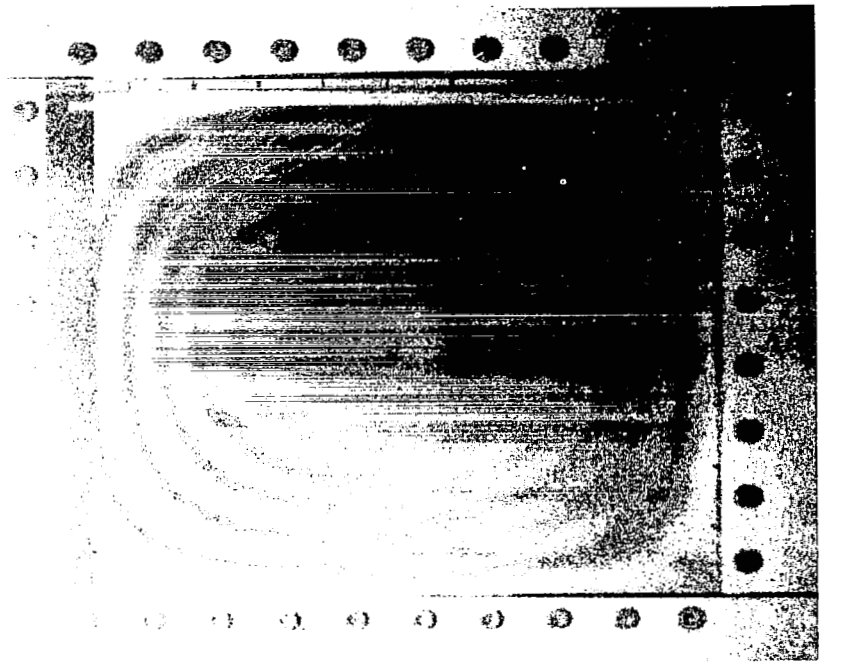

Figure 37(b): Time-average interferogram of the
First Mode (m = 1, n = 1) f = 128 cps

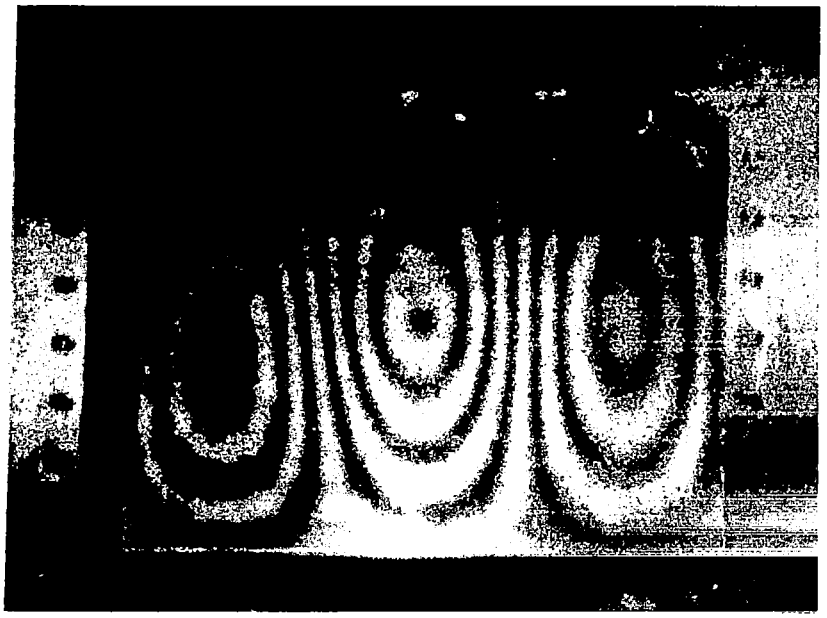

Figure 38(a): Pulsed differential hologram of the 3 x 1 Mode (f = 465 cps)

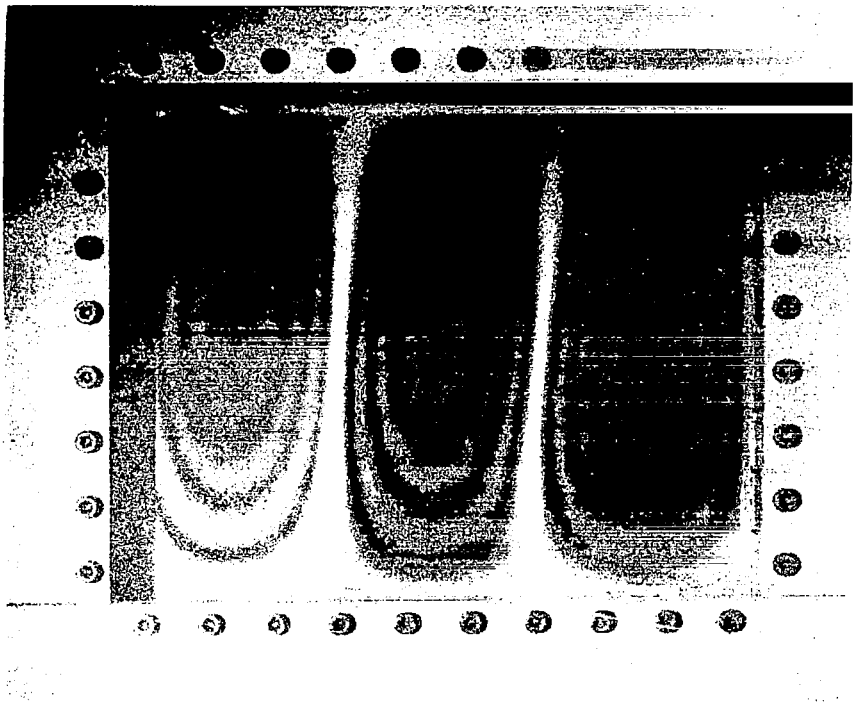

Figure 38(b): Time-Average Interferogram of the 3 x 1 Mode (f = 467 cps)

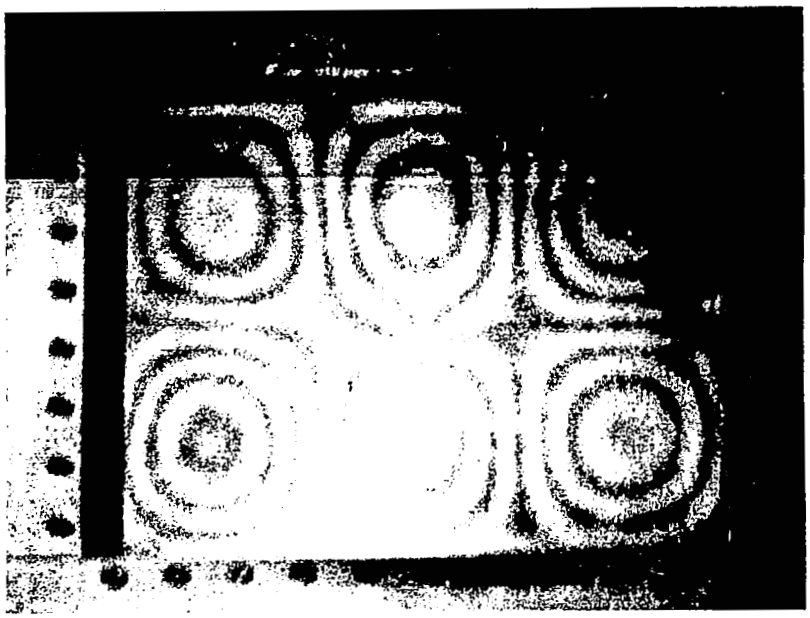

Figure 39(a): Pulsed differential hologram of the 3 x 2 Mode (f = 673 cps)

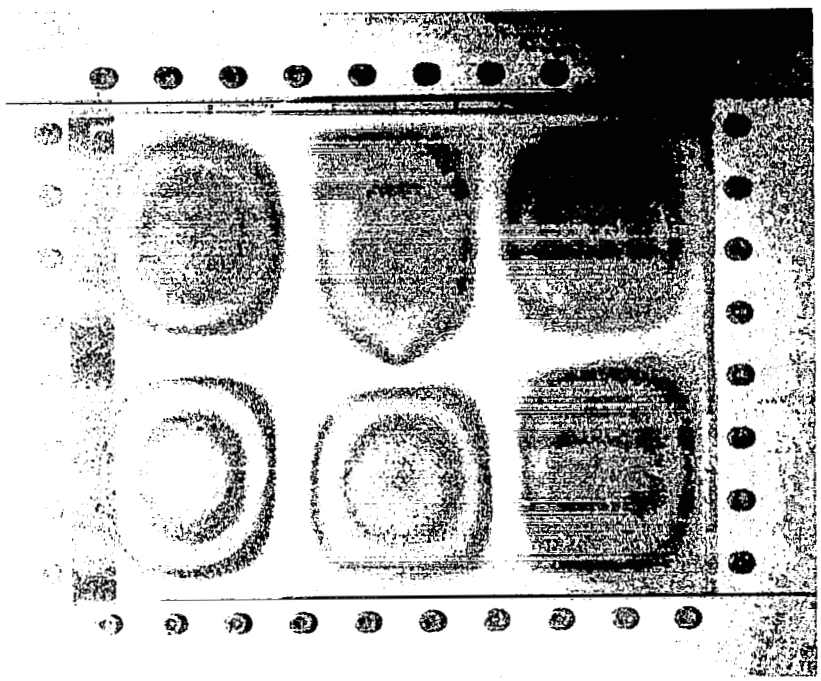

Figure 39(b): Time-Average Interferogram of the 3 x 2 Mode (f = 674 cps)

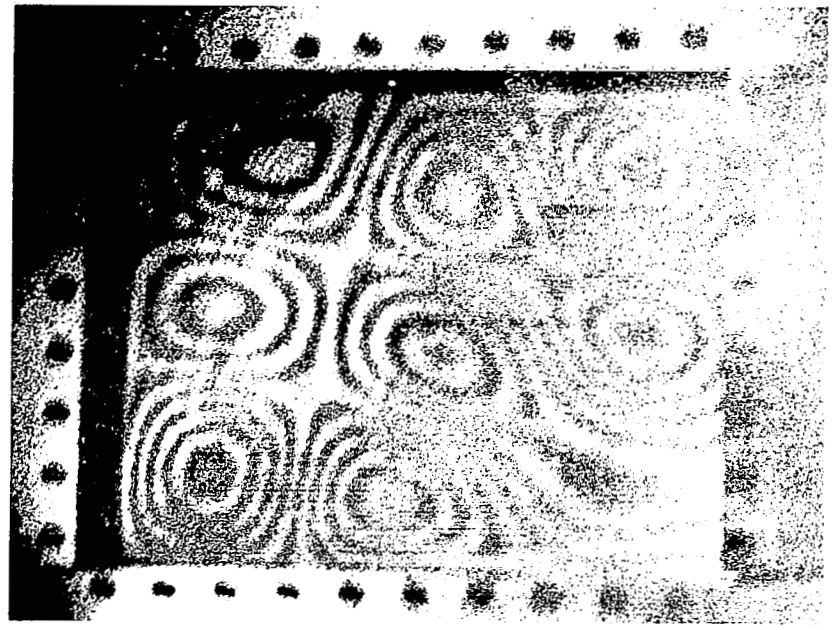

Figure 40(a): Pulsed differential hologram
of the 3 x 3 Mode (f = 1003 cps)

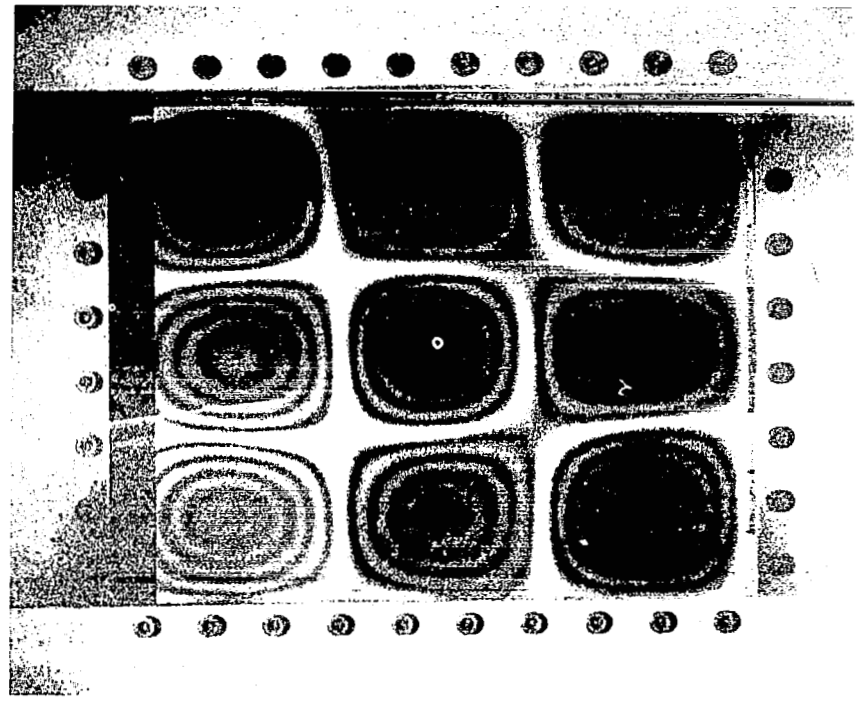

Figure 40(b): Time-Average Interferogram
of the 3 x 3 Mode (f = 994 cps)

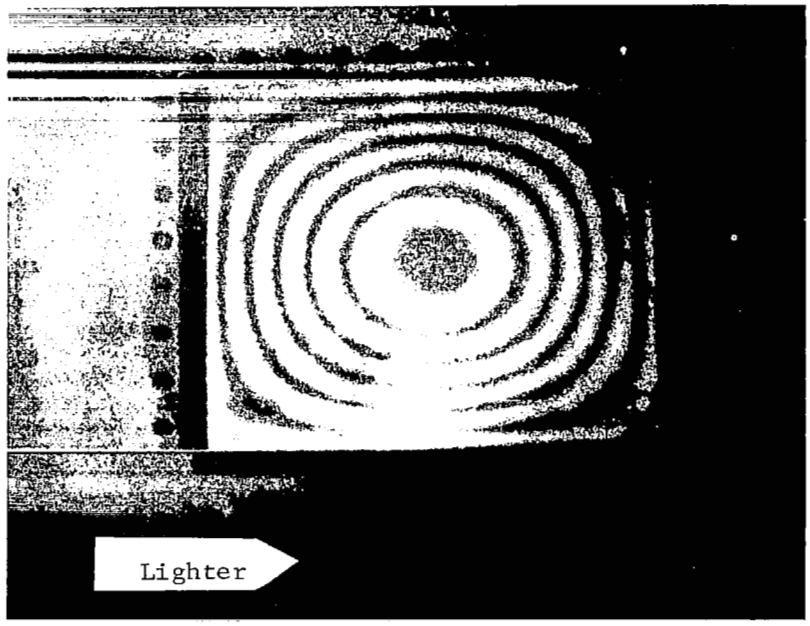

Figure 41 - Differential Hologram of the Fundamental Mode, Undisturbed by Thermal Convection Currents. (Lighted cigarette lighter in foreground; flame is not visible)

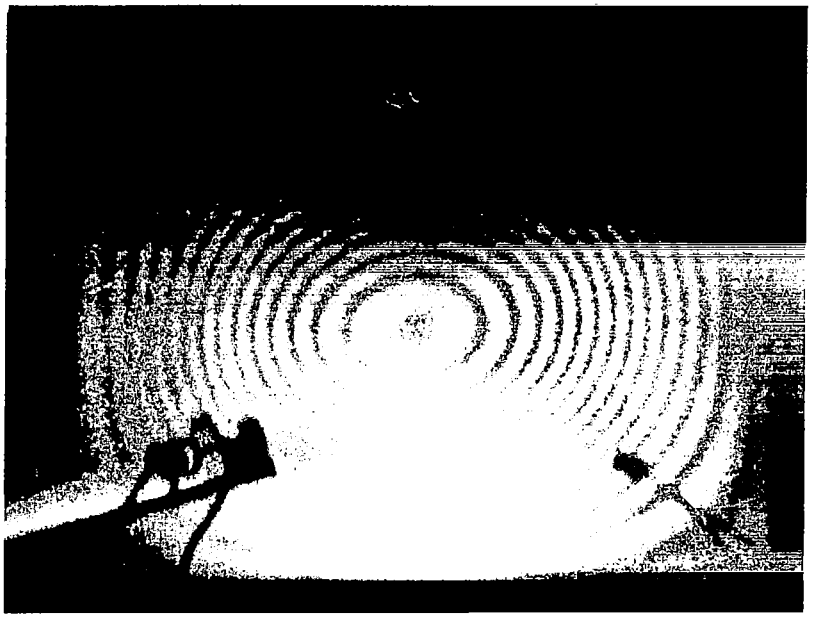

Figure 42 - Differential Hologram of the Fundamental Mode (1 x 1) at 225°F (f = 156 cps, Δt = 50 μs)

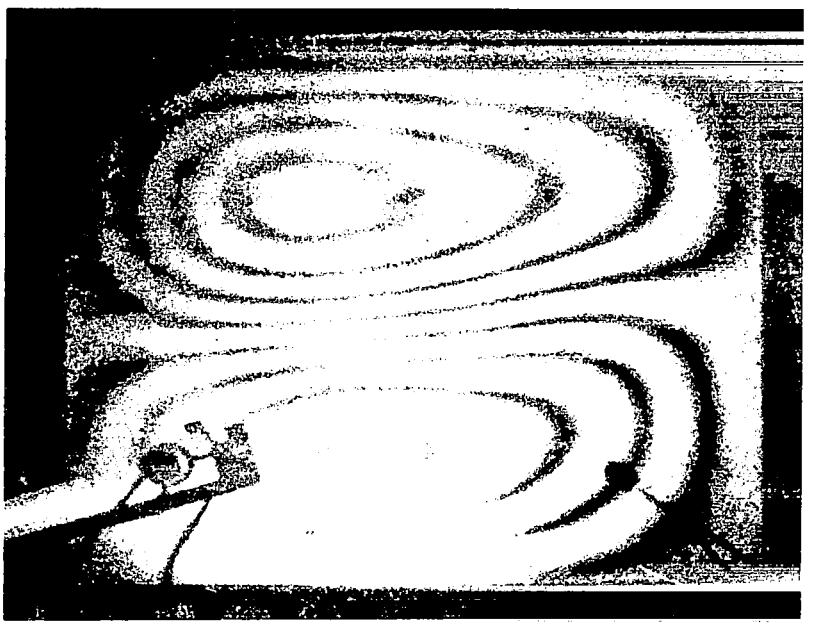

Figure 43 - Differential Hologram of the 1 x 2 Mode at 255°F (f = 346 cps, Δt = 50 μs)

(6) If an interferogram (produced in this fashion) does not contain enough fringes (e.g., no fringes form, or perhaps just one) the resonance can be excited again, and the vibration amplitude increased to obtain more fringe contours.

(7) When enough modes had been recorded at a particular temperature, more heat was applied to raise the temperature and the modal survey was repeated.

It should be noted that in this test procedure (Steps 1 through 7), the plate was allowed to reach thermal equilibrium before each modal survey. The thermocouple reading was recorded (when each hologram was made) and the thermal stability was such that the temperature varied by at most a few degrees ($\pm$5°F).

Using this test procedure, a few modes were recorded at intermediate temperatures of approximately 255°F, 515°F, and 708°. The corresponding interferograms are shown in Figures 44 through 47. Then the temperature was raised to 1040°F and a more detailed survey was conducted, resulting in the modes shown in Figures 48 through 55.

The time-delay used throughout these tests was 50 μs simply chosen because it was a convenient setting of the laser control unit. From a research standpoint, it would have been interesting to maintain a particular temperature (Θ = 1000°F, say) and then make differential holograms using larger-and-larger time-delays to determine when the thermal convection noise N(t) began to corrupt the hologram. (See the discussion of thermal noise and convection given in Section 3.0). Although the laser can be operated over a wide range of Δt , as illustrated in Figures 15 and 16, the mode shapes recorded at 1000°F using Δt = 50 μs appeared to be quite symmetrical, clean, and undistorted, which made it unnecessary to use another time-delay.

The high-temperature tests (ranging from 255° up to 1050°F) were conducted in a period of approximately four (4) hours of actual testing time. Approximately 40 differential holograms were made in this period, and mode shapes were successfully recorded on approximately two-thirds of the shots. Various minor problems contributed to give unsuccessful holograms, such as insufficient vibration amplitude at the high-frequencies ($\simeq$ 1000 cps), occasional mis-firing of the laser (one pulse, but not two), etc.

The final hologram of this test series was made of the fundamental mode using two single pulses of the laser, with a long time-delay (several seconds) between exposures. The first pulse was made at time t_1, and the second pulse was made at time $t_2 = t_1 + \Delta t + mT$ (i.e., an integral number of cycles mT later). The result is shown in Figure 56, which shows no contour fringes on the plate, despite the fact that it had been vibrating between exposures. The thermal convection noise N(t) prevented the interferogram from forming near the heated plate (See Equation 2-6). Note that black interference fringes did form on the support frame (around the 8" x 10" central opening) where the thermal convection was greatly reduced.

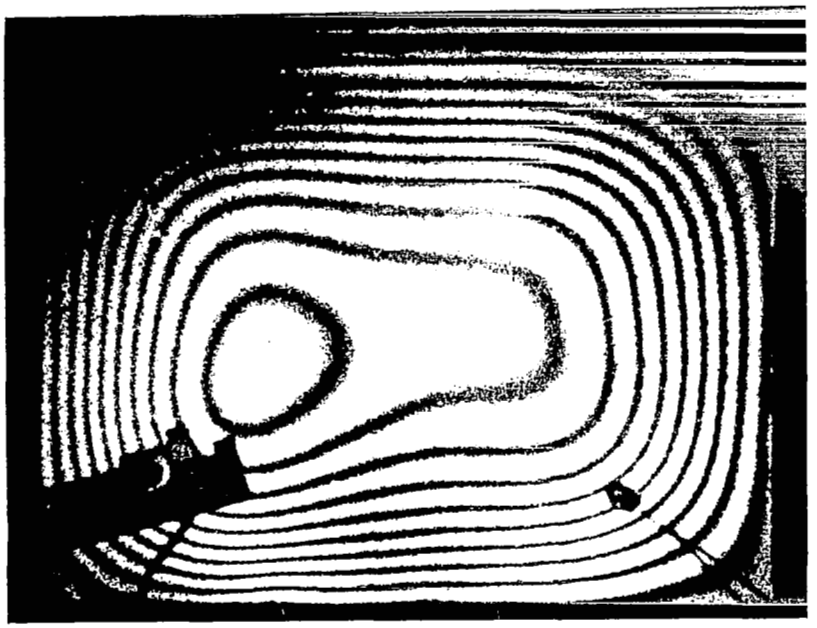

Figure 44: Differential hologram of the fundamental mode (1 x 1) at 514°F. (f = 230 cps, Δt = 50 μsec)

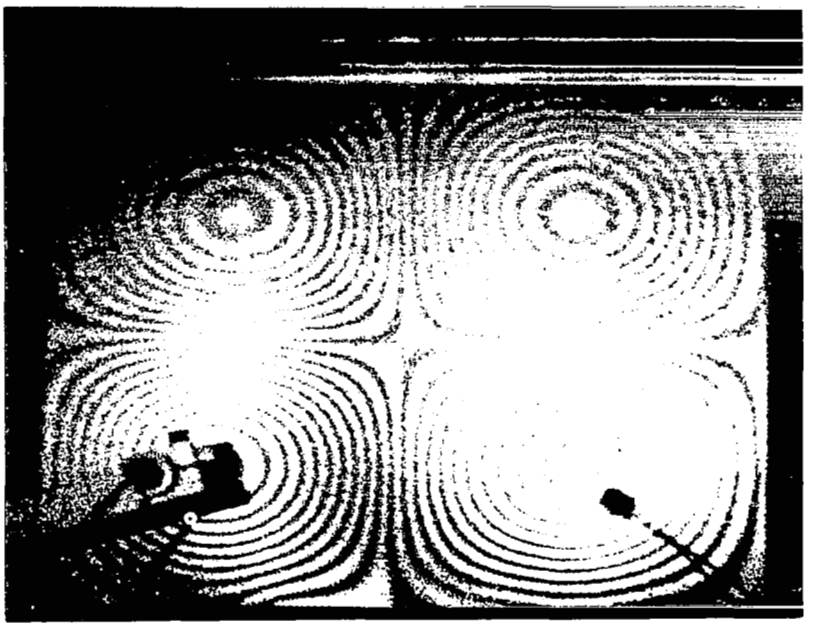

Figure 45: Differential hologram of the 2 x 2 mode at 515°F. (f = 492 cps, Δt = 50 μsec)

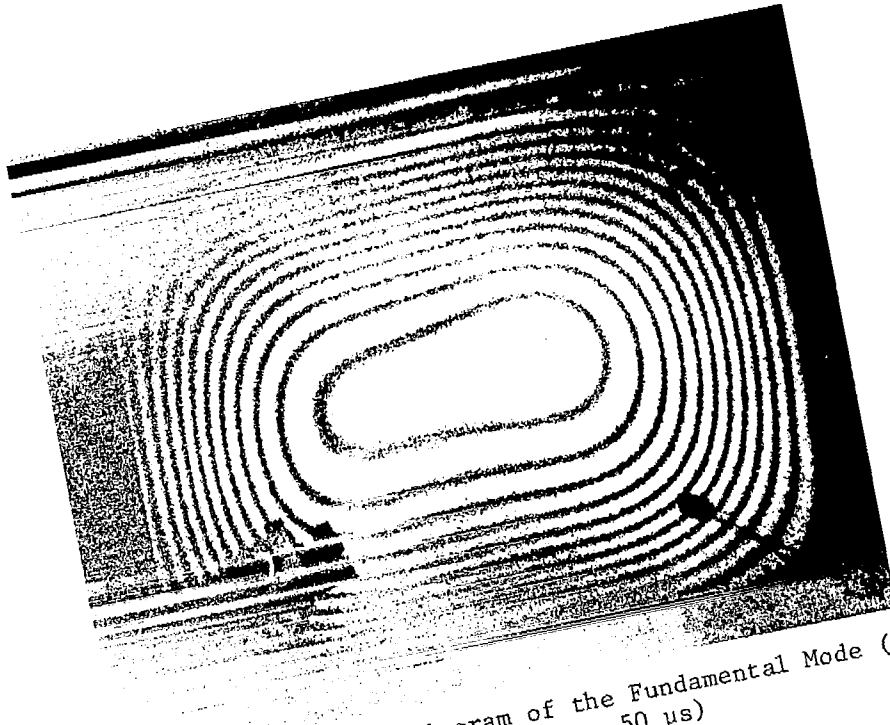

Figure 46 - Differential Hologram of the Fundamental Mode (1 x 1) at 708°F (f = 217 cps, Δt = 50 μs)

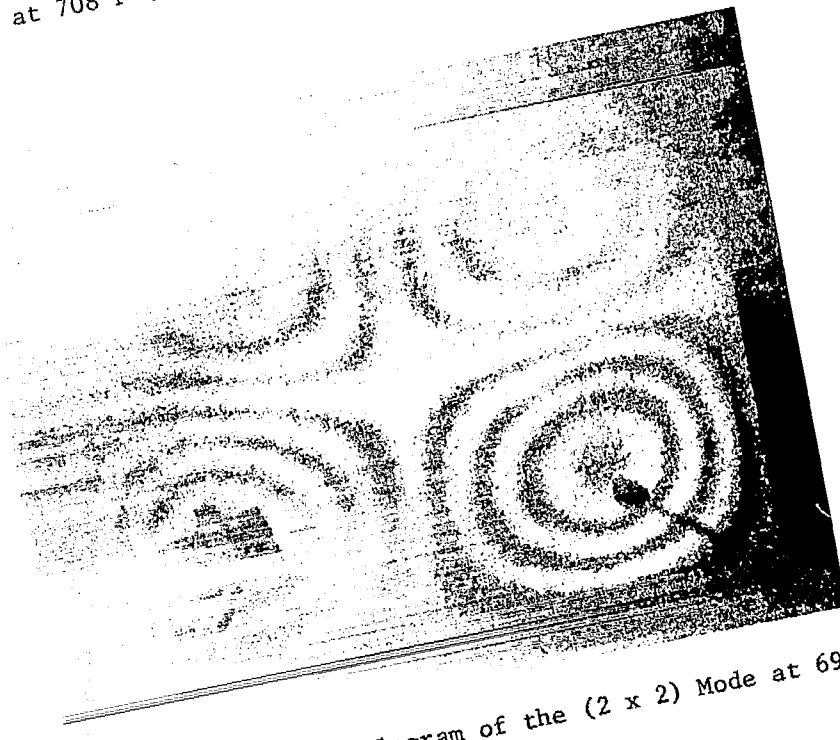

Figure 47 - Differential Hologram of the (2 x 2) Mode at 692°F (f = 489 cps, Δt = 50 μs)

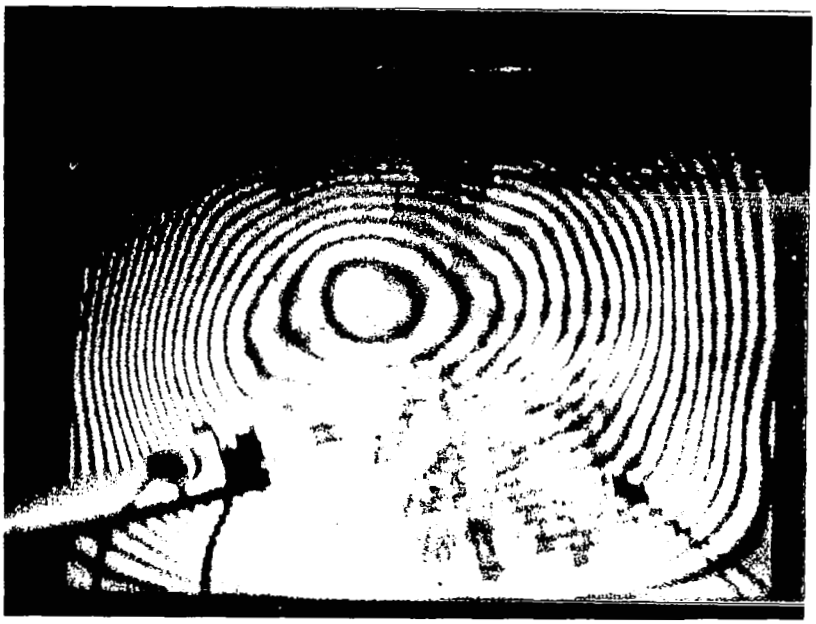

Figure 48 - Differential Hologram of the Fundamental Mode (1 x 1) at 1046°F. (f = 200 cps, Δt = 50 μs)

Figure 49 - Differential Hologram of the 2 x 1 Mode at 1049°F (f = 326 cps, Δt = 50 μs)

Figure 50 - Differential Hologram of a "Combination Mode" at 1053°F. (Looks like the 1 x 2 Mode Combined with the 2 x 1 Mode). (f = 324 cps, Δt = 50 μs)

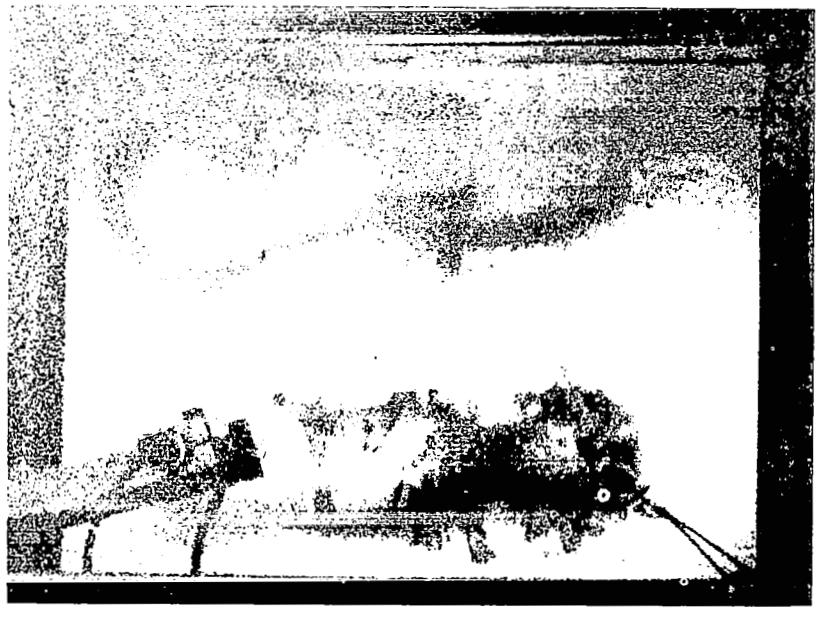

Figure 51 - Differential Hologram of the 1 x 2 Mode at 1056°F. (f = 332 cps, Δt = 50μs)

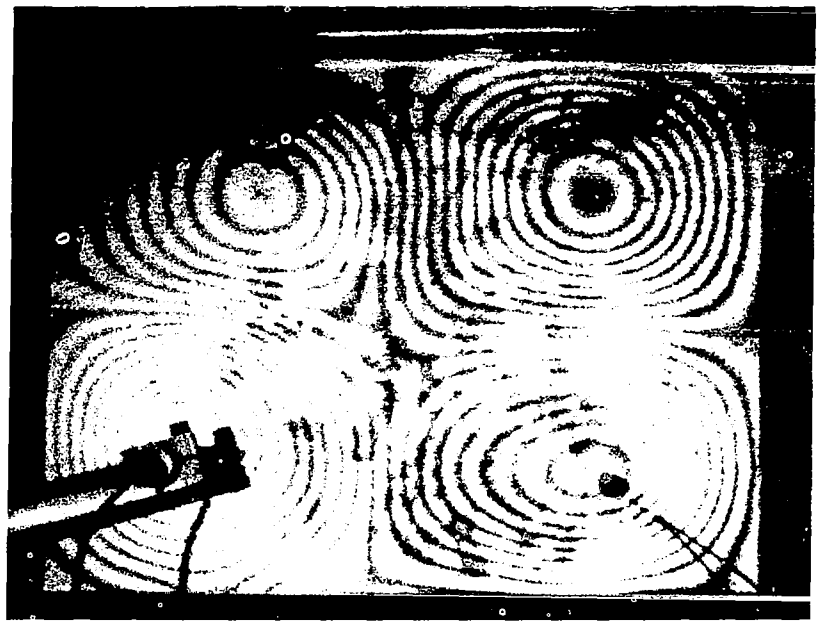

Figure 52 - Differential Hologram of the 2 x 2 Mode at 1040°F
(f = 506 cps, Δt = 50 μs)

Figure 53 - Differential Hologram of the 3 x 1 Mode at 1052°F
(f = 544 cps, Δt = 40 μs)

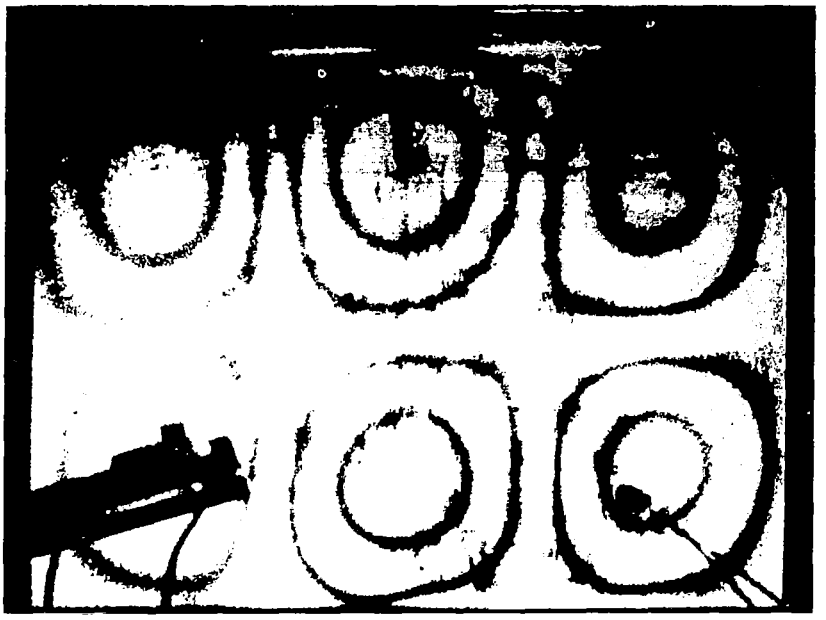

Figure 54 - Differential Hologram of the 3 x 2 Mode at 1050 °F
(f = 692 cps, Δt = 50 μs)

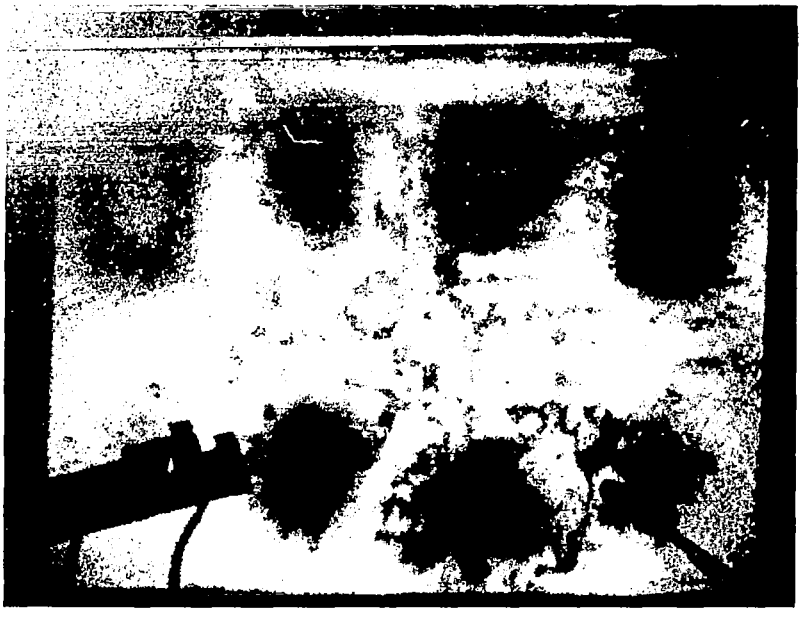

Figure 55 - Differential Hologram of the 4 x 2 Mode at 1044°F
(f = 962 cps, Δt = 50 μs)

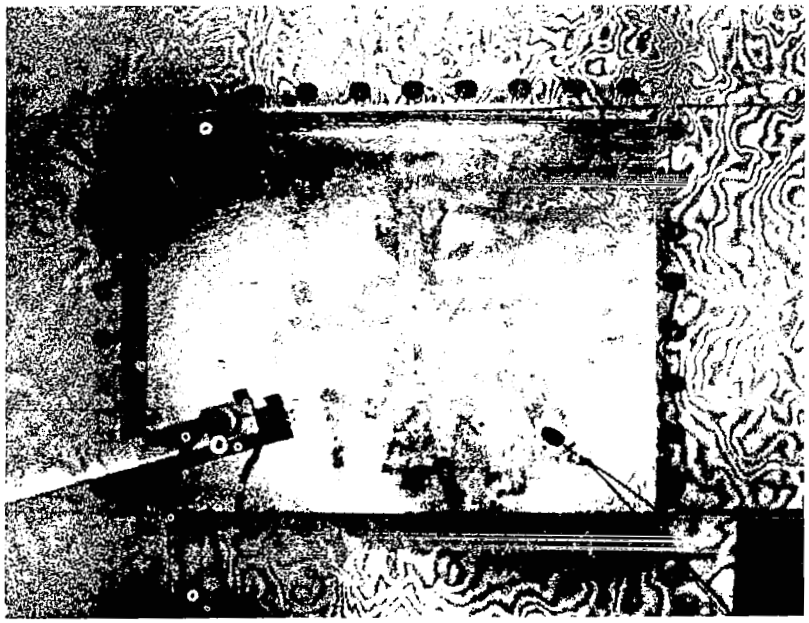

Figure 56 - Double-Pulse Hologram, made with a Long Time-Delay (~2 seconds) Between Exposures. (The plate was at 1050°F, and vibrating strongly.)

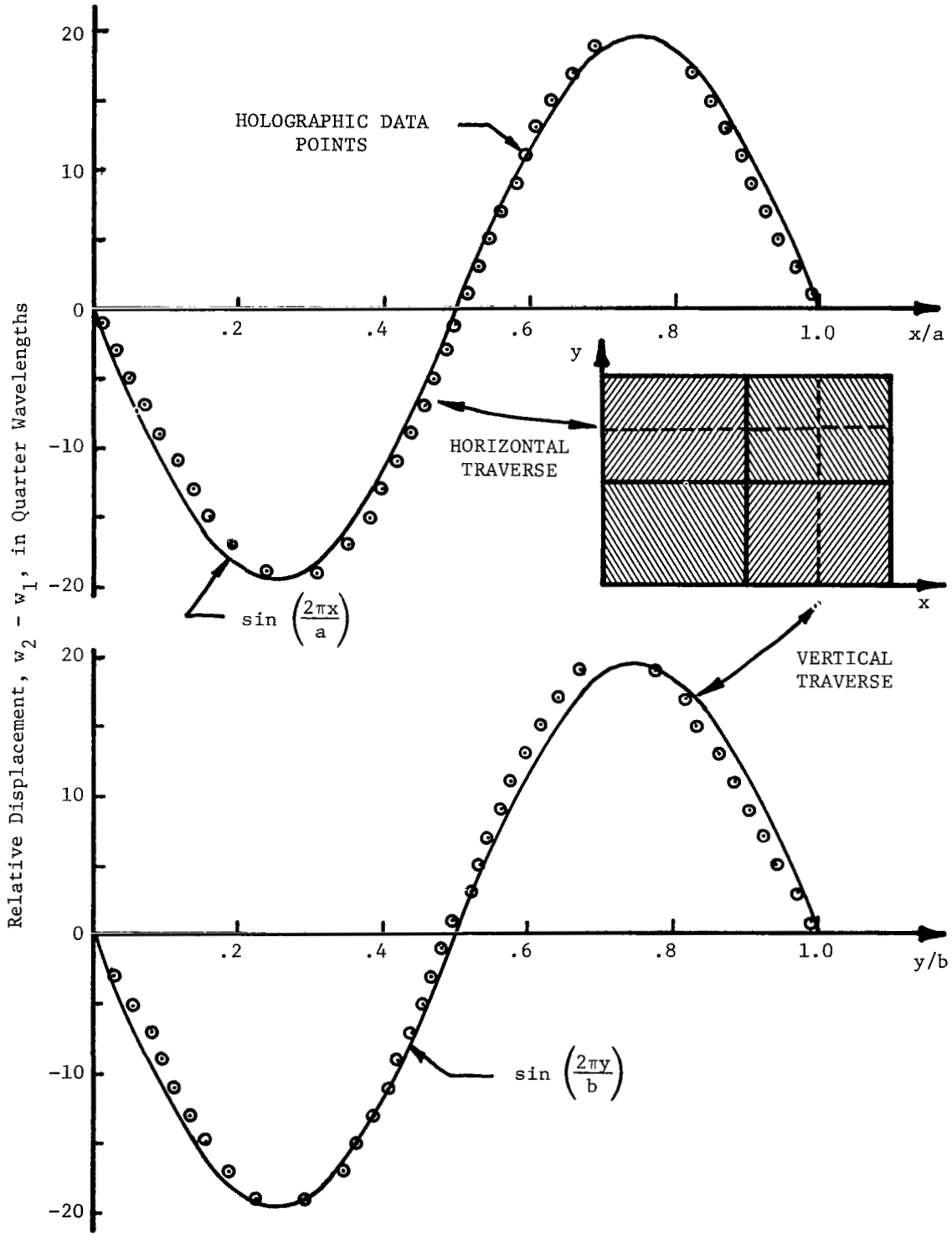

Figure 57 - Mode Shape Data from the Interferogram of Figure 45
(2 x 2 Mode, 515°F, f = 492 cps)

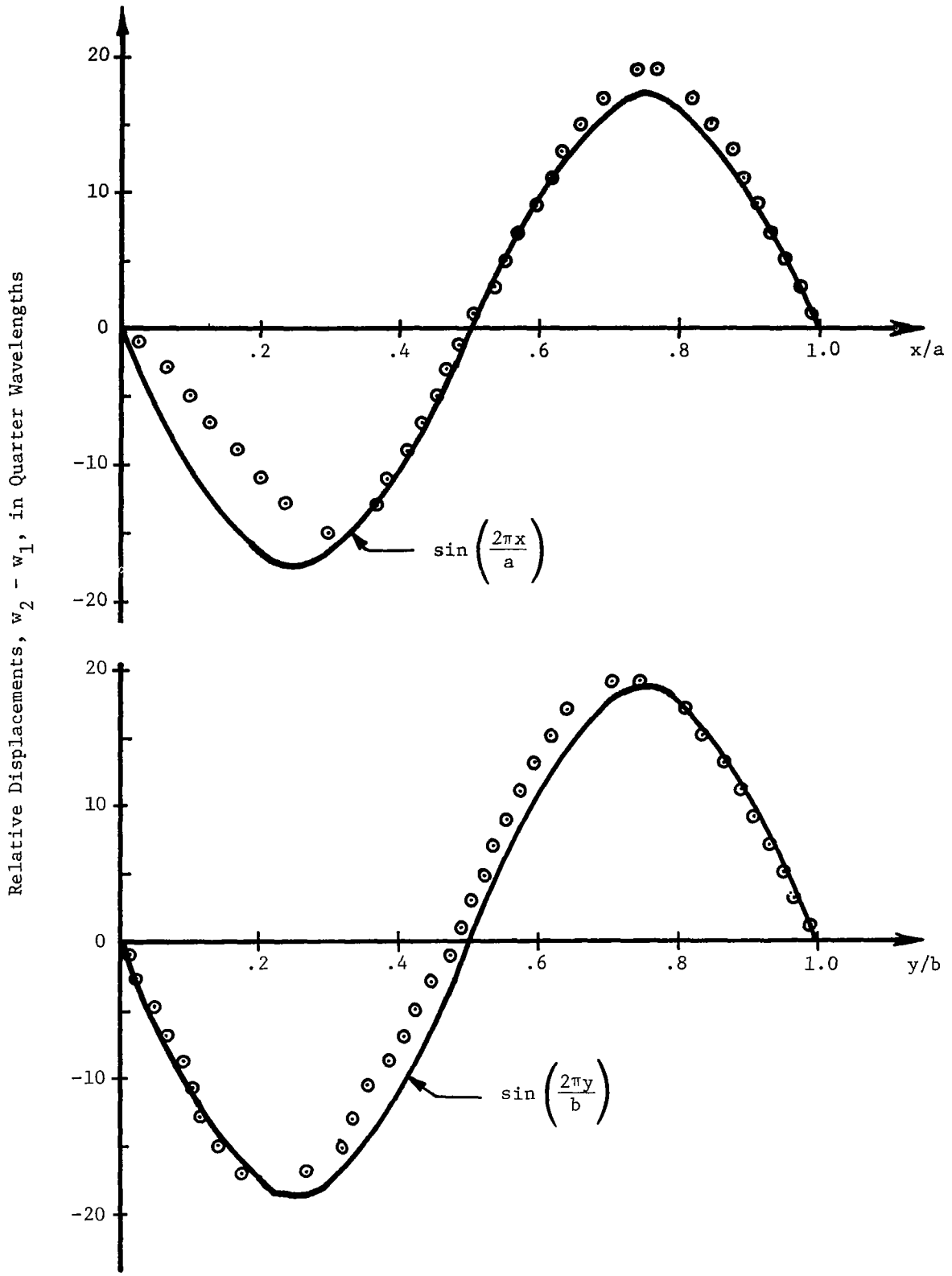

Figure 58: Mode shape data from the interferogram of Figure 52 (2 x 2 mode, 1040°F, f = 506 cps)

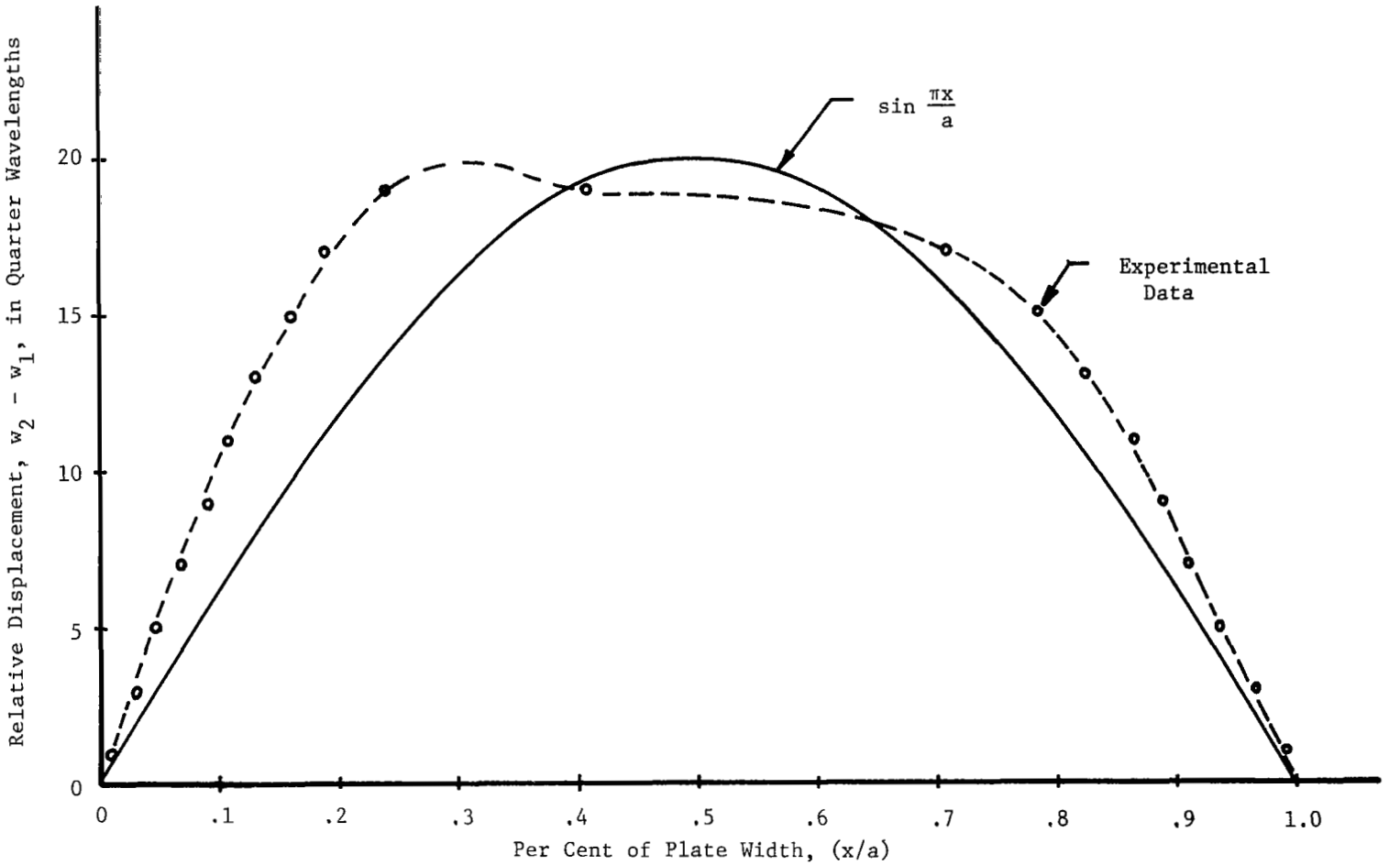

Figure 59 - Mode Shape Data from the Interferogram of Figure 44
(514°F, f = 230 cps, Fundamental Mode)

Results and Discussion

The differential holograms of the heated vibrating plate are shown in Figures 42 through 55, with the corresponding plate temperature ranging from 255°F to 1050°F. The thermocouple recorded the temperature in the lower right-hand quadrant of the plate, and at 1000°F the plate exhibited an orange-reddish glow that appeared symmetric with the central axes of the plate. The plate was cooler at the edges than in the middle, but nevertheless the vibration modes were still very symmetric and undistorted, for the most part. (See Figures 42, 45, 47, 49, 52 and 54). The fundamental mode experienced some distortion (See Figures 44, 46, and 48) primarily near the point where the drive spring contacted the plate.

For a uniform simply-supported rectangular plate with uniform in-plane loading (e.g., compression N_x or N_y), the vibration modes and buckling modes coincide (See Ref. 23). Furthermore, the plate normally buckles in its lowest mode (i.e., the fundamental). A non-uniform in-plane loading of the form

$$N_x = N_o + \Delta N \sin^2 \frac{\pi y}{b} \qquad (4\text{-}1)$$

(where b is the width of the plate in the y-direction)

would be expected to influence the fundamental mode most strongly and the higher modes less-and-less. Such a loading (eq. 4-1) might arise due to the non-uniform temperature of the plate. This decreased sensitivity of the higher modes (to loadings like 4-1) may account for the relative lack of distortion in the modes above the fundamental.

In most cases, the vibration amplitude was sufficient to produce several fringe contours. For the "weaker" resonances, however, only one or two fringe contours were recorded (e.g. Figures 49, 51 and 55). Thus, for Figure 49, the relative displacement $w_2 - w_1$, was just slightly greater than a quarter-wavelength ($\lambda/4$ equals one fringe) between exposures.

Regarding the actual shape of the vibration mode, the interpretation of the black interference fringes as contour lines gives a clear understanding of the holograms. For example, Figures 45, 47, and 52 are readily interpreted as the 2 x 2 mode, corresponding to the mode shape

$$\Phi_{22}(x,y) = \sin \frac{2\pi x}{a} \sin \frac{2\pi y}{b} \qquad (4\text{-}2)$$

for the classical plate vibration problem (Ref. 23). In equation (4-2), the axes x and y are aligned with the edges of the plate, with the side lengths a and b, respectively. As indicated previously (Sections 2.0 and 3.0) the phase of the vibration is not recorded by the differential hologram. Thus, it is not apparent from the interferograms as to which contours enclose the (positive) "hills" of the mode, as opposed to the (negative) "valleys".

The fringe contours are each spaced a distance $\lambda/2$ apart, corresponding to a difference of one fringe order in the equation

$$\Delta w = w_2 - w_1 = \frac{(2n - 1)\lambda}{4} \tag{2-15}$$

discussed previously in Section 2.0. By placing a ruler across the photograph (e.g. Figure 45) and recording the location of each fringe, the mode shape can be determined using equation (2-15). That is, each fringe location (x_i, say) has a corresponding fringe order (n_i) which corresponds to a relative displacement (Δw_i) at that location. This procedure was used to obtain the mode shapes presented in Figures 57 through 59. For comparison purposes, the sine waves (e.g., equation 4-2) appropriate to classical plate theory are shown as solid lines in the figures.

The undistorted behavior of the 2 x 2 mode is readily apparent in Figure 57, just as the distortion of the fundamental mode is clear from Figure 59. These results clearly demonstrate the capability of pulsed differential holography to record vibration modes at 1000°F. Similar experiments were conducted to demonstrate that vibration modes can also be measured at higher temperatures (e.g., 2000°F). These results are presented in Section 5.0 which follows.

5.0 TESTS AT 2000°F

Introduction

With the successful completion of the vibration tests at 1000°F, the theory of holographically recording mode shapes in the presence of turbulent convection currents had been demonstrated to work. At this point, the decision was made to extend the tests to higher temperatures (e.g., 2000 - 2200°F) which are thought to be representative for the NASA/Space Shuttle TPS panels. Of particular interest were such practical considerations as making measurements on the heated side of the plate, at small grazing angles, and with a view cluttered by heat lamps and other fixtures. Other problems, such as operating a vibration transducer at 2000°F for an extended period of time, and making holograms in the presence of intense white light from the quartz lamps, were successfully overcome. The experimental set-up, test procedure, and resulting mode shapes at 2000°F are discussed in the following paragraphs.

Plate Specimen and Support Structure

A problem encountered in the previous tests (Section 4.0) was that of achieving sufficiently high temperature. The individual reflector units (which hold eight quartz lamps) are rated to operate at a maximum input of approximately 8 kilowatts. For comparison purposes, an area 8" by 10" (the original plate planform) radiates approximately 5 kilowatts if heated to a temperature of 1500°F. Thus, the question of putting enough energy into the plate to raise its temperature to 2000°F became a design problem. This problem was solved by

- Reducing the plate area from 8" x 10" to 4" x 8"
- Designing the plate supports to carry electrical current, producing resistance heating of the plate (I^2R)
- Using the quartz lamps in addition to the resistance heating

A schematic diagram of the plate and its support structure are shown in Figure 60. Figure 61 is a photograph of the actual hardware. The plate specimen was stainless steel (302 or 304), four inches wide, and cut to a length of 12 inches. Stainless steel was selected as the plate material because of its desirable electrical resistivity and high melting temperature. An energy balance (between electrical input and thermal radiation out) was used to select the plate thickness. Initial tests were conducted using a thickness h = .047 inches.

One end of the plate specimen was clamped to the support frame, and three stainless steel springs were used to apply a slight tension load at the other end of the plate. * An intermediate support was placed between the clamped end and the springs, giving the test section an 8-inch span (See Figures 60 and 61). The electrical connections for resistance heating were

*The tension springs were used to take up the thermal expansion and prevent buckling of the plate.

made at the clamped end and the intermediate support; thus, just the 8-inch span was electrically heated. The electrical current was brought in through large, bolted connectors, and heavy support clamps (like buss-bars) were used to obtain fairly uniform current density in the plate. (The connectors and clamps are visible in Figure 61.)

With this arrangement, the combination of resistance heating and quartz lamps were sufficient to heat the plate to 2000°F. The temperature was recorded using a chrome-alumel thermocouple, mounted on the cold side of the plate. From a structural standpoint, the eight-inch heated span of the plate acted much like a wide beam (i.e., 4" wide, 8" long, and .047" thick). The ends of the beam were essentially "clamped" (i.e., fixed at $x = 0$, and $x = 8$") as opposed to being "simply-supported". The other two edges of the test specimen were stress-free.

Excitation and Detection of Resonance

The electrodynamic shaker was again used to vibrate the plate (as in Section 4.0) using the tubular sting and stainless-steel compression spring arrangement. The actual set-up is shown in Figure 62 for the 2000°F test. The Bently-Nevada inductance-type displacement transducer was used to detect resonance, as previously discussed in Section 3.0. One test series was conducted without cooling the transducer, and it eventually failed to operate. The transducer was replaced and provided with water cooling. The copper tubing and the cooling coils are visible around the transducer in Figure 63. The critical areas of the excitation and detection problem were (1) the stainless steel drive spring and (2) the inductance vibration transducer. Both operated successfully for plate temperatures as high as 2000°F.

"Cluttered View", and Small Grazing Angles

A single reflector unit (containing a bank of eight quartz heat lamps) was positioned near the front side of the plate. (A schematic diagram is shown in Figure 64, and the actual set-up in Figure 65). The close proximity of the heat lamps to the surface of the plate allowed only small angles for illuminating and viewing the plate (cf. Figure 12, Section 2.0). This experimental arrangement, with small grazing angles (ε_i and ε_v) and heat lamps mounted close to the plate, was meant to demonstrate some of the practical problems which are likely to occur in applying holography to actual NASA vibration tests of heated Space Shuttle panels. Figures 64 and 65 illustrate the practical problems of a "cluttered view", and small grazing angles.

Experimental Set-Up

A schematic diagram of the experimental set-up is shown in Figure 66. An overall view of the actual test set-up and hardware is given in Figure 67. The laser and optics (corresponding to the schematic) are shown in Figure 68. Additional details of the test fixtures and geometry are given in Figures 60 to 65 and 69 to 72. The oscillator-amplifier

combination used to drive the shaker are visible in Figure 67, along with the transducer electronics and the oscilloscope. A chrome-alumel thermocouple was used to measure the plate temperature. The thin leads from the thermo-couple are visible in Figure 62. The quartz heat lamps (one reflector unit) were mounted about 1-1/2 to 2 inches from the plate surface (see Figure 69).

The optical arrangement used to make the holograms is shown in Figures 66 and 68. Note the use of a mechanical shutter (in front of the hologram) and an optical band-pass filter (Wratten filter #70) shown in Figure 66. During the tests, intense white light radiated from the quartz lamps (cf. Figures 67 and 69). It was necessary to prevent this light from exposing (i.e., fogging) the hologram. The shutter and optical filter (in the object beam, coming from the vibrating plate) were used to allow the laser light to reach the hologram while restricting the exposure to the light from the quartz lamps. The shutter is visible in Figures 70 and 71, along with an aluminum sheet that served as a baffle.

The light baffle was used to prevent white light (from the quartz lamps) from reaching the back of the hologram and causing fogging. Additional light baffles (in the form of a cardboard "tunnel") were used along the path of the reference beam to restrict the passage of spurious light from the heat lamps. (The cardboard baffle is shown in Figure 72.)

Timing of the Laser Pulses

Preliminary tests were run using a timing arrangement similar to that described in Section 3.0. The mechanical shutter was set at 1/25th of a second and connected with the electronics using a "logical-and circuit". With this arrangement, the laser was fired when (i) the shutter was open, and (ii) the plate velocity was a maximum. (It was necessary for the shutter to be open during a full vibration period with this synchronization scheme.) This timing method was used in early tests made at room temperature.

When the heat lamps were turned on, however, the slow shutter speed allowed the white light to fog the hologram. Thus, it became necessary to use a faster shutter speed (1/400th of a second), which did not allow synchronization with the plate motion. The electrical arrangement for firing the laser with the mechanical shutter is given in Figure 73.

The shutter was manually controlled, and when opened, it completed a circuit which triggered the laser flash lamp. After an 850 μsec time-delay (from the flash lamp triggering) the Pockels cell Q-switch was activated, resulting in the first laser pulse (t_1). The second laser pulse occurred 50 μsec later, giving the desired time-delay Δt between

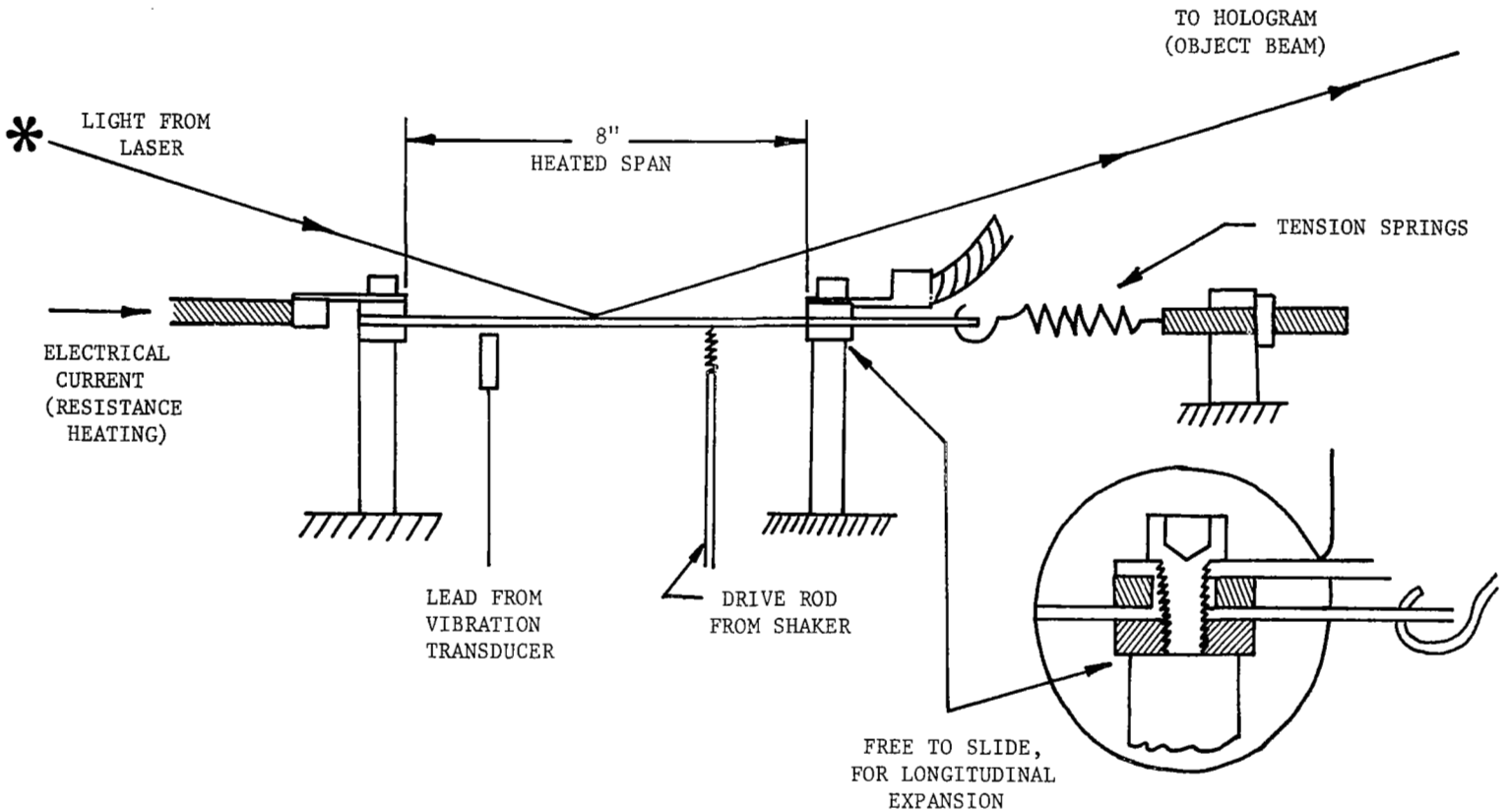

Figure 60 - Schematic Diagram of Plate Specimen and Support Structure

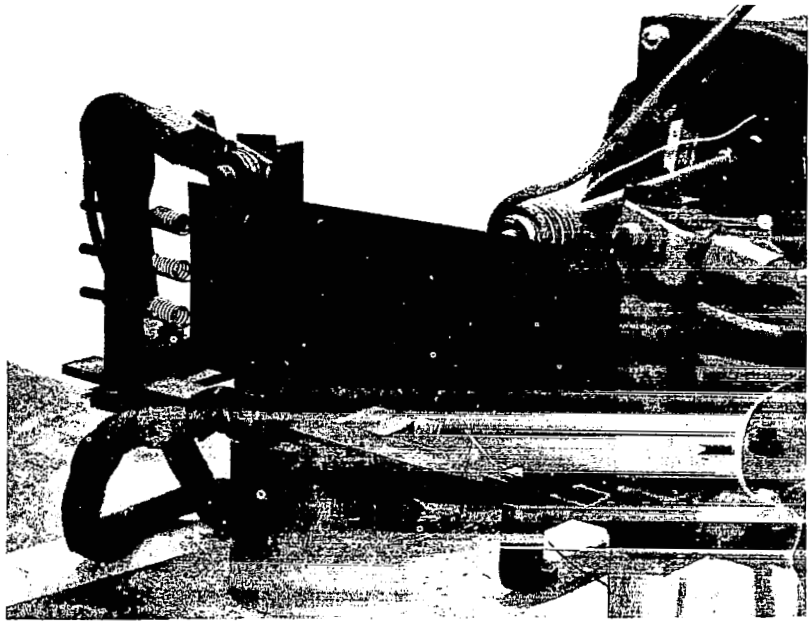

Figure 61: Plate and support structure. (The heated span is 8" long and 4" wide.)

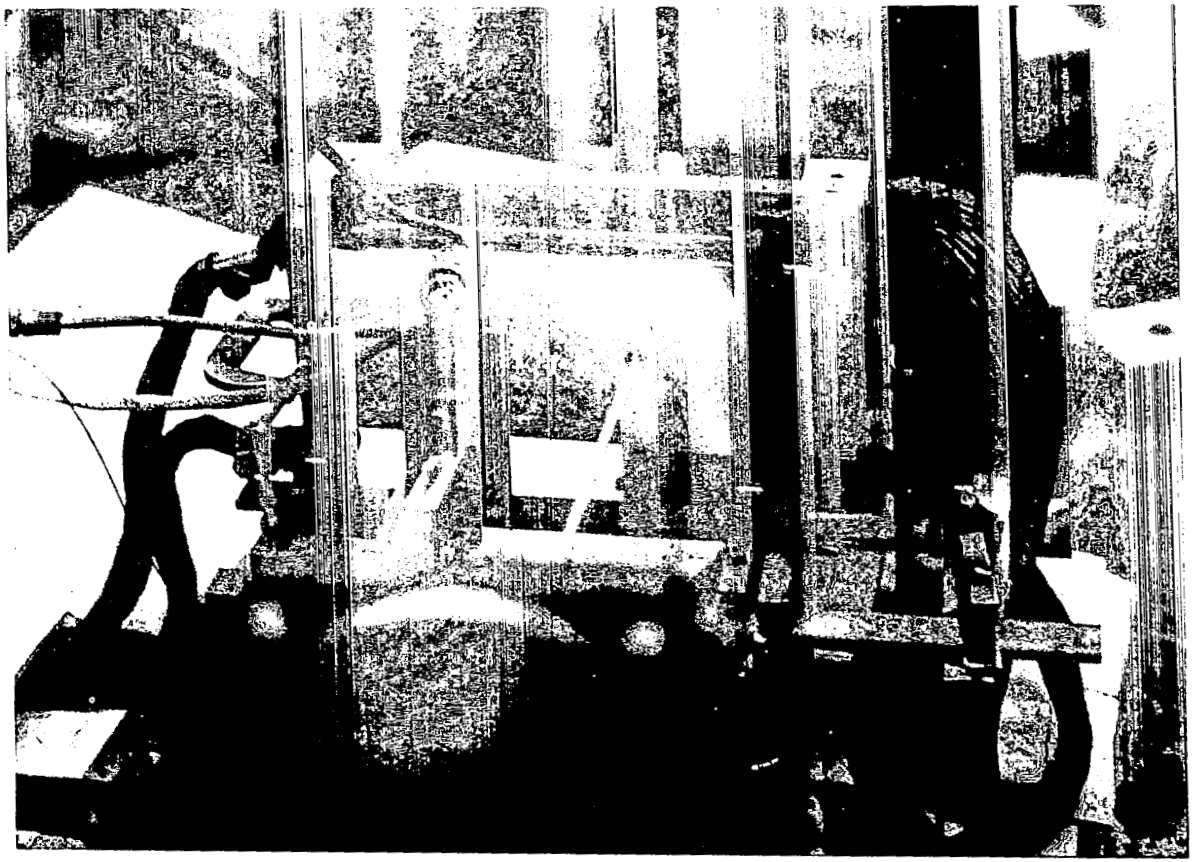

Figure 62: View showing shaker, drive rod, and spring. (Note tension springs on right.)

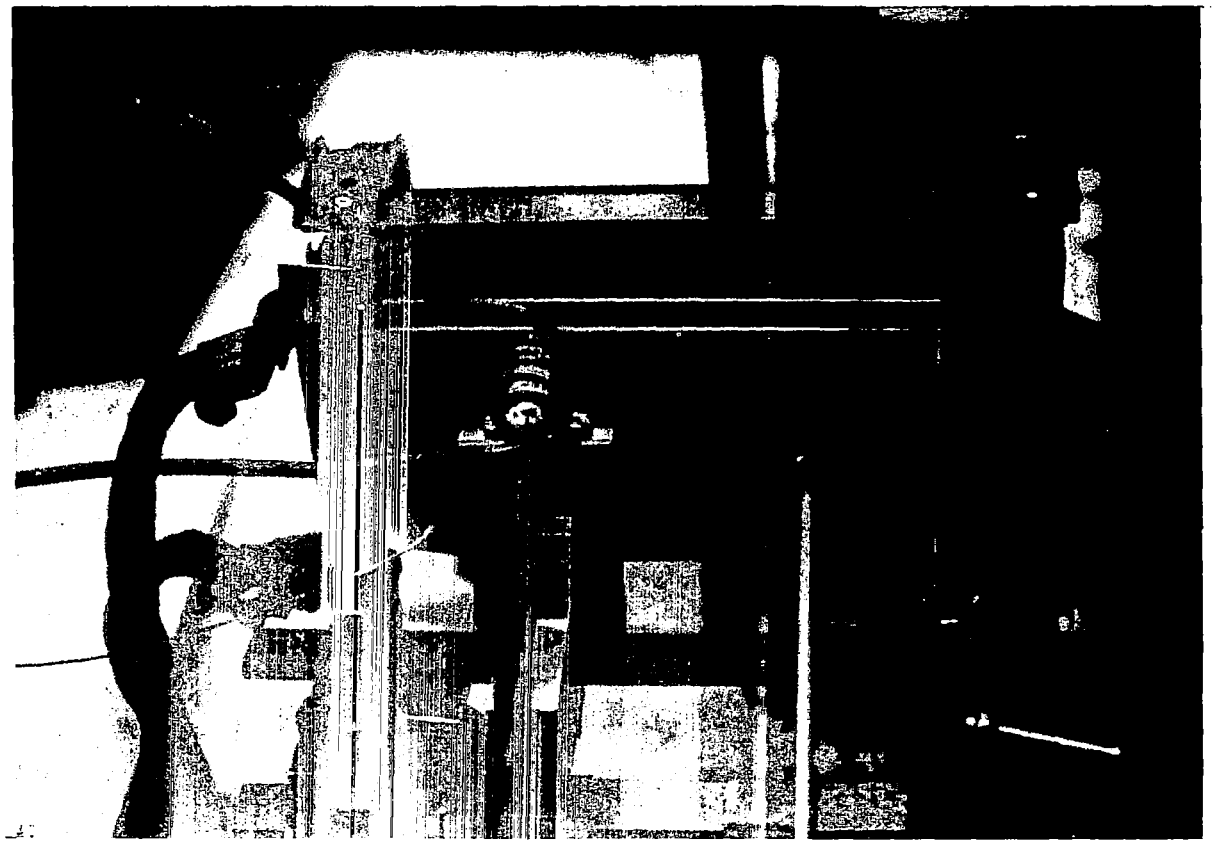

Figure 63: View showing transducer (cooling coils) and drive rod with spring to excite plate.

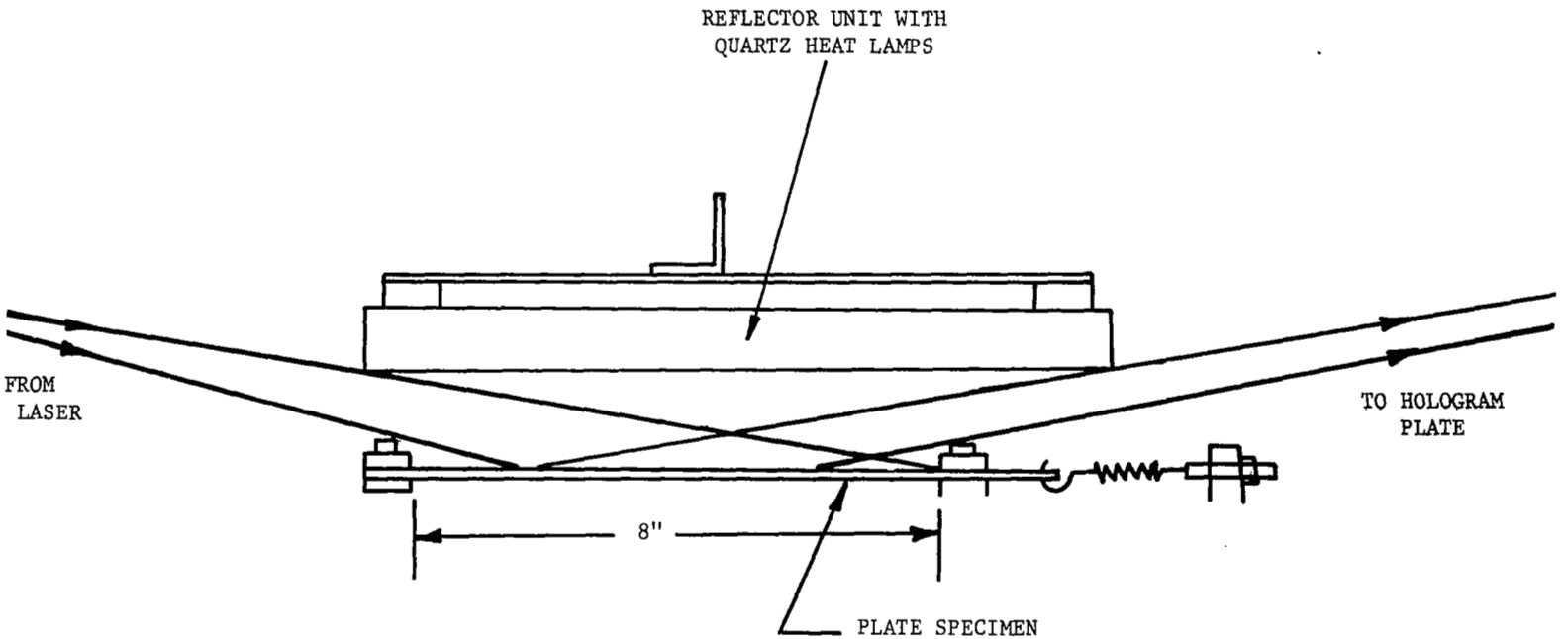

Figure 64 - Schematic Diagram of Quartz Heat Lamps Close to the Plate, Showing the Small Grazing Angles of Illumination and Viewing

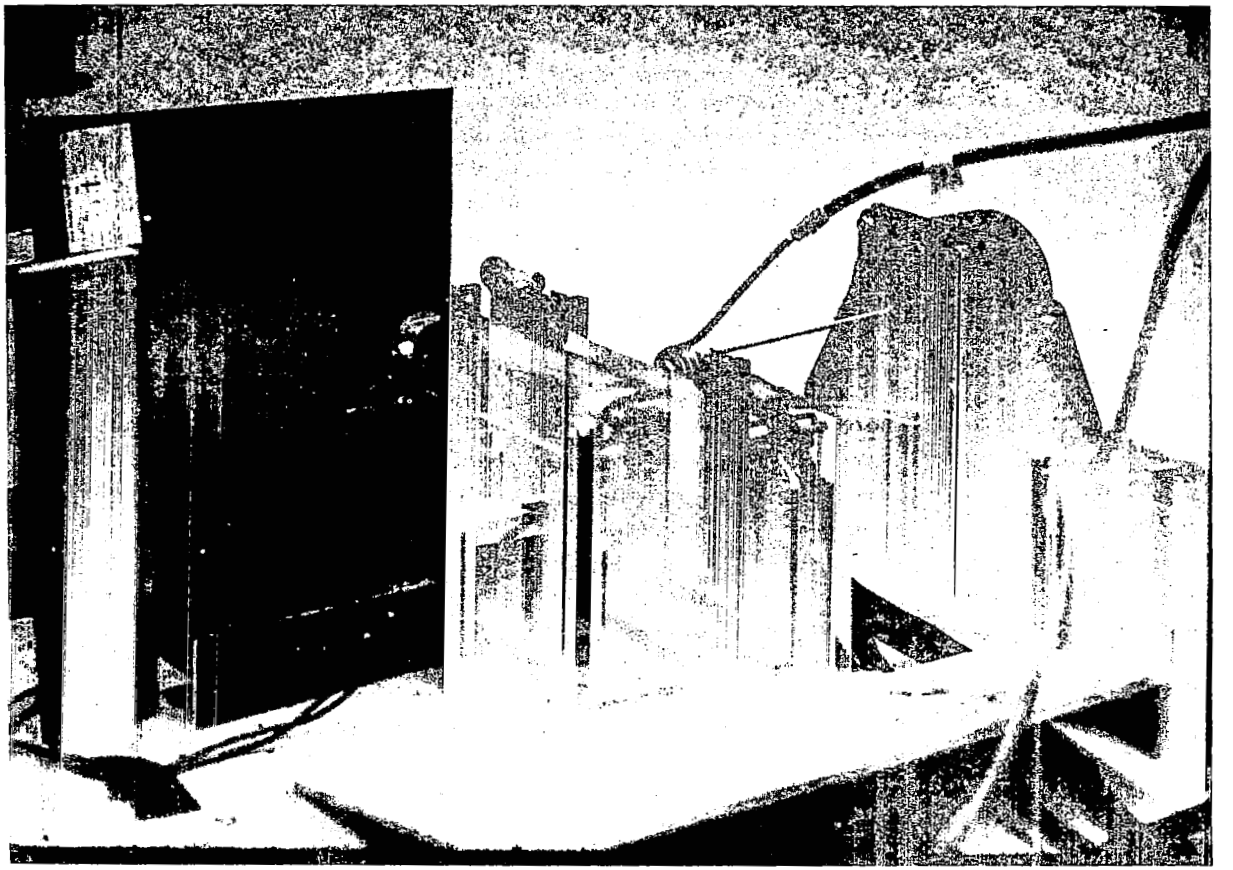

Figure 65: Quartz lamps mounted close to the plate, illustrating the "cluttered view".

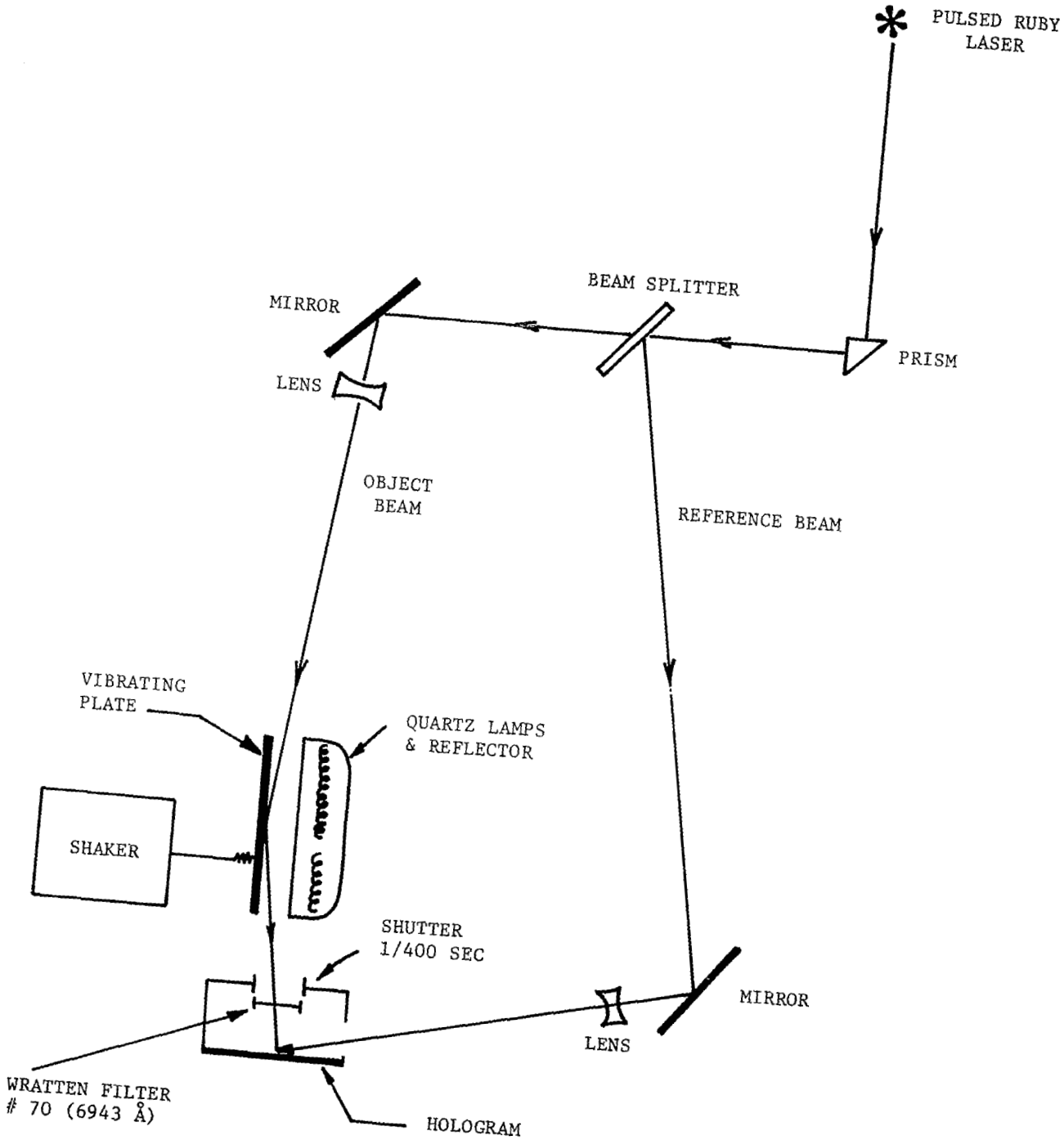

Figure 66 - Schematic of Holographic Set-up for the 2000°F Test

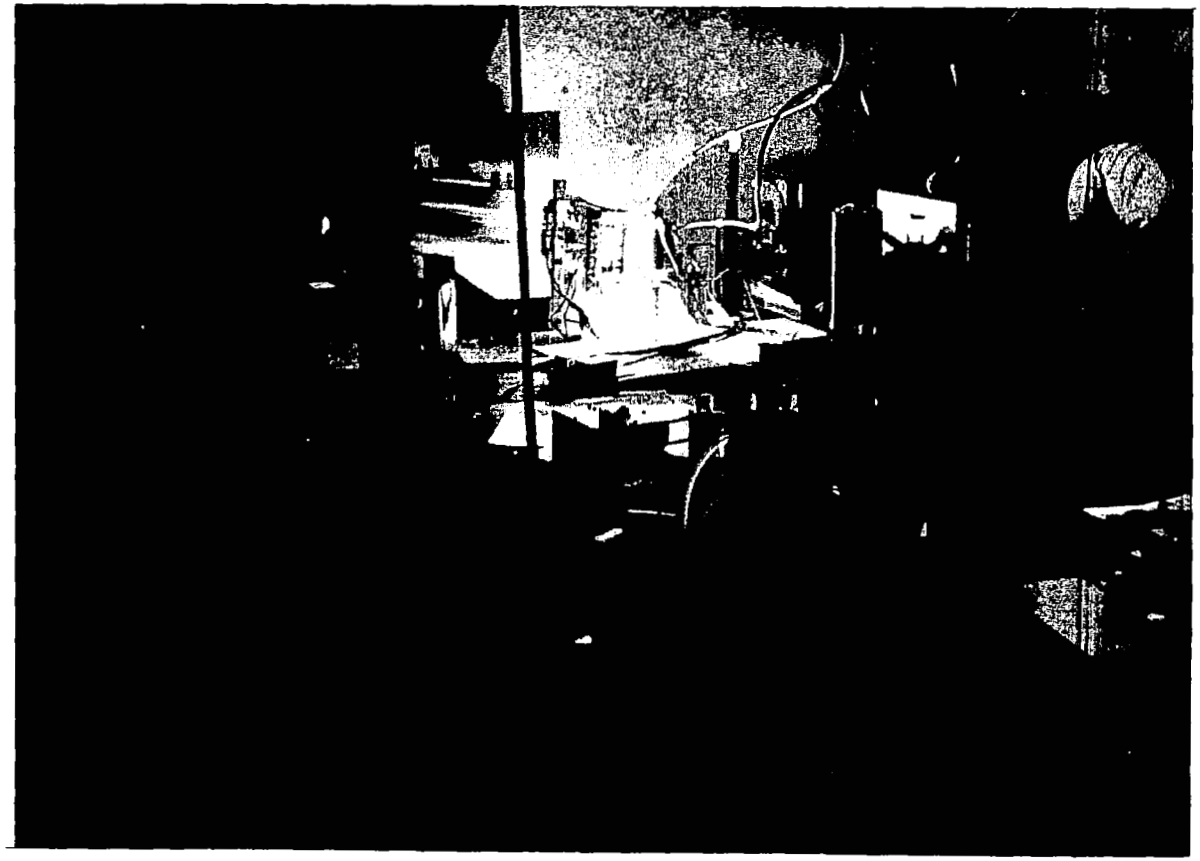

Figure 67: Overall view of the test set-up

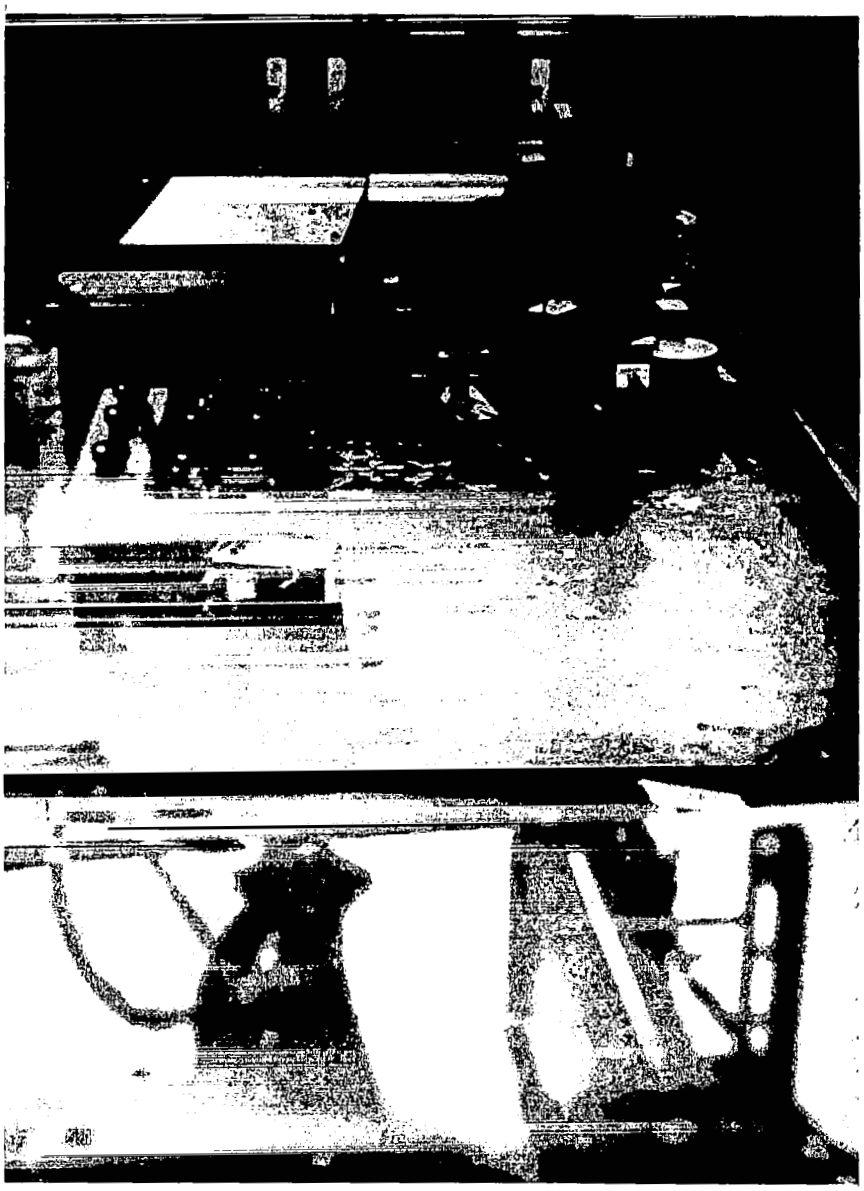

Figure 68: Photograph showing arrangement of the laser and optics

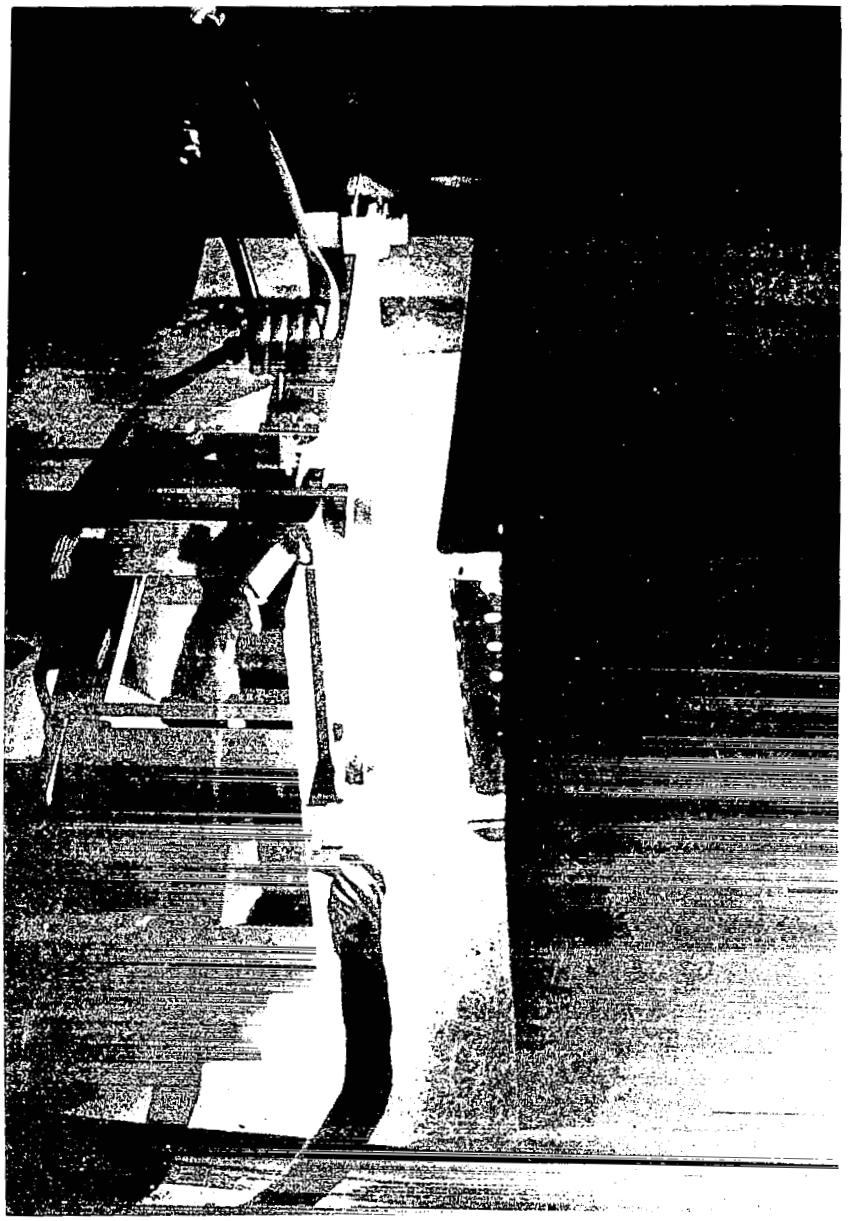

Figure 69: View illustrating spacing between quartz lamps and the plate

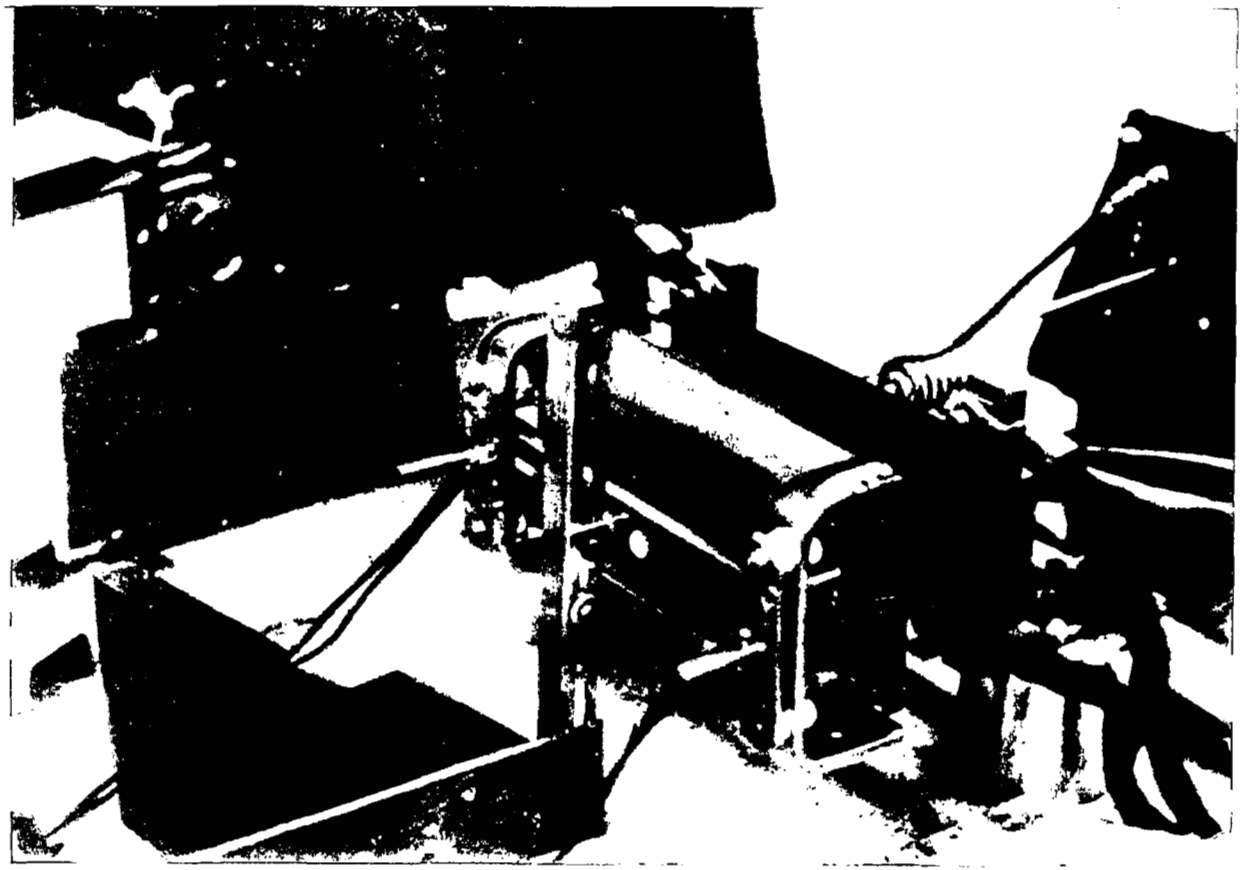

Figure 70: Relative position of shutter and vibrating plate

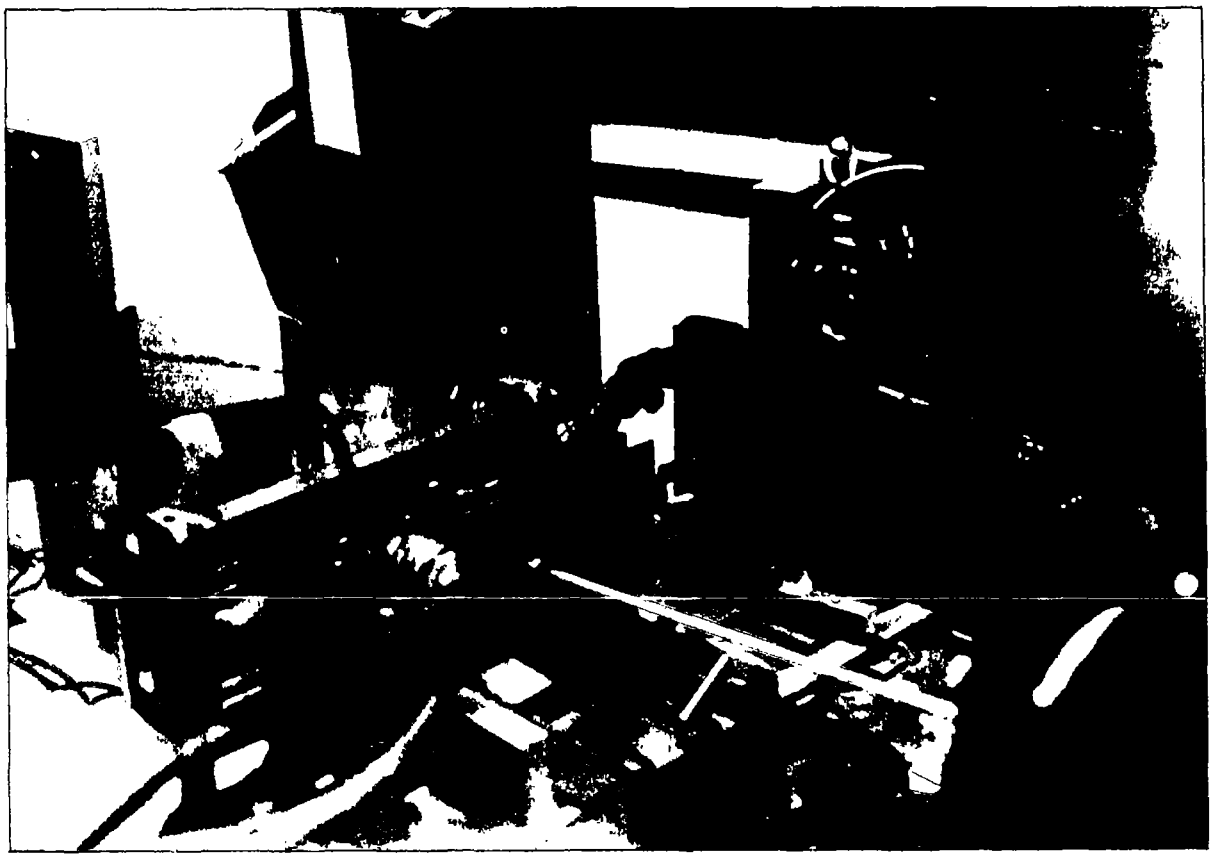

Figure 71: View showing shutter (in front of hologram plate) and light baffles

Figure 72: View showing tunnel-like baffle for the reference beam

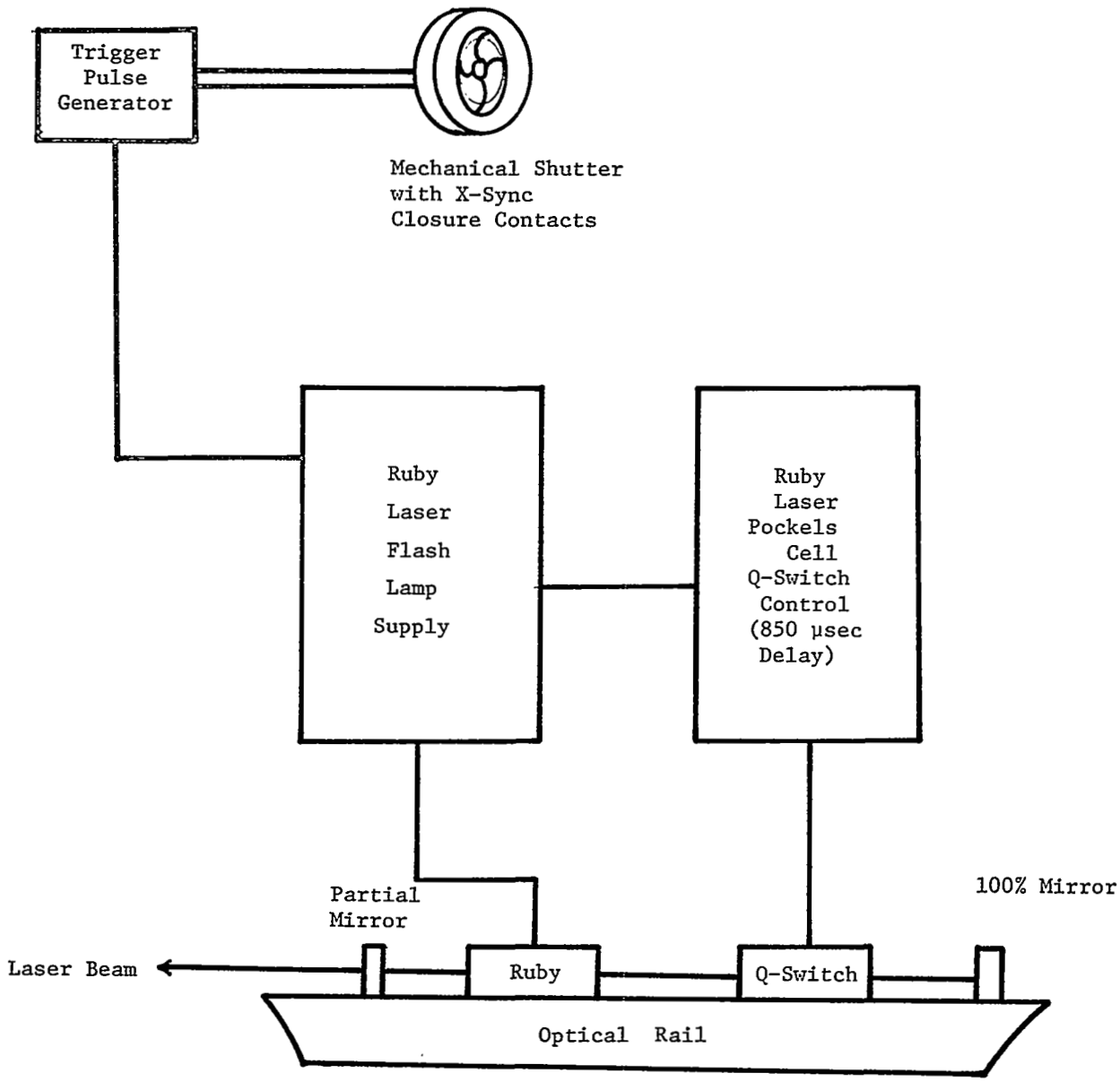

Figure 73: Schematic showing shutter and electrical connections

pulses. For a plate vibrating at 100 cps, the corresponding vibration period is T = 10 millisec. In this case, the manual shutter would be open for only 1/400 = 2.5 millisec, or one-fourth of the vibration period. Since the shutter opening (2.5 ms) could fall anywhere within the vibration cycle, we have the case of "random firing of the first laser pulse", discussed in Section 3.0. (It should be noted that the initial laser pulse was controlled by the mechanical shutter and occurred at a definite time during the 1/400 sec shutter opening.)

Some Preliminary Results

Initial tests were made at room temperature, and they demonstrated the ability of differential holography to record vibration modes using small grazing angles and a cluttered view. The differential interferograms of four modes (at room temperature) are shown in Figures 74 to 77. The mode shapes are readily apparent from the interferograms, and the nodal lines are illustrated in the diagrams (Figures 74 to 77).

Quantitative data can be obtained from the interferograms, using Equation (3-22)

$$w_2 - w_1 = \frac{(2n \pm 1)\lambda}{2(\sin \varepsilon_i + \sin \varepsilon_v)} \tag{3-22}$$

The experimental set-up was such that the viewing angle (ε_v) was in the range

$$6.6^\circ \leq \varepsilon_v \leq 9.6^\circ \tag{5-1}$$

and the illuminating angle (ε_i) was bounded by the same range

$$9.6 \geqslant \varepsilon_i \geqslant 6.6^\circ \tag{5-2}$$

These angles varied (slightly) with the distance (x) along the length of the plate, such that the sum

$$(\sin \varepsilon_i + \sin \varepsilon_v) \cong \varepsilon_i + \varepsilon_v \tag{5-3}$$

was very nearly constant. Thus, Equation (3-22) gives

$$w_2 - w_1 = \frac{(2n \pm 1)\lambda}{2(\varepsilon_i + \varepsilon_v)} \simeq \frac{(2n + 1)\lambda}{2(.14)} \tag{5-4}$$

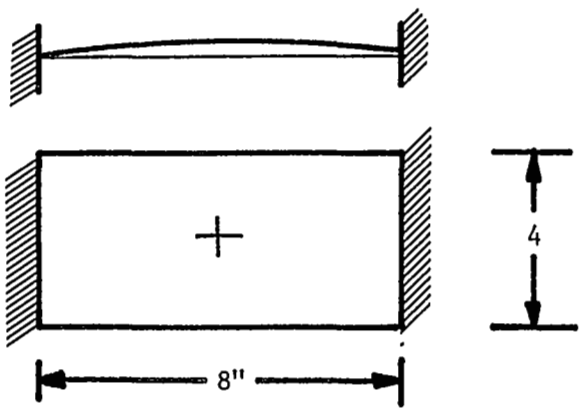

FUNDAMENTAL MODE
(WIDE BEAM)

Figure 74: Fundamental mode (f = 120 cps room temperature)

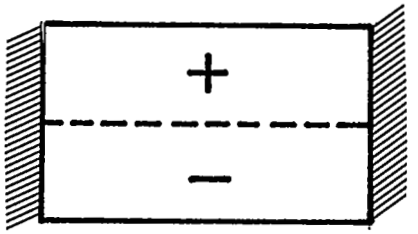

FIRST TORSION MODE

Figure 75 - First torsion mode (f = 223 cps, room temperature)

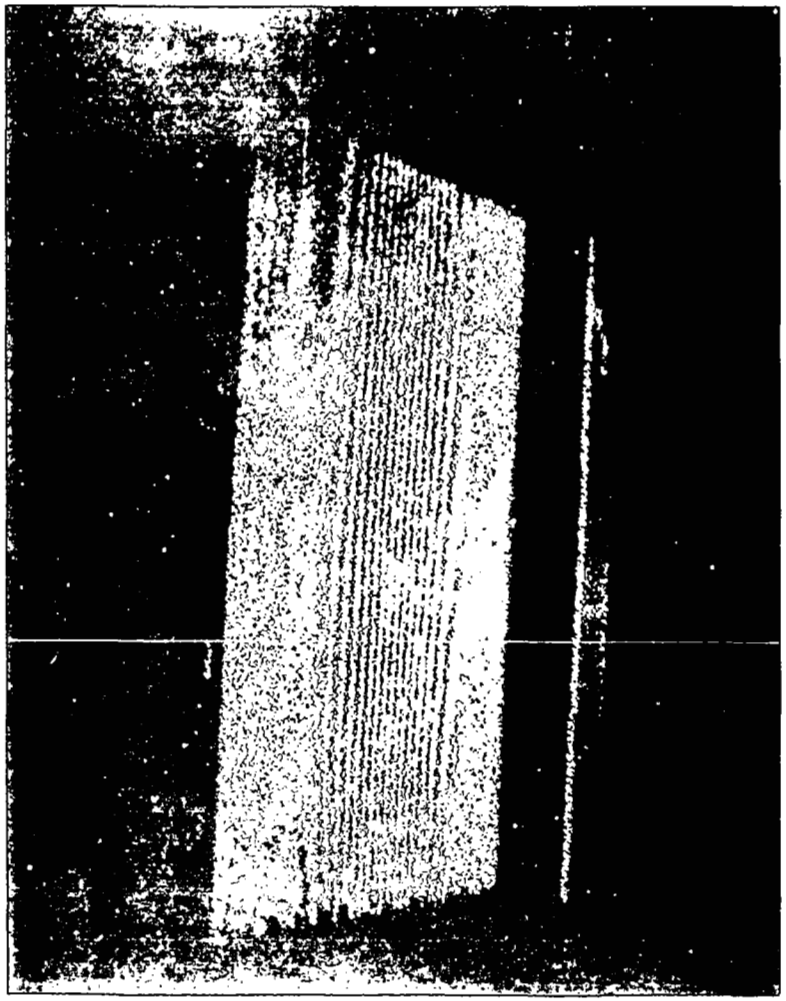

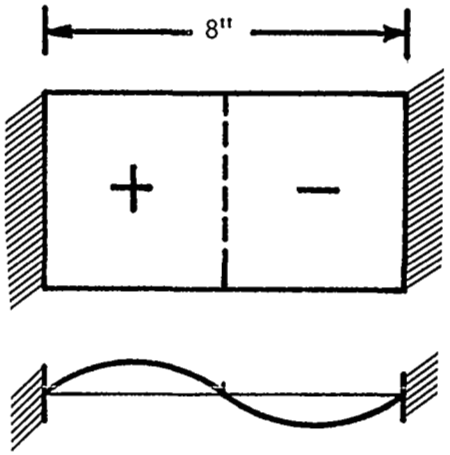

SECOND BENDING MODE

Figure 76: Second bending mode (f = 307 cps, room temperature)

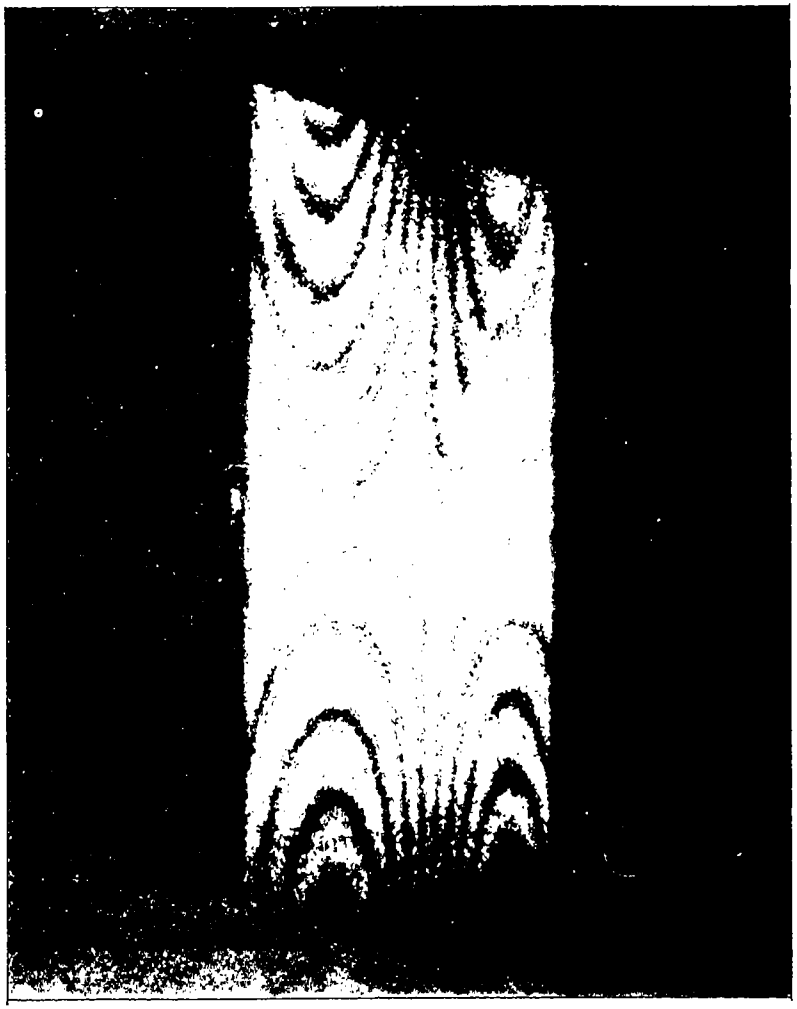

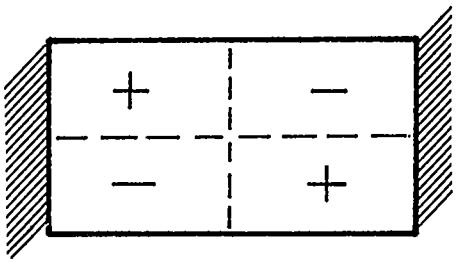

SECOND TORSION MODE

Figure 77: Second torsion mode (f = 486 cps, room temperature)

where $(\varepsilon_i + \varepsilon_v) \cong .14$ radians (e.g., 8.1°) for our test set-up. Equation (5-4) was used to determine the quantitative mode shape data shown in Figure 78.

Test Procedure

The test procedure used was similar to that presented in Section 3.0, with slight modifications. In general, the individual steps in the 2000°F tests were as follows:

(1) Turn on the electrical heating current to the plate (causing I^2R heating)

(2) Turn on the quartz lamps, and continue to raise the plate temperature

(3) Monitor the temperature with the thermocouple, and allow the plate to stabilize at the desired temperature

(4) Vary the frequency and amplitude of the shaker and tune-in a resonance of the plate. The plate response was monitored by the displacement transducer

(5) Load the film plate in its holder and then manually operate the shutter, which fired the laser to make the differential recording

(6) Develop the hologram and tune in another resonant mode; repeat Steps 4 and 5 to record another mode

(7) If the developed hologram did not contain an adequate number of fringes, the mode in question can be re-tuned and another attempt made to record it

This procedure was used to record resonant modes of the vibrating plate at temperatures ranging from 1600°F to 2025°F. The results are presented in the following paragraphs.

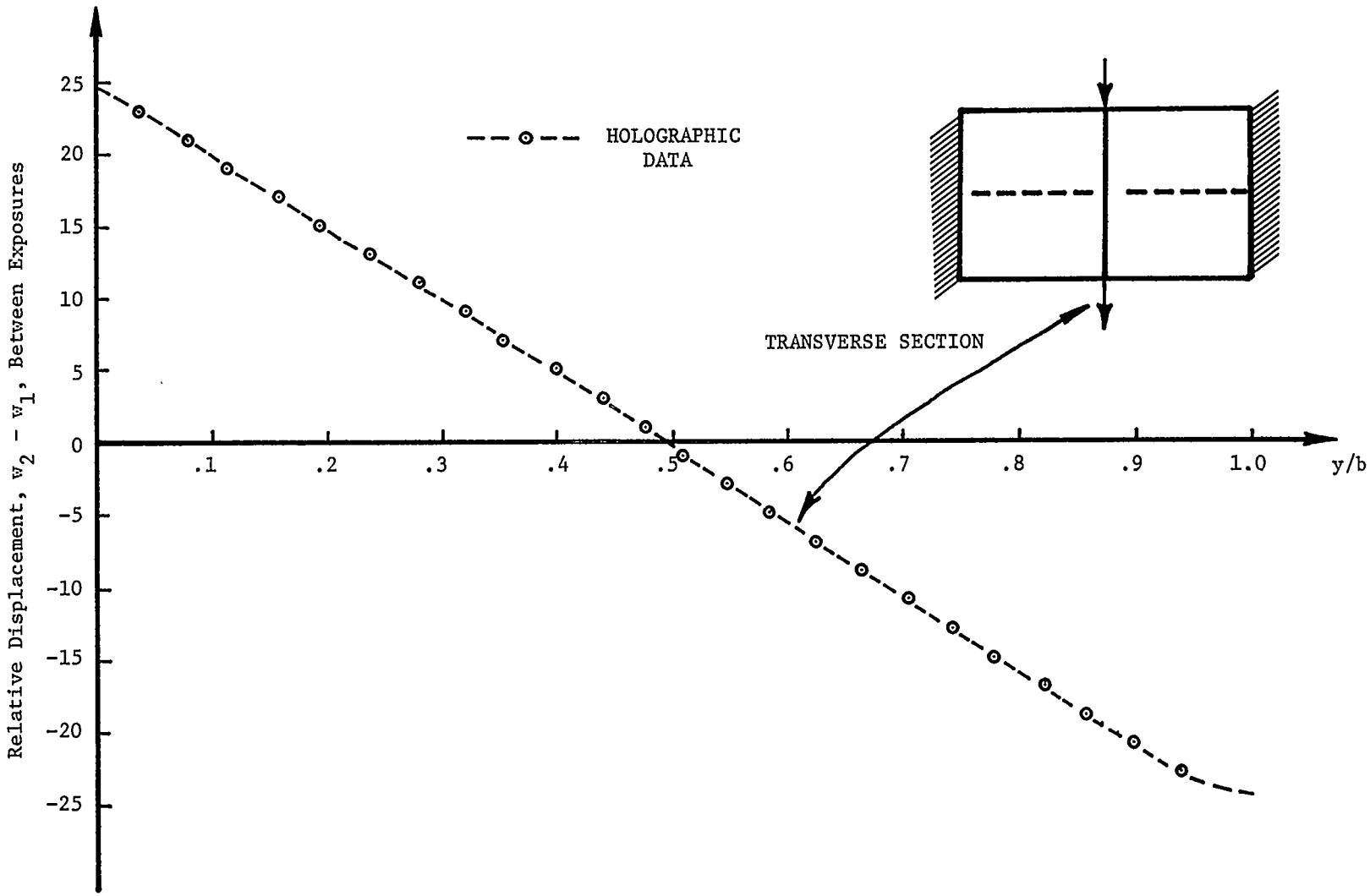

Figure 78 - Mode Shape Data from the Interferogram of Figure 75
(first torsion mode, f = 223 cps, room temperature)

Results and Discussion

Initial high-temperature tests were conducted by heating the plate to 1950°F and recording modes using the procedure just described. A typical interferogram is shown in Figure 79, which is the first torsion mode at 1950°F (cf. Figure 75, the corresponding mode at room temperature).

Figure 79 contains several black vertical lines which resulted from surface oxidation of the plate. In addition, the interference fringes are of low-contrast, and the hologram was fogged slightly (due to the spurious white light). The Wratten Filter (6943Å) was added to the test set-up (see Figure 66) for the subsequent experiments, to inhibit fogging of the holograms.

At this point, the .047" plate specimen was replaced by a thinner sheet (.031") in an attempt to increase the resistive heating and reach higher temperatures. Tests were run using the thinner plate, and a temperature of 1975°F was reached. Modes were recorded at this temperature, but again the fringe contrast was somewhat weak. (This test was stopped abruptly when the gold film boiled off the reflective heating unit and the lamps burned out.)

The final test series was also conducted using a plate .031" thick. In this test sequence, the plate reached a temperature of approximately 1600°F by resistance heating alone. Several high-quality interferograms were made at this temperature, and the various modes are shown in Figures 80-86. The results are similar in many respects to the modes recorded at room temperature and presented previously in Figures 74 to 77. The quartz lamps were then turned on and a maximum temperature of 2025°F was achieved. Mode shapes were successfully recorded at this temperature, as shown in Figures 87 and 88.

These differential interferograms can be interpreted using Equations (5-4) or (3-22) presented previously. An example of such data reduction was given in Figure 78. However, the interferograms themselves provide a good qualitative indication of the mode shape, not unlike the familiar Chaldni sand patterns. In many cases, this qualitative information is sufficient for the vibrations analyst, since it often can be used to compare with computed mode shapes or nodal patterns.

Figure 79: Differential hologram showing first torsion mode of a 4" x 8" stainless steel plate at 1950°F. The black vertical lines are due to surface oxidation. (f = 200 cps, Δt = 50 μsec)

Figure 80: Fundamental mode at 1573°F (f = 82 cps, Δt = 50 μsec)

Figure 81: Fundamental mode at 1602°F (f = 83 cps, Δt = 50 μsec)

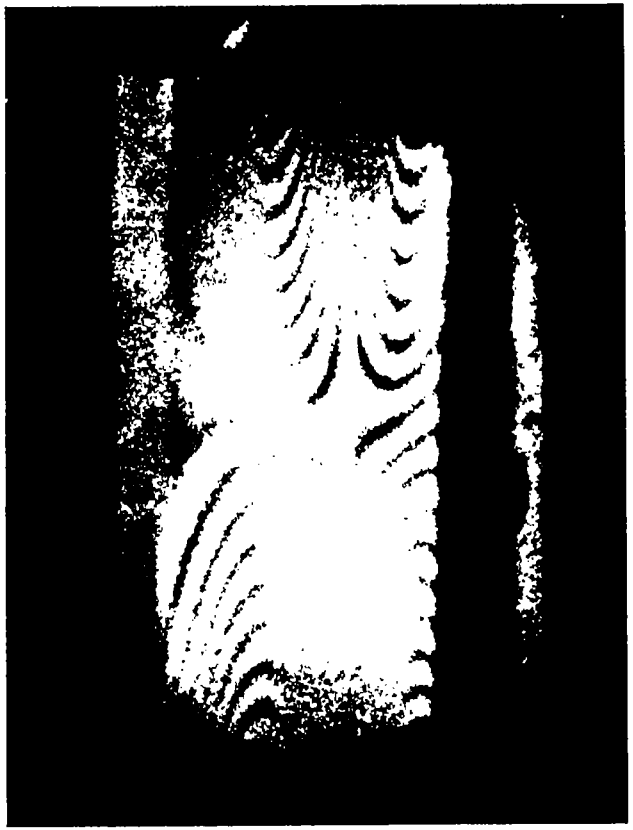

Figure 82: Second torsion mode at 1447°F (f = 290 cps, Δt = 50 μsec)

Figure 83: Combination mode at 1602°F (f = 135 cps, Δt = 50 μsec)

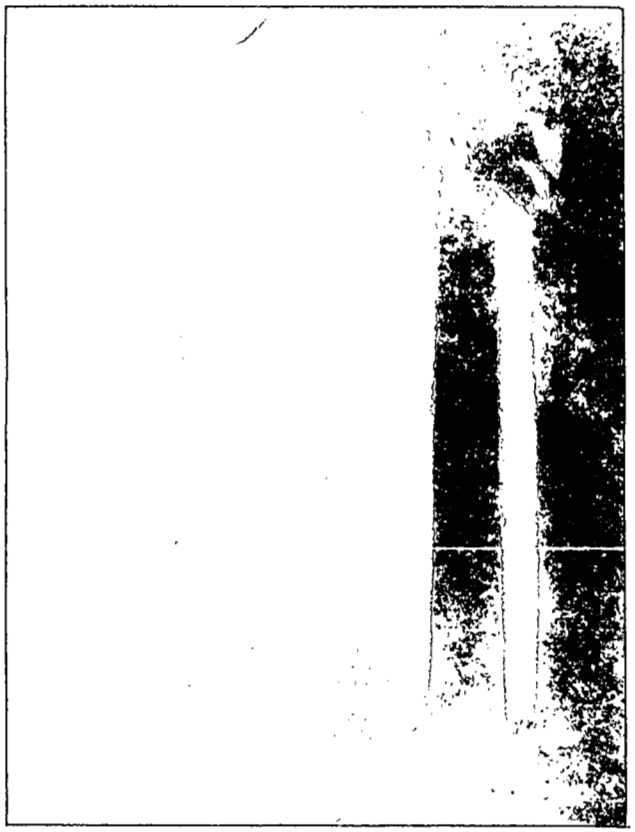

Figure 84: Second torsion mode at 1630°F (f = 293 cps, Δt = 50 μsec)

Figure 85: Second bending mode at 1630°F (f = 239 cps, Δt = 50 μsec)

Figure 86: Combination mode at 1630°F (f = 230 cps, Δt = 50 μsec)

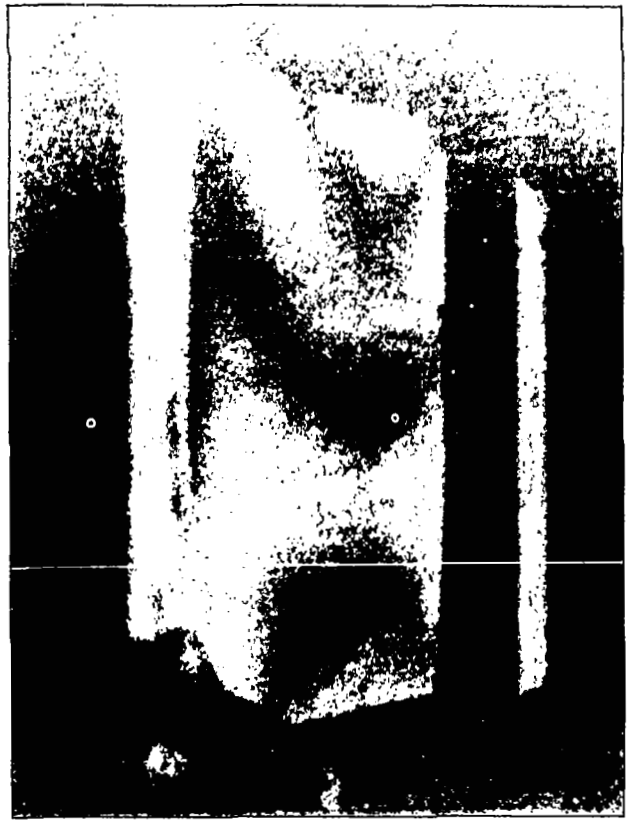

Figure 87: Fundamental mode at 2025°F (f = 60 cps, Δt = 50 μsec)

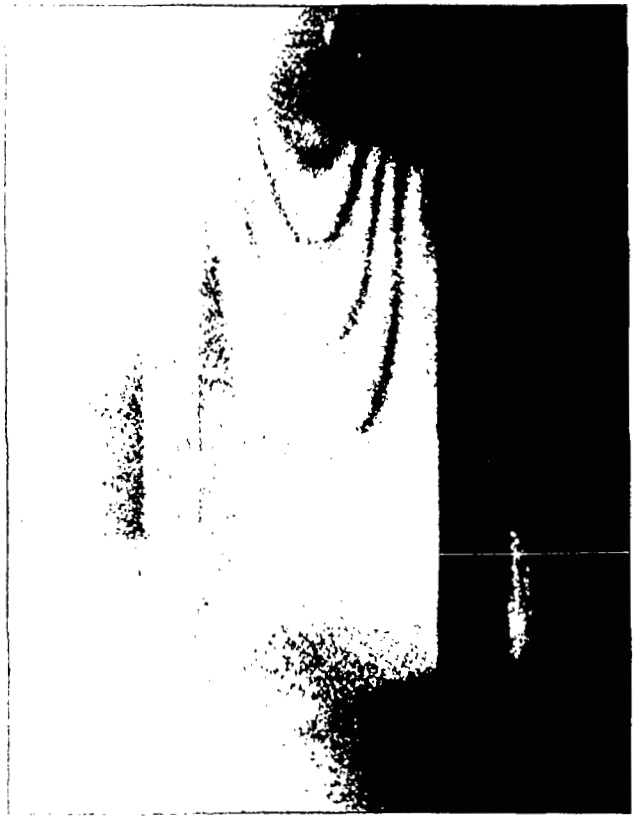

Figure 88: First torsion mode at 2012°F (f = 171 cps, Δt = 50 μsec)

6.0 CONCLUDING REMARKS

The primary result of this study is as follows: It demonstrated that pulsed differential holography can be used to measure vibration modes of heated plates (in the atmosphere) at temperatures up to 2000°F. Since the free convection boundary layer is turbulent for these elevated temperatures we can generalize this conclusion to state "Pulsed differential holography allows measurements of structural deformations through turbulent boundary layers." Based upon the holographic equations given herein, it is possible to analyze similar situations where it is desired to make structural deformation measurements in the presence of random, noisy environments. One example of such calculations is the measurement of flutter modes through a random, turbulent boundary layer.

Other results of secondary importance include the fact that the basic equations which govern pulsed differential holography (for harmonic vibrations involving amplitude, frequency, and the time delay Δt) have been verified experimentally. Results have been presented in which the laser was synchronized to the vibration and also for "random timing" of the laser. Both these approaches have been analyzed mathematically herein and demonstrated to work experimentally. These and related results, such as the vibration sensitivity curves given herein, will be of use to other workers who apply pulsed differential holography to other mechanics problems.

Finally, the reader should note that the question of "noise", and "noisy mechanical environments" has been considered herein and a preliminary analysis given. For the experiments reported herein, there were virtually no problems that arose due to noise, spurious vibrations, or lack of mechanical stability. Wooden tables and ordinary laboratory benches were used to support the optics, the plate specimen, the shaker, etc., and little or no attempt was made at vibration isolation of these components. This represents the extent of the stability problems which were encountered experimentally. The development of precise limitations on noise (which are less stringent than those presented herein) will very likely depend on future applications of pulsed laser holography in noisy environments.

7.0 REFERENCES

1. D. Gabor, "Microscopy by Reconstructed Wavefronts," Proc. Roy. Soc. (London) Series A, Vol. 197, 1949, pp. 457-484.

2. E. N. Leith and J. Upatnieks, "Wavefront Reconstruction with Diffuse Illumination and Three-Dimensional Objects," Journal Opt. Soc. Am., Vol. 54, No. 11, November 1964, pp. 1295-1301.

3. J. B. Develis and G. O. Reynolds, Theory and Applications of Holography, Addison-Wesley Publ., Reading, Mass., 1967.

4. J. W. Goodman, Introduction to Fourier Optics, McGraw-Hill, 1968, pp. 209-268.

5. H. Smith, Principles of Holography, John Wiley & Sons, 1969.

6. L. O. Heflinger, R. F. Wuerker and R. E. Brooks, "Holographic Interferometry," Journal of Applied Physics, Vol. 37, February 1966, pp. 642-649.

7. K. A. Haines and B. P. Hildebrand, "Surface Deformation Measurement Using the Wavefront Reconstruction Technique," Applied Optics, Vol. 5, No. 4, April 1966, pp. 595-602.

8. G. M. Brown, R. M. Grant, and G. W. Stroke, "Theory of Holographic Interferometry," J. Acous. Soc. Amer., Vol. 45, No. 5, May 1969, pp. 1166-1179.

9. E. B. Aleksandrov and A. M. Bonch-Bruevich, "Investigation of Surface Strains by the Holographic Techniques," Soviet Physics, Technical Physics, Vol. 12, No. 2, August, 1967, p. 258.

10. R. Aprahamian and K. R. Overoye, "Holographic Stress Analysis of Turbine Blades," Presented at the NASA/MSFC Conf. on Holog. and Optical Filtering, May 1971. To be Published in the Conference Proceedings.

11. R. Aprahamian, D. A. Evensen, J. S. Mixson and J. E. Wright, "Application of Pulsed Holographic Interferometry to the Measurement of Propagating Transverse Waves in Beams," Experimental Mechanics, J. Soc. for Experimental Stress Analysis, July 1971, pp. 309-314.

12. R. Aprahamian, D. A. Evensen, J. S. Mixson and J. L. Jacoby, "Holographic Study of Propagating Transverse Waves in Plates," Experimental Mechanics, J. Soc. for Experimental Stress Analysis, August 1971, pp. 357-362.

13. W. G. Gottenberg, "Some Applications of Holographic Interferometry," Experimental Mechanics, Proc. Soc. for Experimental Stress Analysis, September, 1968. Also published as TRW Report No. EM 17-13, August 1967.

14. I. K. Leadbetter and T. Allan, "Holographic Examination of the Pre-Buckling Behavior of Axially Loaded Cylinders," in The Engineering Uses of Holography, Ed: E. R. Robertson and J. M. Harvey (Strathclyde, 1968) Cambridge Univ. Press, 1970.

15. R. Aprahamian and D. A. Evensen, "Vibration Analysis by Differential Holographic Interferometry," AIAA Journal, Vol. 9, No. 1, January 1971, pp. 186-188.

16. R. L. Powell and K. A. Stetson, "Interferometric Vibration Analysis by Wavefront Reconstruction," Journal Opt. Soc. Am., Vol. 55, No. 12, December 1965, pp. 1593-1598.

17. D. A. Evensen and R. Aprahamian, "Applications of Holography to Vibrations, Transient Response, and Wave Propagation," TRW Systems Report No. AM 70-11, May 1970. Also available as NASA CR-1671, December 1970.

18. F. J. Mottier, "Holography of Randomly Moving Objects," Appl. Phys. Ltrs., Vol. 15, No. 2, July 15, 1969, pp. 44-45.

19. C. C. Aleksoff, "Temporally Modulated Holography," Applied Optics, Vol. 10, No. 6, pp. 1331-1332, June 1971.

20. E. R. G. Eckert and R. M. Drake, Heat and Mass Transfer, McGraw-Hill, 1959.

21. J. P. Waters, H. G. Aas, and R. K. Erf, "Investigation of Applying Interferometric Holography to Turbine Blade Stress Analysis," Final Report J990798-13, on Contract N00019-69-C-0271, United Aircraft Research Laboratories, February 1970.

22. J. E. Wright (Private Communication), TRW Systems Group, Redondo Beach, California.

23. (Lord) Rayleigh, The Theory of Sound, First Am. Ed., Vols. I and II, Dover Publ., 1945 (Chapter X, Vibrations of Plates).

24. W. B. Davenport and W. L. Root, Random Signals and Noise, McGraw-Hill, 1958.

25. J. S. Bendat and A. G. Piersol, Measurement and Analysis of Random Data, Wiley & Sons, 1966.

26. M. Francon, Optical Interferometry, Academic Press, 1966.